

Evolution of reaction center mimics to systems capable of generating solar fuel

Benjamin D. Sherman · Michael D. Vaughn ·
Jesse J. Bergkamp · Devens Gust · Ana L. Moore ·
Thomas A. Moore

Received: 2 November 2012 / Accepted: 17 January 2013 / Published online: 11 February 2013
© Springer Science+Business Media Dordrecht 2013

Abstract Capturing and converting solar energy via artificial photosynthesis offers an ideal way to limit society's dependence on fossil fuel and its myriad consequences. The development and study of molecular artificial photosynthetic reactions centers and antenna complexes and the combination of these constructs with catalysts to drive the photochemical production of a fuel helps to build the understanding needed for development of future scalable technologies. This review focuses on the study of molecular complexes, design of which is inspired by the components of natural photosynthesis, and covers research from early triad reaction centers developed by the group of Gust, Moore, and Moore to recent photoelectrochemical systems capable of using light to convert water to oxygen and hydrogen.

Keywords Artificial photosynthesis · Solar energy conversion · Biomimicry · Sustainability

Abbreviations

NPP	Net primary production of photosynthesis
HANPP	Human appropriation of net primary production of photosynthesis
OEC	Oxygen evolving complex
NADPH	Nicotinamide adenine dinucleotide phosphate
ATP	Adenosine triphosphate
ADP	Adenosine diphosphate
P _i	Inorganic phosphate
P–Q	Porphyrin–quinone
C–P–Q	Carotenoid–porphyrin–quinone
C–P–C ₆₀	Carotenoid–porphyrin–fullerene
BPEA	Bis(phenylethynyl)anthracene
DHI	Dihydroindolizine
BT	Betaine
Tyr _Z –His190	Tyrosine _Z –histidine190
PCET	Proton coupled electron transfer
BiP	Benzimidazolephenol
TCNP	Tetracyanoporphyrin
FTO	Fluorine-doped tin oxide
PEC	Photoelectrochemical cell
CEPA	2-Dicarboxyethylphosphonic acid
Pg	Petagram
APP	Artificial photosynthetic production

B. D. Sherman · M. D. Vaughn · J. J. Bergkamp · D. Gust ·
A. L. Moore (✉) · T. A. Moore
Department of Chemistry and Biochemistry, Arizona State
University, Tempe, AZ 85287, USA
e-mail: amoore@asu.edu

D. Gust
e-mail: gust@asu.edu
URL: <http://solarfuel.clas.asu.edu/>

T. A. Moore
e-mail: tmoore@asu.edu

B. D. Sherman · M. D. Vaughn · J. J. Bergkamp · D. Gust ·
A. L. Moore · T. A. Moore
Center for Bio-Inspired Solar Fuel Production, Arizona State
University, Tempe, AZ 85287, USA

B. D. Sherman · M. D. Vaughn · J. J. Bergkamp · D. Gust ·
A. L. Moore · T. A. Moore
Center for Bioenergy and Photosynthesis, Arizona State
University, Tempe, AZ 85287, USA

Introduction

Human activity and especially our reliance on burning fossil fuels has affected planet wide systems, resulting in a

precarious future for the global ecosystem (Rockström et al. 2009). The magnitude of the energy reaching the Earth from the sun makes solar energy conversion a likely part of any alternative energy future that does not rely on the use of fossil fuel yet still satisfies society's energy demand (Armaroli and Balzani 2007). The immense scale of solar irradiance, however, means little without an efficient means of converting it to useful forms such as electricity or an energy-dense and transportable fuel. Developing a system for converting an abundant and readily available precursor into a fuel using solar radiation as the sole energy input is the primary goal of artificial photosynthesis (Bard and Fox 1995; Gust et al. 2009).

The motivation for and possible impact of the wide scale use of artificial photosynthesis to meet human societal energy needs can be illustrated with reference to Fig. 1. Taking into account reflection and absorption of light by the atmosphere, around 65,000 TW reaches the hydrosphere and 15,600 TW reaches land (Sorensen 2010). Photosynthesis converts a portion of this irradiance into energy stored in reduced carbon, with the net amount of biomass produced in a year [net primary production (NPP)] totaling ~ 112 Pg of fixed carbon (Ito 2011). Converting this amount of reduced biomass produced per year to a rate of energy conversion using the conversion factor of 41.3 kJ g^{-1} of fixed carbon (Archer and Barber 2004) yields an average rate of ~ 156 TW, evenly distributed

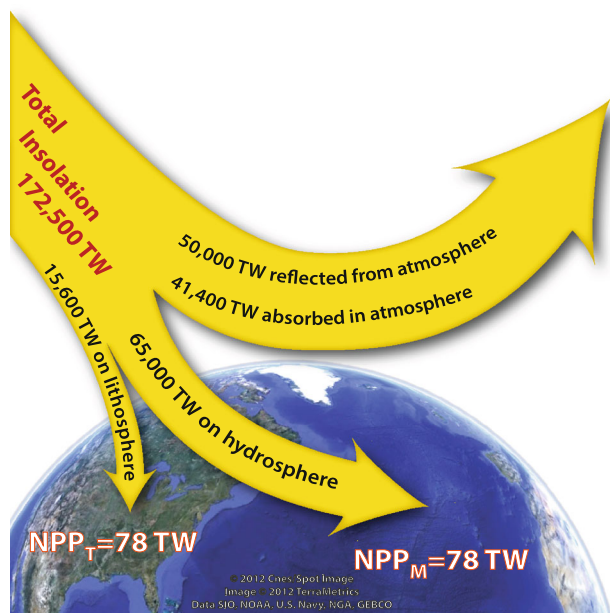


Fig. 1 Solar radiation and photosynthetic conversion. Rates of solar energy reaching various portions of the Earth system (Sorensen 2010). While $\sim 80,000$ TW reach the surface of the Earth, only 15,600 TW fall on land. About half is within the wavelength range of the photosynthetic pigments; a small fraction of this is stored as chemical energy for the biosphere, i.e., NPP, at an average rate of ~ 156 TW

between terrestrial and marine production (Cramer et al. 1999; Field et al. 1998; Ito 2011). This biomass in turn supports nearly all life on the planet. Humans consume an increasing portion, currently $\sim 25\%$ (Haberl et al. 2007). An important issue we face is that human appropriation of net primary production (HANPP) comes at the expense of the remainder of biology, and continued population growth will increase the human demand on NPP for food and material. The conversion of land to support HANPP is thought to be driving several Earth systems over boundaries established by natural cycles operating on the geological time scale (Barnosky et al. 2012; Rockström et al. 2009).

Therefore, any solar-to-fuel system must be vetted against its impact on HANPP; an increase will accentuate an already tenuous ecological situation (Barnosky et al. 2012; Rockström et al. 2009). Figure 2 outlines energy accounts comparing terrestrial NPP, HANPP, the remainder of NPP after human harvest, and the current non-food energy consumption of modern society. Part (a) illustrates the current state: the human requisition of NPP sums to 20 TW (Haberl et al. 2007). Driving the global gross domestic product currently consumes ~ 17 TW, mainly supplied by fossil fuels (IPCC 2011). Fully displacing fossil fuels with crop-derived biofuel, as shown in (b), must come directly out of NPP. Though carbon neutral, such a scenario is not sustainable as HANPP would increase to nearly 50% NPP. Such a substantial consumption of the total available terrestrial biomass would likely upend the balance of life on the planet as it has been known for the entirety of human existence. Alternatively, as shown in (c), an artificial photosynthetic system (possibly including a synthetic biological organism or photosynthetic microbe, the culture of which does not displace native organisms or crops) could supply human energy needs while not depleting the biomass needed to support the global ecosystem. We term this converted solar energy APP or artificial photosynthetic production. This situation would have to satisfy several caveats. For instance any such system should occupy surface area already altered by human activity and minimize the amount of additional land converted for human use. This basic argument seeks not only to focus just on the surface footprint needed to convert solar irradiance to forms of energy usable by humans but also to consider that any system should not compete for sunlight or land currently used for food production or accessible to nature. To do so will only increase HANPP and further endanger the stability of the global ecosystem.

In order to exceed current productivity without increasing HANPP, the field of artificial photosynthesis seeks the development of solar-to-fuel systems capable of converting light energy to chemical energy stored in a dense, transportable fuel with efficiencies much greater than those of natural photosynthesis. Such a system, as

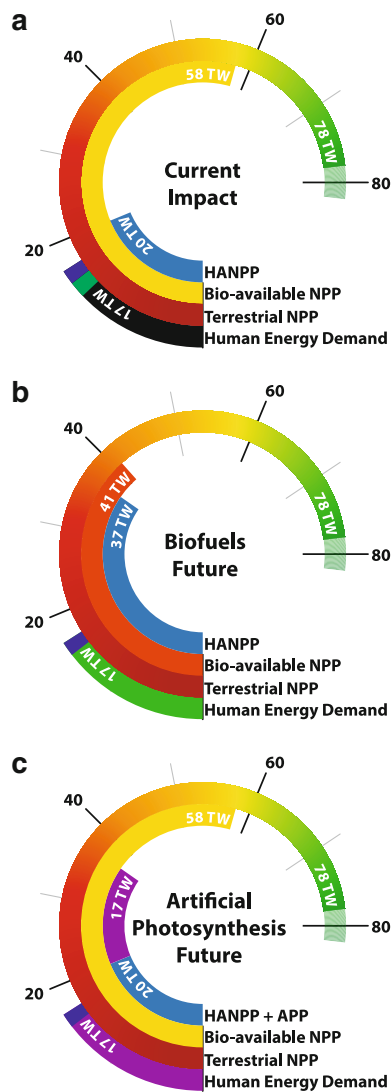


Fig. 2 Impact of human society on the NPP and the biosphere. **a** Current impact of human society. NPP is estimated from a consensus of recent models (Ito 2011) (NPP prior to industrialization is indicated by the shaded extension to 82 TW) and transformed into TW using a previous conversion (Haberl et al. 2007). HANPP is indicated relative to the amount remaining for all biota (Haberl et al. 2007). Human energy demands are met using primarily fossil reserves (*black fill*), while current renewable sources are designated as renewable biofuels (*green fill*) and renewable nonbiofuels (*dark blue fill*) (IPCC 2011). **b** Future scenario with complete replacement of fossil fuels by biofuels (*green fill*), bioavailable NPP is reduced by half, which has catastrophic effects on biodiversity. **c** Future scenario with NPP enhanced by higher efficiency APP deployed within existing footprint of human society, purple fill indicates enhancements to productivity from APP

opposed to that of solar-to-electricity (photovoltaic cells), allows for the storage of solar energy and separates its points of generation and utilization in both time and space. As such, artificial photosynthesis can provide a direct substitute for fossil fuels, which are ideal energy carriers with respect to their high energy densities and easy

transport. Although designing and constructing such a system comes with enormous challenges, the natural process of oxygenic photosynthesis offers us a guide.

Oxygenic photosynthesis uses the energy of visible light to carry out the oxidation of water and reduction of carbon dioxide to form oxygen and reduced carbon fuel. Absorption of actinic photons by antennas and reaction center pigments of the photosynthetic machinery initiates charge separation and migration in the reaction center, generating spatially separated oxidizing and reducing equivalents. This conversion of solar energy into electrochemical energy is followed by the production of oxygen from water at the oxygen evolving complex (OEC), the generation of reduced nicotinamide adenine dinucleotide phosphate (NADPH), and creation of a proton gradient across the thylakoid membrane. Dissipation of this proton motive force across the membrane produces adenosine triphosphate (ATP) via ATP synthase, and ATP and NADPH then power the dark reactions of the Calvin–Benson cycle leading to the assimilation of CO₂.

Artificial photosynthesis does not seek to reproduce the natural process, but rather to adapt its basic science to meet the needs of humans. Akin to the process of photosynthesis, an artificial reaction center for solar fuel production needs to absorb light in the visible and near-infrared, generate a charge-separated state upon photo-excitation, spatially separate and stabilize the charge-separated state, and then transport the photo-generated oxidizing and reducing equivalents to catalysts to carry out the chemical reactions necessary for the production of a fuel (e.g., oxidation of H₂O and production of H₂). In addition, efficient solar-to-fuel systems incorporating abundant materials are paramount. The study of the underlying photophysical and photochemical processes of model constructs and photo-electrochemical cells will inform the design and aid in the development of such systems.

Much of the research of the Gust, Moore, and Moore group has centered on the development and study of artificial reaction centers with the ultimate objective of constructing solar-to-fuel systems. Here, we provide an overview of this work from the first triad reaction centers to the solar water splitting photochemical systems currently under study. The focus of this review is intended as a concise summary of how the group has approached the major challenge of developing sustainable solar energy to fuel technologies, a task that needs input from and is being addressed by many research groups.

Molecular reaction centers

An artificial reaction center seeks to perform the same photochemical processes as those observed in the natural

system. With the ultimate goal of using light energy to form a fuel, the key functions include: absorption of light across the visible and near-infrared spectra, rapid and efficient transfer of excitation energy from antenna pigments to the reaction center, fast photoinduced charge separation with quantum yields near unity, and prevention of photodamage. Artificial constructs capable of emulating many aspects of the photosynthetic process have been studied, but developing complete systems capable of efficient conversion of light energy into a fuel remains a challenge. The work outlined below shows a research trajectory aimed at this ultimate goal.

Triad reaction centers

Covalently linking two molecular analogs of the cofactors involved in the photosynthetic reaction center (e.g., chlorophylls, carotenoids, pheophytins, quinones) produces some of the simplest artificial reaction centers. Study of porphyrin–quinone (P–Q) constructs in particular guided early work in the field carried out by many different researchers. While a P–Q dyad could form the P^+-Q^- charge-separated state with proper illumination, the extremely fast decay of this state limits its usefulness (Gust and Moore 1989). In the natural system, sequential electron transfer steps following photoinduced charge separation spatially separate positive and negative charges across a substantial distance, which greatly slows recombination. Following this design principle, incorporating a third

component, one thermodynamically competent for carrying out a second electron transfer after photoinduced charge transfer, proved essential for prolonging the lifetime of the charge-separated state. Synthesis and subsequent study of a carotenoid–P–Q triad (C–P–Q) (Moore et al. 1984) marked a major improvement in stabilizing charge separation in an artificial reaction center and established a platform for engineering improved artificial reaction centers as well as studying other processes characteristic of photosynthesis.

This first triad reaction center, compound **1**, consisted of a ditolylporphyrin covalently bonded via amide linkages to a benzoquinone electron acceptor and a carotenoid secondary electron donor. Molecule **1** and subsequent carotenoporphyrin-acceptor triads characteristically adopt a linear conformation in solution without folding of the appended groups back over the plane of the porphyrin (Gust et al. 1987; Moore et al. 1984). Transient spectroscopic studies of C–P–Q show that illumination with visible light (600 nm) generates the porphyrin first excited singlet state, $C-^1P-Q$, with a portion of this species then decaying to the first charge-separated state, $C-P^+-Q^-$. Competing with recombination, a second electron transfer from the carotenoid to the porphyrin radical cation produces the final charge-separated state C^+-P-Q^- . Monitoring the transient absorbance of the oxidized carotenoid moiety (in the 970 nm region) shows that the final charge-separated state has a lifetime of 170 ns in dichloromethane, increasing to 2.5 μ s in electrolyte-saturated solvent. Table 1 contains a summary of the results for **1** and several

Table 1 Final charge-separated state lifetimes, quantum yield for the formation of the final charge-separated state, and experimental conditions for selected artificial reaction centers

Compound	Solvent	τ^a	Φ^a	$\lambda_{\text{excitation}}$ (nm)	Reference
1	Dichloromethane	170 ns	0.04	600	Moore et al. (1984)
	Dichloromethane ^b	2.5 μ s	0.25	600	Moore et al. (1984)
2	2-Methyltetrahydrofuran	60 ns	0.96	590	Bahr et al. (2000)
3	2-Methyltetrahydrofuran	57 ns	0.95	600	Kodis et al. (2004)
4	2-Methyltetrahydrofuran	170 ns	0.14	590	Liddell et al. (1997)
	2-Methyltetrahydrofuran ^c	1.5 μ s	0.10	590	Liddell et al. (1997)
5	2-Methyltetrahydrofuran	340 ns	0.88	590	Kuciauskas et al. (2000)
6	2-Methyltetrahydrofuran	1.3 ns	0.69	560	Kuciauskas et al. (1999)
7	2-Methyltetrahydrofuran	240 ns	0.86	560	Kodis et al. (2002)
8^d	2-Methyltetrahydrofuran	8.9 ns	0.80	480	Kodis et al. (2006)
8^e	2-Methyltetrahydrofuran	15.3 ns	0.96	480	Kodis et al. (2006)
9	1,2-Difluorobenzene	230 ps	~ 1	480	Terazono et al. (2009)
11	Benzonitrile	3.8 μ s	0.52	740	Megiatto et al. (2012)

^a Lifetime and quantum yield given for the final charge-separated state of the respective reaction center

^b Saturated with tetra-n-butylammonium tetrafluoroborate

^c 77 K (all other values in table at room temperature)

^d $M = 2H$ (freebase form, see Fig. 5)

^e $M = Zn$ (Zn inserted form, see Fig. 5)

other reaction centers described herein. The final state preserves 1.1 eV of the 1.9 eV of the porphyrin first excited singlet state (Gust et al. 1993a). The improved stability of the final charge-separated state of this complex relative to those of the preceding dyads resides in the greater spatial separation, and therefore electronic decoupling, of the separated charges and the endergonic steps hindering the overall energetically favorable charge recombination.

The C–P–Q triad in turn provided a foundation for further elaboration and improvement in reaction center design and function. Several iterations of the triad reaction center are shown in Fig. 3. Alterations of the electronic coupling, as in changing the orientation of the amide linker in **4** and **5** (Kuciauskas et al. 2000), redox properties (Kodis et al. 2004), and type of acceptor moiety (Gust et al. 1991; Liddell et al. 1997) in the reaction center led to triad complexes with improved lifetimes and yields of the final charge-separated state. The extension of the triad design

led to the creation of tetrad and pentad complexes which demonstrated the feasibility of carrying out multiple electron transfer steps across larger complexes resulting in greater spatial separation of the charges and long lifetimes for the charge-separated state (Gust et al. 1993b; Gust et al. 1990; Gust et al. 1988a, b).

The introduction of a fullerene electron-accepting unit in place of a quinone advanced the performance of the artificial reaction centers (Liddell et al. 1997). Although, not observed in any known biological system, the use of a fullerene acceptor moiety offers definite advantages in imitating the photochemical processes observed in natural photosynthesis. With small solvent and internal reorganizational energies upon reduction and relative insensitivity of the radical anion to the solvent dielectric constant compared to quinones, fullerenes perform remarkably well in reaction center constructs (Imahori et al. 1996; Liddell et al. 1997, 1994). In comparison with triad complexes employing quinones, those with fullerene acceptor moieties in general show more rapid

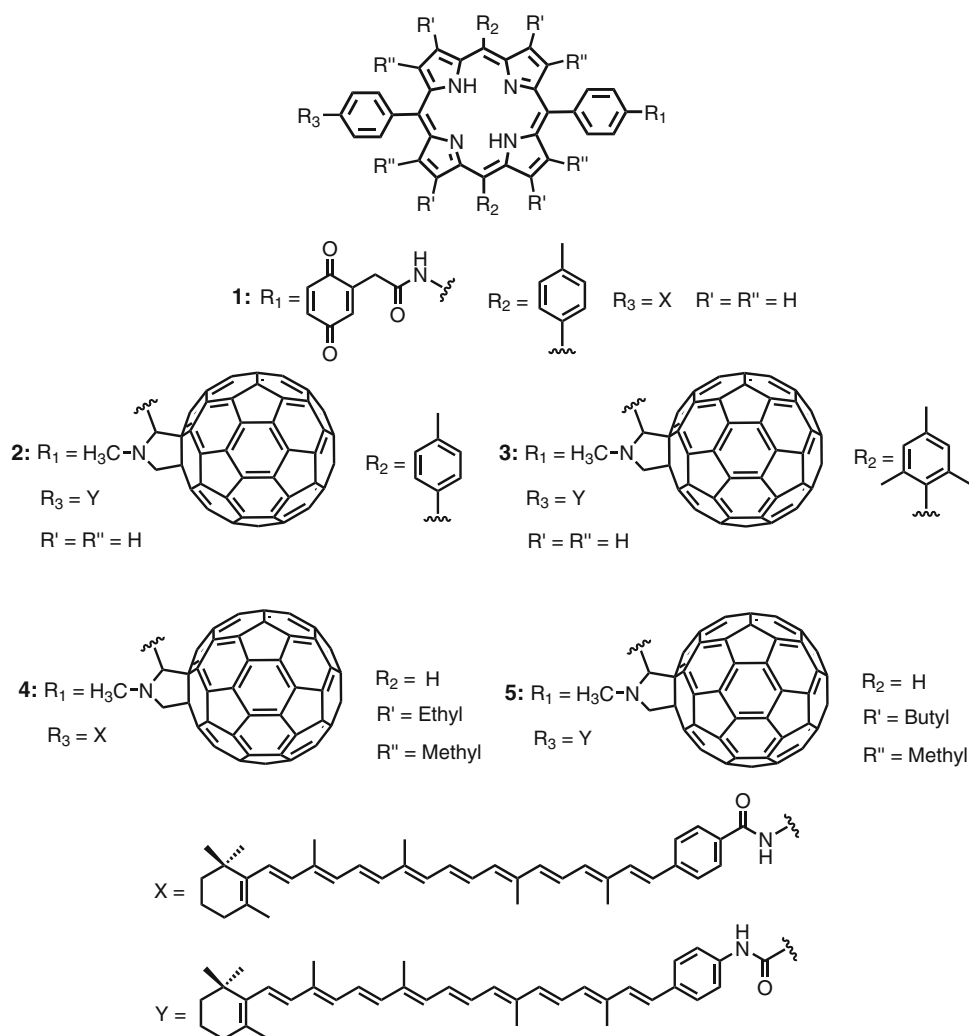


Fig. 3 Chemical structures for triad reaction centers 1–5

photoinduced charge separation and slower charge recombination, can perform charge separation in a variety of solvents and even at low temperature in glasses (Kuciauskas et al. 2000; Liddell et al. 1997), and can recombine to triplet excited states rather than the ground state (Kodis et al. 2004; Liddell et al. 1997). Such behavior is characteristic of the natural system, making fullerenes an ideal example where compounds alien to biology can substantially aid in the development and performance of overall biomimetic artificial systems (Kodis et al. 2002).

The first iteration of the C–P–C₆₀ based triad featuring a β -alkyl substituted porphyrin, **4**, formed the final C⁺–P–C₆₀[–] state with a yield of 0.14 in 2-methyltetrahydrofuran (Liddell et al. 1997). Spectroscopic studies showed that the decay of this state, with a lifetime of 170 ns, led to the formation of the carotenoid triplet state, ³C–P–C₆₀. Progressive molecular engineering of the complex by introduction of a lower potential carotenoid (compare **4** and **5**) (Kuciauskas et al. 2000), introduction of a ditolylporphyrin in **2** (Bahr et al. 2000), and then dimesitylporphyrin in **3** (Kodis et al. 2004) steadily improved the performance of the reaction center, producing complexes capable of obtaining quantum yields for the final charge-separated state near unity. The trajectory of triad reaction centers from the first C–P–Q complexes to the later fullerene-containing analogs demonstrated the ability of synthetic molecular constructs to transform efficiently light energy to chemical potential with charge-separated state lifetimes long enough for conversion of the conserved excitation energy to a useful form, for example by formation of chemical bonds or generation of a pH gradient across a membrane (Steinberg-Yfrach et al. 1997, 1998).

Antenna-reaction centers

The single chromophore in a triad reaction center limits the total usable region of the spectrum; nature, by contrast, employs several different pigment molecules such as chlorophylls, carotenoids, cyanobilins, and erythrobilins for wide coverage of the solar spectrum. In the photosynthetic process, antenna pigment-protein complexes absorb most of the actinic light and channel the resultant excitation energy to the reaction center leading to charge separation (Blankenship 2002).

In an artificial context, multiporphyrin antenna-reaction center complexes provided the basis for later multichromophore arrays and also established a means of studying energy transfer to a reaction center. An antenna moiety consisting of four Zn(II)tetrarylporphyrins—a central Zn(II)porphyrin connected to the meso positions of three peripheral porphyrins—was attached to a free base porphyrin-fullerene reaction center [(P_{ZP})₃–P_{ZC}–P–C₆₀, **6**]. This system established the feasibility of specifically

exciting the antenna to induce charge separation in the attached reaction center (Fig. 4) (Kuciauskas et al. 1999). Optimizing the design of the (P_{ZP})₃–P_{ZC}–P–C₆₀ reaction center by replacing the diarylporphyrin of **6** with tetraarylporphyrin in **7**, and thereby increasing the potential of the electron donating porphyrin, provided more thermodynamic driving force for electron transfer from the antenna porphyrins to the radical cation of the freebase porphyrin and led to a hole delocalization in the antenna and longer lifetime of the final charge-separated state (Kodis et al. 2002). The structural differences between **6** and **7** also led to different HOMO orbital types in the freebase porphyrin moieties: the β -alkyl substituents of the freebase porphyrin in **6** induce an a_{1u}-type HOMO with nodes at the meso positions, whereas the freebase porphyrin of **7** without β substituents and mesityl groups at the 10,20-meso positions exhibits an a_{2u}-type HOMO with lobes at the meso positions. These differences in the HOMO orbital structure combined with the steric influence of the β -alkyl groups of **6**, which results in an increased average dihedral angle and less π – π overlap between the meso aryl group and the porphyrin macrocycle, also create a substantial increase in the rate of singlet–singlet energy transfer rates, better antenna function, and increased quantum yield of final charge separation for **7** as compared to **6** (Kodis et al. 2002). Extending the concept of this design, an antenna-reaction center complex comprised of five bis(phenylethynyl)anthracene (BPEA) antenna molecules linked to a hexaphenylbenzene core and covalently linked to a porphyrin–fullerene complex **8** (Fig. 5), carried out efficient charge separation with better coverage of the spectrum from 430 to 480 nm (Kodis et al. 2006).

Further elaboration of the antenna-reaction center came with the development of complex **9** (Fig. 6), consisting of several different chromophore moieties. Centered on a hexaphenylbenzene core, two BPEA, two borondipyrromethene, and two Zn(II)tetraarylporphyrin dyes comprised an antenna complex with coverage across the visible spectrum (Terazono et al. 2009). Coordination of a dipyriddy functionalized fullerene to the two adjacent Zn(II)porphyrins of the antenna complex completed the formation of a multi-antenna-reaction center complex **9**. Excitation of any of the antenna pigments in the complex leads to rapid light-induced electron transfer to the fullerene. Developing molecular design strategies for broad spectral coverage with funneling of excitation energy to charge transfer centers, such as those outlined above, plays a central role in the development of efficient solar-to-fuel systems.

Photoregulation

During photosynthesis, the process of non-photochemical quenching enables the organism to avoid the buildup of

Fig. 4 Chemical structures for antenna-reaction centers **6** and **7**

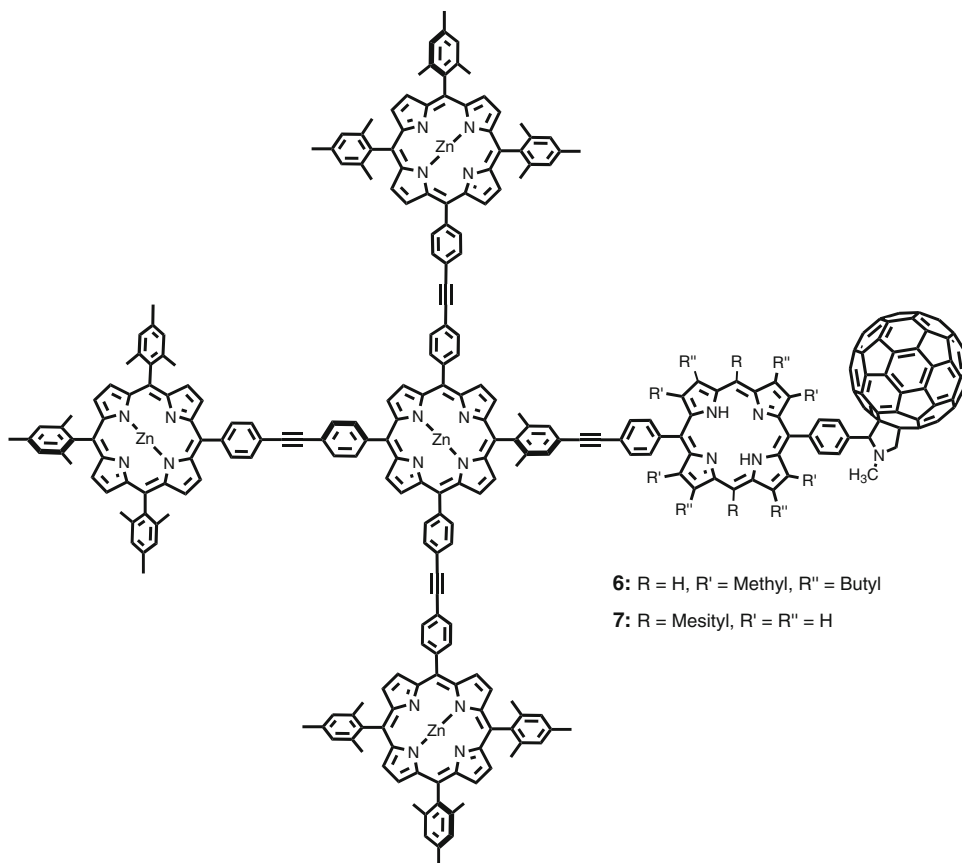
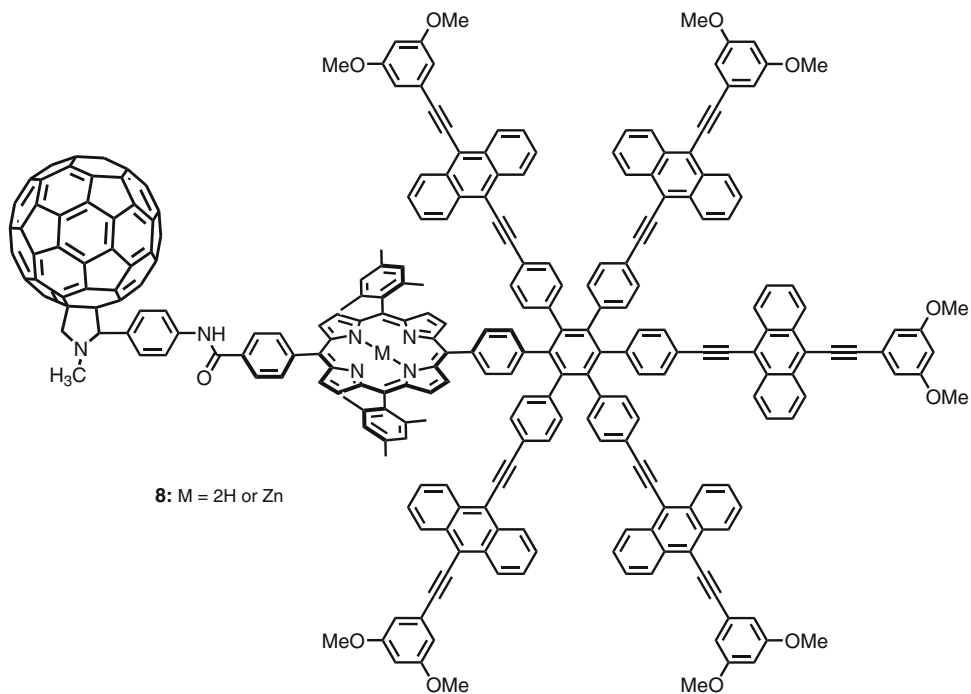


Fig. 5 Antenna-reaction center complex **8**



energetic, and damaging, intermediates that would otherwise form under high light intensities (Horton et al. 2012; Müller et al. 2001). Avoiding destructive intermediates

formed under such conditions could likely increase the longevity of artificial systems in a similar manner. A pentad reaction center, consisting of a porphyrin primary

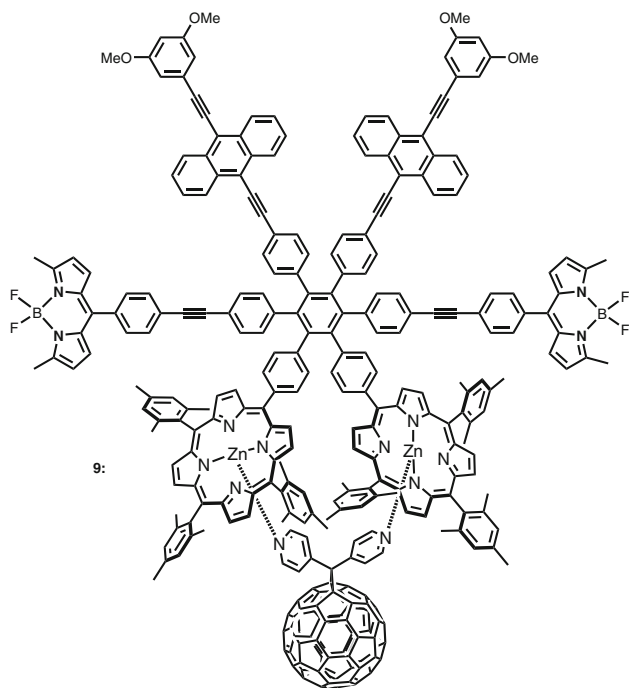


Fig. 6 Antenna-reaction center complex **9**

donor, fullerene acceptor, two antenna pigments, and a dihydroindolizine (DHI) photochrome control moiety, demonstrated the ability of an artificial reaction center to reversibly change the quantum yield of charge separation based on the intensity of incident light (Straight et al. 2008). Under low white light levels, in which the DHI exists primarily in the closed form, the reaction center carries out light-induced charge separation with a quantum yield of 0.82. Under high white light intensities, the quantum yield of a solution of the pentad decreases to 0.27 as photoisomerization converts some of the photochrome to its open, betaine form (BT), a conformation competent for rapidly quenching the porphyrin excited singlet state by energy transfer. Upon forming BT at high white light intensities, the quenching of the porphyrin excited state prevents charge separation in the reaction centers of the isomerized molecules, markedly reducing the overall quantum yield for this process.

Charge separation across a membrane

Along with light capture and formation of a charge-separated state, an artificial solar-to-fuel system must convert incident light energy to some other useful form. In photosynthesis, photoinduced charge transfer across the thylakoid membrane is coupled to proton shuttling across the bilayer, thereby establishing a proton gradient. Dissipation of the proton imbalance back across the membrane then drives the production of ATP via a transmembrane ATP-synthase

enzyme. Producing constructs capable of mimicking this process can offer insight into the design and development of artificial systems for solar energy conversion.

A study to this end demonstrated that illumination of a phospholipid bilayer impregnated with C–P–Q type reaction centers and separating a solution containing a sacrificial electron donor from that with an acceptor species results in the passage of photocurrent in a circuit bridging the bilayer membrane (Seta et al. 1985). Building off this work, imbedding a similar C–P–Q type reaction center in the bilayer of a liposome set the basis of a system capable of pumping protons across the lipid layer (Steinberg-Yfrach et al. 1997). The overall amphiphilic nature of the C–P–Q complex used directs the asymmetric insertion of the reaction center into the liposome with the carotenoid moiety toward the interior and the more polar quinone to the exterior. Excitation of the complex generates an oxidizing potential inside and a reducing potential around the periphery of the liposome. A freely diffusing quinone electron/proton carrier within the membrane of the liposome with a midpoint potential between that of the oxidized carotenoid and reduced quinone moieties of the reaction center shuttles protons across the membrane, resulting in the acidification of the interior of the liposome. This results in the creation of a light-induced potential gradient across the bilayer.

In order to harness the proton motive force generated in this system, a CF_0F_1 -ATP synthase was incorporated into the liposome along with the reaction center and redox mediator components (Steinberg-Yfrach et al. 1998). With proton translocation driven by the photocycle described above, dissipation of the pH gradient coupled to the catalytic conversion of ADP and P_i to ATP as carried out by the CF_0F_1 -ATP synthase resulted in the net conversion of incident light energy into that of a high-energy chemical species. Quantitative analysis of the system reveals that in low light the absorption of 14 photons results in the production of 1 ATP molecule and, with illumination by 633 nm light, roughly 4 % of the absorbed energy is conserved in the form of a chemical bond.

In a subsequent study, the same C–P–Q reaction center was used in conjunction with a quinone-like molecule, ability to bind Ca^{2+} of which is modulated by the redox status (Bennett et al. 2002). This system was capable of pumping Ca^{2+} ions against a concentration gradient by the asymmetric arrangement of the C–P–Q reaction center in liposomes. Although the quantum yield was only 1 %, a significant electrical potential was measured across the membrane extending Mitchell's mechanism of accumulating membrane potential using a redox loop to divalent cations in addition to protons.

Mimicking proton control during electron transfer

The Tyrosine_Z–Histidine190 (Tyr_Z–His190) pair of photosystem II (PSII) is thought to undergo proton-coupled electron transfer (PCET) as it serves as an electron transfer mediator between P₆₈₀ and the OEC (Faller et al. 2003; Rappaport and Diner 2008). The interaction between Tyr_Z and His190 likely serves to tune the potential of the tyrosine residue so that it lies between that needed for the reduction of the photogenerated P₆₈₀⁺ and the potential for oxidizing the OEC. Serving as an intermediary between P₆₈₀ and the OEC, Tyr_Z–His190 prevents charge recombination that would otherwise compromise the catalytic activity of the Mn₄O₅Ca cluster of the OEC. This is especially important given that four oxidizing equivalents must accrue on the OEC to carry out the oxidation of one molecule of water. To improve artificial systems, utilizing a similar design feature could also aid in preventing back electron transfer after photoinduced charge separation.

With the natural system as a template, we designed a porphyrin construct **10** (Fig. 7) bearing a benzimidazolphenol (BiP) moiety with the phenolic hydrogen capable of forming a hydrogen bond with the lone pair electrons of the imidazole nitrogen (Moore et al. 2008, 2010). Chemically functionalizing the porphyrin to adsorb to the surface of a colloidal TiO₂ nanoparticle enables the assembly of **10** as shown in Fig. 7. This molecule–nanoparticle complex is reminiscent of the triad reaction centers discussed earlier, consisting of a porphyrin light absorber (PF₁₀), TiO₂ primary electron acceptor, and BiP electron donor (Moore et al. 2008). Electron paramagnetic resonance studies of this complex reveal phenoxyl radical formation in the complex upon excitation of the porphyrin as a result of light-induced charge separation. Given that the potential for the oxidation of the BiP moiety lies at 1.00 V versus SCE, the photo-formed BiP⁺–PF₁₀–TiO₂[–] state is thermodynamically competent for water oxidation.

A continuation of this study led to the development of **11** (Fig. 7), a fully organic triad complex with a tetracyanoporphyrin (TCNP) serving as the primary acceptor in place of a TiO₂ nanoparticle (Megiatto et al. 2012). This complex bears considerable similarity to the Tyr_Z–His190–P₆₈₀–Phoe_{D1} portion of the electron transport chain in PSII. Time resolved spectroscopic investigation of this reaction center in benzonitrile reveals that with excitation of TCNP the complex undergoes an initial electron transfer between the PF₁₀ and TCNP resulting in Bi–PhOH–PF₁₀⁺–TCNP[–]. Competing with charge recombination, a second, rapid electron transfer then occurs between the benzimidazolphenol and oxidized PF₁₀, presumably resulting in BiH⁺–PhO[–]–PF₁₀–TCNP[–]. This state forms with a quantum yield of 0.52 and persists with a 4 μs lifetime, which is longer than those of many of the carotenoporphyrin–acceptor

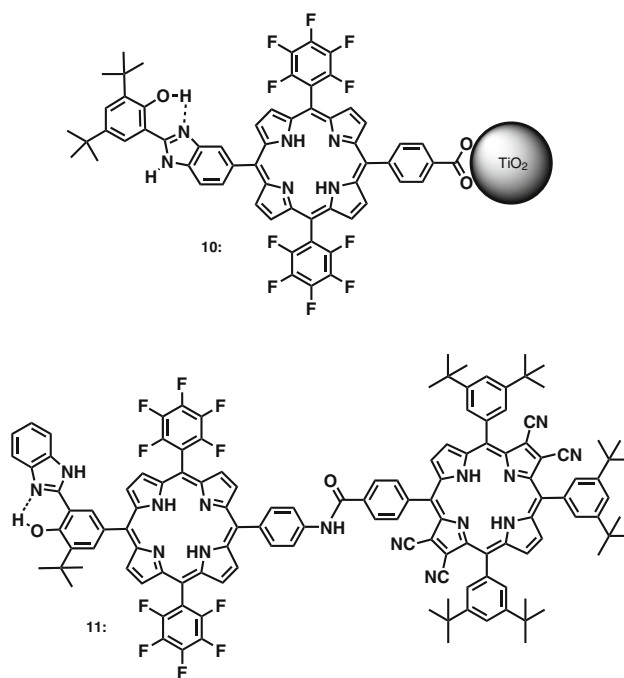


Fig. 7 BiP containing triad reaction centers **10** and **11**

reaction centers of prior studies. Presumably, the final charge-separated state reflects transfer of the phenolic proton to the nitrogen of the benzimidazole. Based on reduction potentials for model compounds (Moore et al. 2010), the PF₁₀⁺ would not generate sufficient driving force for the formation of the Bi–PhOH⁺–PF₁₀–TCNP[–], implying a PCET leading to the formation of the BiH⁺–PhO[–]–PF₁₀–TCNP[–] state. The long-lived charge-separated state and high potential of the oxidized BiH⁺–PhO[–] (1.04 V vs. SCE), make this reaction center type an ideal candidate for incorporation into the photoanode of a photoelectrochemical device for light driven water splitting.

Employing reaction centers for water splitting

Thus far, we have illustrated artificial photosynthetic systems for light absorption and charge separation via photoinduced electron transfer. Fuel production requires “wiring” such reaction centers to catalysts. One approach to doing so is to combine electrode architectures reminiscent of those used in dye sensitized solar cells with artificial reaction centers to produce photoelectrochemical water splitting cells.

In collaboration with the Mallouk lab, we developed a photoanode composed of a transparent fluorine-doped tin oxide (FTO) conductive glass support bearing a nanoparticulate TiO₂ semiconducting layer to which is adsorbed a trisbipyridylruthenium(II) [Ru(bpy)₃²⁺]-hydrated iridium oxide (IrO_x·nH₂O) complex (Fig. 8) (Youngblood et al. 2009). A photoelectrochemical cell (PEC) consisting of

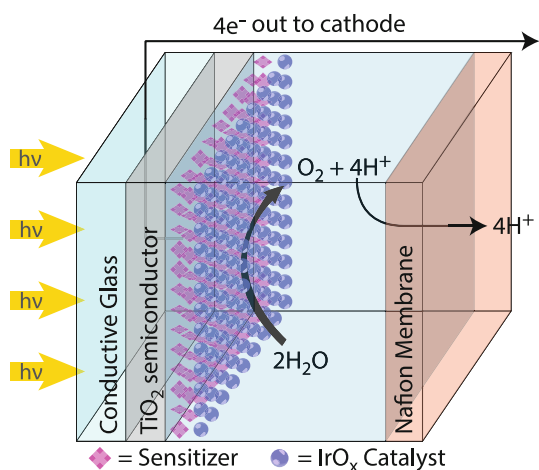


Fig. 8 Schematic representation of the photoanode compartment of a PEC. Electrons and protons from water oxidation migrate to the cathode for fuel production

this electrode in combination with a platinum cathode in aqueous solution demonstrated overall photolytic water splitting to oxygen and hydrogen, with the application of a small bias.

This system resembles a triad-type reaction center with a Ru(bpy)₃²⁺ light absorber and primary electron donor, a TiO₂ primary acceptor, and an IrO_x·nH₂O secondary electron donor. Ideally, four sequential photocycle turnovers consisting of excitation of the Ru(bpy)₃²⁺, electron transfer to the TiO₂ resulting in current flow to the platinum counter electrode, and hole transport to the IrO_x·nH₂O, results in the conversion of water to oxygen at the IrO_x·nH₂O surface and production of hydrogen at the platinum cathode. While overall water splitting was observed, spectroscopic study of the system revealed that the charge recombination from the TiO₂ to the oxidized dye occurred nearly an order of magnitude faster than the forward electron transfer from the IrO_x·nH₂O to regenerate the ground state dye. This charge recombination imposes a major limitation on the performance of the system and represents a critical area for improvement.

In PSII, Tyr_Z serves the function of charge transfer mediator between P₆₈₀ and the OEC and limits the occurrence of charge recombination. In order to address the analogous recombination in our system, we turned to the use of the benzimidazolephenol of the BiP–PF₁₀–TiO₂ triad (Fig. 7) as a redox mediator in the photoelectrochemical system. Chemically modifying the BiP with a dicarboxylate functionality enabled the production of colloidal IrO_x·nH₂O particles decorated with both the BiP mediator and 2-dicarboxyethylphosphonic acid (CEPA) (Zhao et al. 2012). Study of a PEC similar to that of the earlier work but using an FTO–TiO₂ photoanode bearing co-immobilized Ru(bpy)₃²⁺ dye and BiP/CEPA–IrO_x·nH₂O shows that the BiP mediator improves the performance of

the system. As compared to a cell without the mediator (using only CEPA capped IrO_x·nH₂O), higher photocurrents and greater overall efficiency (about a factor of three) are observed. Transient bleaching recovery traces showed that the improved performance results from faster regeneration of the ground state dye from the first oxidized state with the presence of BiP in the system (Zhao et al. 2012). Thus, BiP serves a similar role to that of Tyr_Z in PSII by preventing recombination losses after light-induced charge separation.

Conclusion

This account shows our research group's trajectory from building simple molecular reaction center constructs to developing complete systems for the conversion of solar energy to a fuel. Efficient and economical systems which can generate a sustainable fuel from sunlight and a widely available precursor such as water are requisite to meeting future human energy demand in a way that does not endanger the diversity of life on the planet or the health and wellbeing of its inhabitants. Developing and improving the technologies for such systems represents a principal challenge of the modern world. The complications of fulfilling energy demand requires a host of sustainable technologies for varying locales. Certainly, solar energy will play a substantial role, and chemical fuels provide the greatest possible flexibility of usage.

We have pursued this challenge through the study of artificial reaction centers designed to mimic aspects of photosynthesis. As the only process capable of converting solar energy to a chemical fuel on a planet wide scale, photosynthesis provides a model for doing so by artificial means. The development and study of molecular reaction centers has culminated in the development of a first generation of dye-sensitized PECs for solar-to-fuel conversion. Substantial work remains in advancing the viability of this system. For instance, we are exploring the synthesis and use of new dye-catalyst constructs (Sherman et al. 2011) and catalytic materials based on more abundant elements (Wee et al. 2011). Ultimately, the grand challenge of supplying sustainable energy requires contributions from many researchers and all fields of science; our best hope lies in developing a range of renewable energy technologies and contributing to a well informed and well equipped global society.

Acknowledgments This work was supported by the Center for Bio-Inspired Solar Fuel Production, an Energy Frontier Research Center funded by the U.S. Department of Energy, Office of Science, Office of Basic Energy Sciences under award Number DE-SC0001016. Some of the research described in this review was supported by the National Science Foundation (CHE-0352599) and U.S. Department of Energy

(DE-FG02-03ER15393). M.D.V. thanks the National Science Foundation for support from the Graduate Research Fellowship Program (GRFP).

References

- Archer MD, Barber J (2004) Molecular to global photosynthesis. Imperial College Press, London
- Armadori N, Balzani V (2007) The future of energy supply: challenges and opportunities. *Angew Chem Int Ed Engl* 46:52–66. doi:10.1002/anie.200602373
- Bahr JL, Kuciauskas D, Liddell PA et al (2000) Driving force and electronic coupling effects on photoinduced electron transfer in a fullerene-based molecular triad. *Photochem Photobiol* 72:598–611. doi:10.1562/0031-8655(2000)0720598DFAECE2.0.CO2
- Bard AJ, Fox MA (1995) Artificial photosynthesis: solar splitting of water to hydrogen and oxygen. *Acc Chem Res* 28:141–145. doi:10.1021/ar00051a007
- Barnosky AD, Hadly EA, Bascompte J et al (2012) Approaching a state shift in Earth's biosphere. *Nature* 486:52–58. doi:10.1038/nature11018
- Bennett IM, Farfano HMV, Bogani F et al (2002) Active transport of Ca^{2+} by an artificial photosynthetic membrane. *Nature* 420:398–401. doi:10.1038/nature01209
- Blankenship RE (2002) Molecular mechanisms of photosynthesis. Wiley-Blackwell, Oxford
- Cramer W, Kicklighter DW, Bondeau A et al (1999) Comparing global models of terrestrial net primary productivity (NPP): overview and key results. *Glob Chang Biol* 5:1–15. doi:10.1046/j.1365-2486.1999.00009.x
- Faller P, Goussias C, Rutherford AW, Un S (2003) Resolving intermediates in biological proton-coupled electron transfer: a tyrosyl radical prior to proton movement. *Proc Natl Acad Sci* 100:8732–8735. doi:10.1073/pnas.1530926100
- Field CB, Behrenfeld MJ, Randerson JT, Falkowski P (1998) Primary production of the biosphere: integrating terrestrial and oceanic components. *Science* 281:237–240
- Gust D, Moore TA (1989) Mimicking photosynthesis. *Science* 244:35–41. doi:10.1126/science.244.4900.35
- Gust D, Moore TA, Liddell PA et al (1987) Charge separation in carotenoporphyrin–quinone triads: synthetic, conformational, and fluorescence lifetime studies. *J Am Chem Soc* 109:846–856. doi:10.1021/ja00237a035
- Gust D, Moore TA, Moore AL et al (1988a) Photoinitiated charge separation in a carotenoid–porphyrin–diquinone tetrad: enhanced quantum yields via multistep electron transfers. *J Am Chem Soc* 110:321–323. doi:10.1021/ja00209a068
- Gust D, Moore TA, Moore AL et al (1988b) A carotenoid–diporphyrin–quinone model for photosynthetic multistep electron and energy transfer. *J Am Chem Soc* 110:7567–7569. doi:10.1021/ja00230a064
- Gust D, Moore TA, Moore AL et al (1990) Efficient multistep photoinitiated electron transfer in a molecular pentad. *Science* 248:199–201. doi:10.1126/science.248.4952.199
- Gust D, Moore TA, Moore AL et al (1991) Long-lived photoinitiated charge separation in carotene–diporphyrin triad molecules. *J Am Chem Soc* 113:3638–3649. doi:10.1021/ja00010a002
- Gust D, Moore TA, Moore AL (1993a) Molecular mimicry of photosynthetic energy and electron transfer. *Acc Chem Res* 26:198–205. doi:10.1021/ar00028a010
- Gust D, Moore TA, Moore AL et al (1993b) Photoinduced electron and energy transfer in molecular pentads. *J Am Chem Soc* 115:11141–11152. doi:10.1021/ja00077a011
- Gust D, Moore TA, Moore AL (2009) Solar fuels via artificial photosynthesis. *Acc Chem Res* 42:1890–1898. doi:10.1021/ar900209b
- Haberl H, Erb KH, Krausmann F et al (2007) Quantifying and mapping the human appropriation of net primary production in Earth's terrestrial ecosystems. *Proc Natl Acad Sci USA* 104:12942–12947. doi:10.1073/pnas.0704243104
- Horton P, Ruban AV, Walters RG (2012) Regulation of light harvesting in green plants. *Annu Rev Plant Physiol Mol Biol* 47:655–684. doi:10.1146/annurev.arplant.47.1.655
- Imahori H, Hagiwara K, Aoki M et al (1996) Linkage and solvent dependence of photoinduced electron transfer in zincporphyrin– C_{60} dyads. *J Am Chem Soc* 118:11771–11782. doi:10.1021/ja9628415
- IPCC (2011) Special report on renewable energy sources and climate change mitigation. p 1–1088
- Ito A (2011) A historical meta-analysis of global terrestrial net primary productivity: are estimates converging? *Glob Chang Biol* 17:3161–3175. doi:10.1111/j.1365-2486.2011.02450.x
- Kodis G, Liddell PA, la Garza de L et al (2002) Efficient energy transfer and electron transfer in an artificial photosynthetic antenna—reaction center complex. *J Phys Chem A* 106:2036–2048. doi:10.1021/jp012133s
- Kodis G, Liddell PA, Moore AL et al (2004) Synthesis and photochemistry of a carotene–porphyrin–fullerene model photosynthetic reaction center. *J Phys Org Chem* 17:724–734. doi:10.1002/poc.787
- Kodis G, Terazono Y, Liddell PA et al (2006) Energy and photoinduced electron transfer in a wheel-shaped artificial photosynthetic antenna–reaction center complex. *J Am Chem Soc* 128:1818–1827. doi:10.1021/ja055903c
- Kuciauskas D, Liddell PA, Lin S et al (1999) An artificial photosynthetic antenna–reaction center complex. *J Am Chem Soc* 121:8604–8614. doi:10.1021/ja991255j
- Kuciauskas D, Liddell PA, Lin S et al (2000) Photoinduced electron transfer in carotenoporphyrin–fullerene triads: temperature and solvent effects. *J Phys Chem B* 104:4307–4321. doi:10.1021/jp9935135
- Liddell PA, Sumida JP, Macpherson AN et al (1994) Preparation and photophysical studies of porphyrin– C_{60} dyads. *Photochem Photobiol* 60:537–541. doi:10.1111/j.1751-1097.1994.tb05145.x
- Liddell PA, Kuciauskas D, Sumida JP et al (1997) Photoinduced charge separation and charge recombination to a triplet state in a carotene–porphyrin–fullerene triad. *J Am Chem Soc* 119:1400–1405. doi:10.1021/ja9631054
- Megiatto JD, Antoniuk-Pablant A, Sherman BD et al (2012) Mimicking the electron transfer chain in photosystem II with a molecular triad thermodynamically capable of water oxidation. *Proc Natl Acad Sci USA*. doi:10.1073/pnas.1118348109
- Moore TA, Gust D, Mathis P et al (1984) Photodriver charge separation in a carotenoporphyrin–quinone triad. *Nature* 307:630–632. doi:10.1038/307630a0
- Moore GF, Hamburger M, Gervaldo M et al (2008) A bioinspired construct that mimics the proton coupled electron transfer between p680^{+} and the Tyr_z–His190 pair of photosystem II. *J Am Chem Soc* 130:10466–10467. doi:10.1021/ja803015m
- Moore GF, Hamburger M, Kodis G et al (2010) Effects of protonation state on a tyrosine–histidine bioinspired redox mediator. *J Phys Chem B* 114:14450–14457. doi:10.1021/jp101592m
- Müller P, Li X-P, Niyogi KK (2001) Non-photochemical quenching: a response to excess light energy. *Plant Physiol* 125:1558–1566. doi:10.1104/pp.125.4.1558
- Rappaport F, Diner BA (2008) Primary photochemistry and energetics leading to the oxidation of the (Mn)₄Ca cluster and to the

- evolution of molecular oxygen in Photosystem II. *Coord Chem Rev* 252:259–272. doi:[10.1016/j.ccr.2007.07.016](https://doi.org/10.1016/j.ccr.2007.07.016)
- Rockström J, Steffen W, Noone K et al (2009) A safe operating space for humanity. *Nature* 461:472–475. doi:[10.1038/461472a](https://doi.org/10.1038/461472a)
- Seta P, Bienvenue E, Moore AL et al (1985) Photodriven transmembrane charge separation and electron transfer by a carotenoporphyrin–quinone triad. *Nature* 316:653–655. doi:[10.1038/316653a0](https://doi.org/10.1038/316653a0)
- Sherman BD, Pillai S, Kodis G et al (2011) A porphyrin-stabilized iridium oxide water oxidation catalyst. *Can J Chem* 89:152–157. doi:[10.1139/V10-118](https://doi.org/10.1139/V10-118)
- Sorensen BS (2010) *Renewable energy, fourth edition: physics, engineering, environmental impacts, economics & planning*. Academic Press, Oxford
- Steinberg-Yfrach G, Liddell PA, Hung SC et al (1997) Conversion of light energy to proton potential in liposomes by artificial photosynthetic reaction centres. *Nature* 385:239–241
- Steinberg-Yfrach G, Rigaud JL, Durantini EN et al (1998) Light-driven production of ATP catalysed by F₀F₁-ATP synthase in an artificial photosynthetic membrane. *Nature* 392:479–482. doi:[10.1038/33116](https://doi.org/10.1038/33116)
- Straight SD, Kodis G, Terazono Y et al (2008) Self-regulation of photoinduced electron transfer by a molecular nonlinear transducer. *Nat Nanotechnol* 3:280–283. doi:[10.1038/nnano.2008.97](https://doi.org/10.1038/nnano.2008.97)
- Terazono Y, Kodis G, Liddell PA et al (2009) Multiantenna artificial photosynthetic reaction center complex. *J Phys Chem B* 113:7147–7155. doi:[10.1021/jp900835s](https://doi.org/10.1021/jp900835s)
- Wee T-L, Sherman BD, Gust D et al (2011) Photochemical synthesis of a water oxidation catalyst based on cobalt nanostructures. *J Am Chem Soc* 133:16742–16745. doi:[10.1021/ja206280g](https://doi.org/10.1021/ja206280g)
- Youngblood WJ, Lee S-HA, Kobayashi Y et al (2009) Photoassisted overall water splitting in a visible light-absorbing dye-sensitized photoelectrochemical cell. *J Am Chem Soc* 131:926–927. doi:[10.1021/ja809108y](https://doi.org/10.1021/ja809108y)
- Zhao Y, Swierk JR, Megiatto JD et al (2012) Improving the efficiency of water splitting in dye-sensitized solar cells by using a biomimetic electron transfer mediator. *Proc Natl Acad Sci USA*. doi:[10.1073/pnas.1118339109](https://doi.org/10.1073/pnas.1118339109)

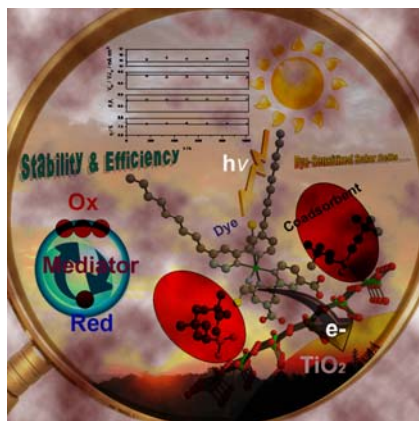
This paper is published as part of a *Dalton Transactions* themed issue on:

Solar Energy Conversion

Guest Editor Villy Sundström

Lund University, Sweden

Published in [issue 45, 2009 of *Dalton Transactions*](#)



Images reproduced with permission of Michael Grätzel

Articles published in this issue include:

PERSPECTIVES:

[Introducing a dark reaction to photochemistry –](#)

[Photocatalytic hydrogen from \[FeFe\]hydrogenase active site model complexes](#)

Sascha Ott and Reiner Lomoth, *Dalton Trans.*, 2009, DOI: [10.1039/b911129h](#)

[Recombinant and *in vitro* expression systems for hydrogenases: New frontiers in basic and applied studies for biological and synthetic H₂ production](#)

Michael Seibert, Katherine Brown, Carrie Eckert, Christine English and Paul King, *Dalton Trans.*, 2009, DOI: [10.1039/b913426n](#)

[Solar energy conversion in a photoelectrochemical biofuel cell](#)

Thomas Moore, Devens Gust, Michael Hambourger, Gerdenis Kodis, Ana Moore and Gary F. Moore, *Dalton Trans.*, 2009 DOI: [10.1039/b912170f](#)

[Transcription regulation of the cyanobacterial bidirectional Hox-hydrogenase](#)

Peter Lindblad and Paulo Oliveira, *Dalton Trans.*, 2009 DOI: [10.1039/b908593a](#)

[How algae produce hydrogen – News from the photosynthetic hydrogenase](#)

Thomas Happe and Sven T. Stripp, *Dalton Trans.*, 2009 DOI: [10.1039/b916246a](#)

Visit the *Dalton Transactions* website for more cutting-edge inorganic and organometallic research
www.rsc.org/dalton

Solar energy conversion in a photoelectrochemical biofuel cell

Michael Hambourger, Gerdenis Kodis, Michael D. Vaughn, Gary F. Moore, Devens Gust,* Ana L. Moore* and Thomas A. Moore*

Received 22nd June 2009, Accepted 22nd September 2009

First published as an Advance Article on the web 15th October 2009

DOI: 10.1039/b912170f

A photoelectrochemical biofuel cell has been developed which incorporates aspects of both an enzymatic biofuel cell and a dye-sensitized solar cell. Photon absorption at a porphyrin-sensitized *n*-type semiconductor electrode gives rise to a charge-separated state. Electrons and holes are shuttled to appropriate cathodic and anodic catalysts, respectively, allowing the production of electricity, or a reduced fuel, *via* the photochemical oxidation of a biomass-derived substrate. The operation of this device is reviewed. The use of alternate anodic redox mediators provides insight regarding loss mechanisms in the device. Design strategies for enhanced performance are discussed.

Introduction

Organisms use enzymatic catalysts to carry out the chemical transformations essential for optimizing the forward transfer of genes. Enzymes possess well-organized, three-dimensional architectures selected to precisely stabilize the transition state of a reaction, while controlling numerous factors including electron and proton motion, the reactivity of intermediates, the binding and release of substrate(s) and product(s), and the local dielectric environment. The tight control of these parameters is responsible for the successful operation of enzymes. *In vivo*, these catalysts are capable of self-assembly and self-repair, allowing such 'soft' materials to constitute remarkably robust catalytic systems. Moreover, enzymes typically operate under mild conditions, using earth-abundant materials, yet catalyze chemical reactions with high efficiency. Some of these reactions, such as water oxidation,

carbon-carbon bond formation/scission, the redox chemistry of N₂, CO₂ reduction, *etc.* continue to offer challenges in the design of human-engineered catalysts for sustainable energy production and use. These many remarkable features of enzymes make them attractive targets for study and emulation. Over the past several years, we have investigated the *in vitro* coupling of redox enzymes to photochemically-generated oxidizing and reducing equivalents in a hybrid photoelectrochemical biofuel cell.¹⁻⁵ This device combines aspects of both enzymatic biofuel cells⁶⁻¹³ and dye-sensitized solar cells.¹⁴⁻¹⁸

In a conventional enzymatic biofuel cell, a biologically-derived fuel is oxidized *in vitro* by enzyme catalysts, with the electrons liberated during this process collected at an electrode and transferred to an external circuit.^{8,11,12} These electrons flow to a cathode, where biological or inorganic catalysts facilitate the reduction of an appropriate oxidant. Consequently, a portion of the chemical energy stored in the biofuel (ultimately solar energy converted by photosynthesis) is converted into electrical energy during the controlled oxidation. Molecular oxygen typically serves as the terminal oxidant, and biofuel cells thus represent a closed fuel

Center for Bioenergy and Photosynthesis, and Department of Chemistry and Biochemistry, Arizona State University, Tempe, Arizona, 85287-1604, USA. E-mail: tmoore@asu.edu; Fax: 001 (480) 965-2747; Tel: 001 (480) 965-3461



Michael Hambourger

Michael Hambourger received his PhD in 2008 from Arizona State University. He is currently an Assistant Professor at Appalachian State University, in Boone, NC. Hambourger maintains interests in research and education as they relate to environmentally responsible energy systems. His research is focused on electrocatalysis and the coupling of single electron photochemical events to multi-electron catalytic reactions.



Gerdenis Kodis

Gerdenis Kodis graduated from Vilnius University (1993) and received his PhD in physics from the Institute of Physics, Lithuania, in 1999. He is currently Research Assistant Professor in the Department of Chemistry and Biochemistry, Arizona State University. His research interests focus on studies of energy and electron transfer in artificial systems, mimicking processes in natural photosynthesis, conjugated polymers, and photochromic supramolecular systems.

cycle. Electrons liberated from water during photosynthesis (and stored in the biofuel) recombine with molecular oxygen (in the biofuel cell) to form water and release a fraction of the solar energy that was initially responsible for formation of the biofuel.¹⁹ Due to the high specificity of enzymes, enzymatic biofuel cells have the potential to operate without membrane separation of the anodic and cathodic solutions.^{20,21} Maximum power densities are generally in the 10^{-6} to 10^{-3} W cm⁻² range,⁸ making enzymatic biofuel cells capable of powering small electronic devices and especially promising as implantable power sources for electrical devices *in vivo*.^{7,21}

In contrast, dye-sensitized solar cells (DSSCs) are capable of converting solar to electrical energy without the intermediate storage of energy/electrons in the chemical bonds of a biological molecule. DSSCs rely upon the sensitization of a semiconductor by a monolayer of dye molecules adsorbed at the semiconductor/electrolyte interface. High surface area, porous semiconductor electrodes are typically used.^{14,22} As only a single-monolayer of dyes in direct contact with the semiconductor is competent for photo-induced electron transfer, the high surface area allows

for drastically improved light harvesting. Most typically an *n*-type semiconductor is used, although DSSCs have also been developed using *p*-type semiconductors.²³ For a sensitized *n*-type semiconductor, the absorption of light by an adsorbed dye molecule gives rise to an excited state of the dye. Due to the electronic coupling between the dye and the semiconductor, as well as the high density of states near the semiconductor conduction band edge, the excited state predominantly decays by ultra-fast electron transfer to the semiconductor,²⁴⁻²⁷ giving rise to a Dye⁺/Semiconductor⁻ charge-separated state. The oxidized dye molecule is reduced by an electron donor in the electrolyte. The injected electron migrates to an underlying transparent conductive oxide (TCO) electrode and travels through an external circuit to a counter electrode. At this cathode, the electron recombines with the oxidized form of the electron donor in the electrolyte. The result is a photoinduced cyclic electron flow, with no net chemical transformation occurring. Over the years, DSSCs have received considerable attention as a low-cost photovoltaic technology,¹⁶ with solar energy conversion efficiencies in excess of 11% reported.²⁸



Gary F. Moore

Gary F. Moore received his PhD (in 2009) from Arizona State University, where he was a National Science Foundation fellow. He is currently working with the Green Energy Consortium at Yale University, New Haven, Connecticut, USA, as The Camille and Henry Dreyfus Foundation Postdoctoral Fellow with the research groups of Gary W. Brudvig, Robert H. Crabtree, Victor S. Batista and Charles A. Schmuttenmaer.



Devens Gust

Devens Gust is a Foundation Professor in the Arizona State University Department of Chemistry and Biochemistry, and Director of the Energy Frontier Research Center for Bio-Inspired Solar Fuel Production.



Ana L. Moore

Ana L. Moore is a Professor in the Arizona State University Department of Chemistry and Biochemistry and team leader in the Center for Bio-Inspired Solar Fuel Production.



Thomas A. Moore

Thomas A. Moore is a Professor in the Arizona State University Department of Chemistry and Biochemistry, and Director of the ASU Bioenergy and Photosynthesis Center.

The photoelectrochemical biofuel cell incorporates aspects of both enzymatic biofuel cells and dye-sensitized solar cells (Fig. 1). The system relies upon charge separation at a porphyrin-sensitized *n*-type semiconductor photoanode, in close analogy with DSSCs. Following photoinduced charge separation, the porphyrin radical cation is reduced by β -nicotinamide adenine dinucleotide (NADH) or by β -nicotinamide adenine dinucleotide phosphate (NADPH) in the aqueous anodic solution, ultimately generating the oxidized form of the mediator, NAD(P)^+ , after two electron transfers to the photoanode. In turn, NAD(P)^+ serves as a substrate for dehydroge-

nase enzymes in the anodic solution, with the enzymatic oxidation of a biofuel leading to the regeneration of NAD(P)H . The enzyme catalyzed, and NAD(P) mediated, electron transfers between the biofuel and the photoanode are reminiscent of enzymatic biofuel cell operation.¹³ However, a larger open-circuit voltage is theoretically achievable in the photoelectrochemical biofuel cell because the photochemical step raises the energy of electrons entering the external circuit at the anode.¹ Unlike traditional DSSCs, the extraction of electrons from the biomass-derived substrate permits the photoelectrochemical biofuel cell to operate with linear electron flow from anode to cathode. This linear electron flow permits the production of either electricity or an energy rich fuel depending upon the chosen cathodic reaction. The energy for this process is provided both by incident photons and the solar energy stored in the chemical bonds of the biomass substrate.⁴ The study of this device provides insight regarding the constraints of coupling redox enzymes to oxidizing and reducing equivalents in a photochemical system.

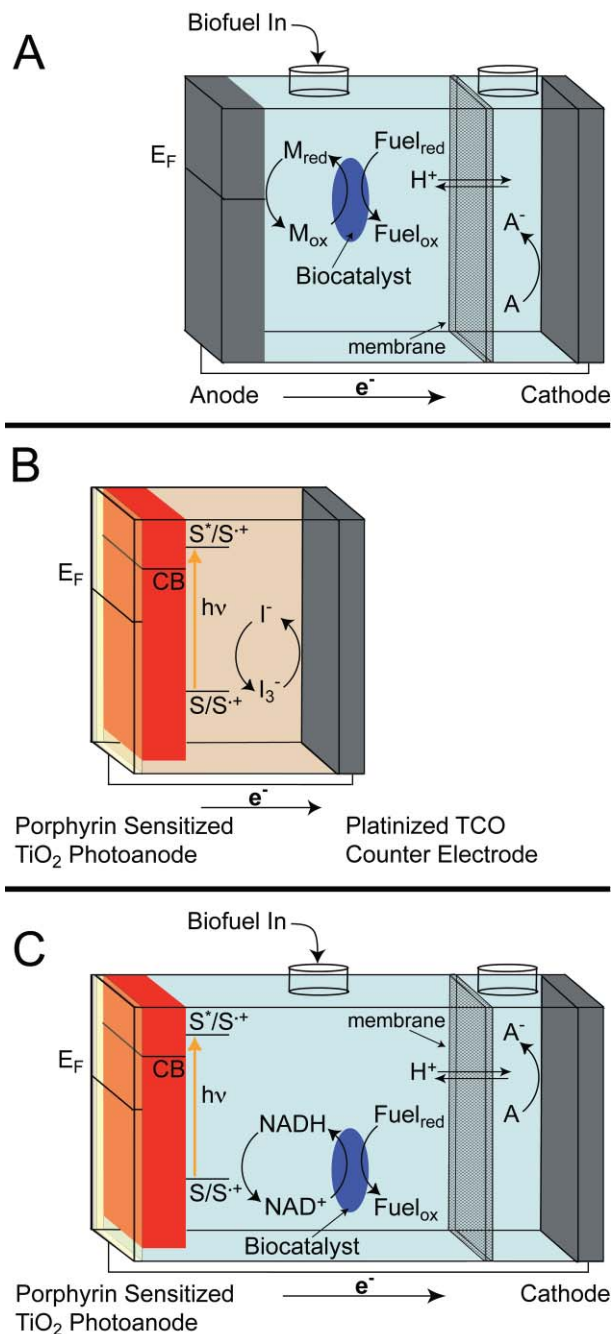


Fig. 1 Schematic representations of (a) an enzymatic biofuel cell, (b) a dye-sensitized solar cell, and (c) the photoelectrochemical biofuel cell. The operation of these devices is as described in the text.

Electricity generation in the photoelectrochemical biofuel cell

As initially conceived, the photoelectrochemical biofuel cell involved a monolayer of 5-(4-carboxyphenyl)-10,15,20-tris(4-methylphenyl)porphyrin (P) adsorbed to a high surface area SnO_2 layer deposited on a TCO electrode.¹ This photoanode was bathed in an aqueous solution containing an equilibrated mixture of NAD(P)^+ , an appropriate dehydrogenase enzyme and a biofuel substrate. Illumination with actinic photons resulted in the oxidation of NAD(P)H , thereby providing the NAD(P)^+ for further oxidation of the biofuel *via* the dehydrogenase enzyme in solution. When wired to a $\text{Hg}/\text{Hg}_2\text{SO}_4$ cathode (bathed in saturated K_2SO_4), the open-circuit voltage was 0.75 V. The performance was comparable with either methanol, ethanol, glucose, or glucose-6-phosphate as the biofuel, demonstrating that the reduction of the porphyrin radical cation depends only upon the availability of NAD(P)H , regardless of its source. With appropriate enzymes, methanol was oxidized in three steps (six electrons) to CO_2 , ethanol was oxidized in two steps (four electrons) to acetate, glucose was oxidized in one step (two electrons) to gluconolactone, and glucose-6-phosphate was oxidized in two steps (four electrons) to ribulose-5-phosphate and CO_2 .

Subsequent work using a TiO_2 -based photoanode demonstrated a higher open-circuit voltage upon illumination (1.10 V), under otherwise comparable conditions with glucose as the biofuel.² The increased open-circuit voltage is readily accounted for by the more negative reduction potential of TiO_2 as compared to SnO_2 . In aqueous solution, both SnO_2 and TiO_2 exhibit a Nernstian 59 mV per pH unit dependence of their reduction potential. At pH 8.0, the TiO_2 conduction band operates near -0.63 V vs. NHE,²⁹⁻³¹ while the SnO_2 conduction band operates near 0.04 V vs. NHE.^{15,32,33} The open-circuit voltage of the cell reflects the difference in potential between the semiconductor quasi-Fermi level upon illumination and the redox couple at the cathode. The increase in the open-circuit voltage with TiO_2 (0.35 V greater than with SnO_2) is less than the estimated difference in the flatband potentials of TiO_2 and SnO_2 (0.67 V difference), suggesting the presence of trap-states positive of the TiO_2 conduction band edge. In turn, the

photoelectrochemical biofuel cell is relatively insensitive to the choice of cathode, operating well with either a Hg/Hg₂Cl₂ (bathed in saturated KCl, *i.e.* a saturated calomel electrode) or a Ag/AgCl (bathed in saturated KCl) cathode, in addition to the Hg/Hg₂SO₄ cathode. However, the open-circuit voltage upon illumination is greater with the higher potential Hg/Hg₂SO₄ cathode.

The photoelectrochemical biofuel cell gives negligible current in the dark, and its function is therefore dependent upon the photochemical formation of a charge-separated state (as described above in the discussion of dye-sensitized solar cells). Fig. 2 shows transient absorption data for a porphyrin-sensitized TiO₂ photoanode in aerobic buffer (pH 8). In the spectrum (inset), the Q-band bleach and the broad absorbance from 650 to 750 nm are consistent with P⁺, validating the formation of the P⁺/TiO₂⁻ charge-separated state. The formation of the charge-separated state occurs within the pulse-width of the laser (4.8 ns) and cannot be resolved. This is consistent with literature reports of porphyrin-sensitized TiO₂ DSSCs,³⁴ which show electron injection into TiO₂ occurring on a sub-picosecond timescale.³⁵ In the absence of NADH, the charge-separated state exhibits a bi-exponential decay, with lifetimes of 7.0 μs (48%) and 54.2 μs (52%), with P⁺ eventually decaying to the ground state *via* charge recombination. The addition of NADH decreases the P⁺ lifetime to 2.0 μs (39%) and 17.1 μs (61%) in the presence of 1 mM NADH, and to 850 ns (44%) and 7.8 μs (56%) in the presence of 2 mM NADH. In the presence of 3 mM NADH, the fast component could not be resolved and the data were fit to a single exponential decay with a 7.5 μs lifetime. These results demonstrate that the charge-separated state is sufficiently long-lived to allow hole transfer to NADH in solution, thereby generating NAD⁺ used for the enzymatic oxidation of the biofuel.

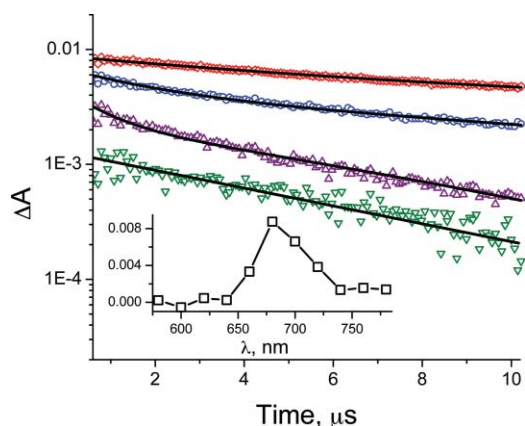


Fig. 2 Transient absorption kinetic traces (650 nm excitation and 700 nm probe) recorded for a porphyrin-sensitized TiO₂ photoanode in aerobic 0.25 M Tris, 0.10 M KCl (pH 8.0) buffer, under open-circuit conditions at 20 °C. Kinetic traces were recorded in the presence of 0 mM (◇), 1 mM (○), 2 mM (△), and 3 mM (▽) NADH. The spectrum (inset) was recorded in the absence of NADH, 4 μs after 532 nm laser excitation.

Due to quenching of the porphyrin radical cation *via* electron transfer from NAD(P)H, the injected electrons in the TiO₂ conduction band are free to migrate through an external circuit to a cathode, thereby generating electricity. The choice of cathode influences the open-circuit voltage of the cell. Fig. 3 compares the performance of the photoelectrochemical biofuel cell operating

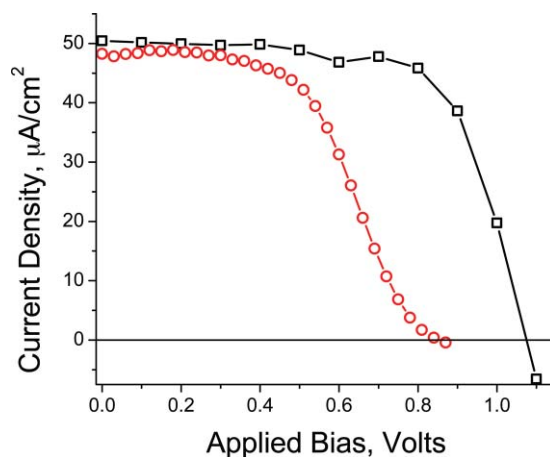


Fig. 3 Current–voltage curves recorded for a porphyrin-sensitized TiO₂ photoanode (operating in 0.25 M TES, 0.10 M KCl (pH 7.8) buffer, with 5 mM NADH present); wired to either a Hg/Hg₂SO₄ (saturated K₂SO₄) cathode (□), or an oxygen reducing platinum cathode (○) operating in 0.25 M TES, 0.10 M KCl (pH 7.8) buffer. Both traces were recorded under monochromatic illumination (520 nm, ~0.9 mW cm⁻²). The higher open-circuit voltage observed with the Hg/Hg₂SO₄ cathode is attributable to this cathode operating at a more positive potential.

with either a Hg/Hg₂SO₄ or a high surface area platinum (oxygen reducing) cathode. The short-circuit currents are comparable, as both cathodes have sufficient area to avoid limiting the current density. The open-circuit voltage is higher with the mercury cathode ($V_{oc} = 1.08$ V) than with the platinum cathode ($V_{oc} = 0.85$ V), indicating that the Hg/Hg₂SO₄ electrode operates at a higher potential than the oxygen-reducing cathode. Interestingly, the Hg/Hg₂SO₄ (saturated K₂SO₄) electrode operates at 0.64 V vs. NHE, while thermodynamically the reduction of oxygen to water occurs at 0.77 V vs. NHE (pH 7.8).³⁶ Hence the data in Fig. 3 suggest that oxygen reduction occurs on the particulate platinum cathode at an overpotential of ~0.36 V.

From an operational perspective, the oxygen reducing cathode offers a significant advantage over the Hg/Hg₂SO₄ cathode since molecular oxygen can be obtained from the ambient environment and the reduction of O₂, presumably to water,¹ is environmentally benign. Fig. 4 shows an action spectrum of the photoelectrochemical biofuel cell operating with an oxygen-reducing cathode. The incident-photon-to-current-efficiency (IPCE) closely tracks the light harvesting efficiency (LHE) of the photoanode across the spectrum, which, in turn, is consistent with the absorption spectrum of the porphyrin sensitizer dye in solution. This observation indicates that photon absorption by porphyrin-sensitizer dyes initiates the photoinduced electron transfers which gives rise to photocurrent and photovoltage.

Hydrogen generation in the photoelectrochemical biofuel cell

When the TiO₂-based photoelectrochemical biofuel cell operates with the same platinum cathode, but under anaerobic conditions, oxygen reduction is no longer feasible at the cathode. Under these conditions hydrogen production becomes the relevant cathodic process.³ Even though hydrogen production is readily observed, the cell is not operating at optimum current and voltage. A V_{oc}

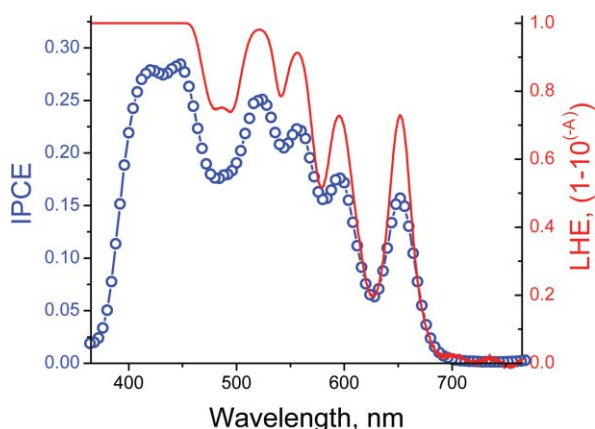


Fig. 4 Action spectrum of a porphyrin-sensitized TiO_2 photoanode (operating in 0.25 M TES, 0.10 M KCl (pH 7.8) buffer, with 8 mM NADH present), wired to an oxygen reducing platinum cathode operating in 0.25 M TES, 0.10 M KCl (pH 7.8) buffer. The incident photon to current efficiency (IPCE, \circ) maxima correspond to the light harvesting efficiency (LHE, —) maxima of the photoanode. The light intensity was $\sim 1 \text{ mW cm}^{-2}$ for each wavelength investigated.

of about 0.15 V was measured with the cathode equilibrated with hydrogen at ambient pressure (hydrogen bubbles forming just before V_{oc} was measured). Driving hydrogen production at this voltage implies that the cell was operating below P_{max} . Nevertheless, under these conditions energy as electromotive force is transformed and stored in the chemical bond of the molecular hydrogen product; any additional use of the electromotive force would result in a decrease in the rate of hydrogen production. Because H_2 is among the most reducing species encountered in biology,³⁷ hydrogen production can be viewed as a proxy for the synthesis of other high value fuels, such as reduced carbon compounds. Moreover, the hydrogen itself could serve as a fuel or be used in the production of liquid fuels.³⁸

Fig. 5 demonstrates the photocurrent and hydrogen product (detected by gas chromatography) generated upon illumination of a porphyrin-sensitized TiO_2 photoanode wired to an anaerobic platinum cathode. Comparison of these two quantities reveals a Faradaic efficiency for hydrogen production of 92%. This value is a lower estimate, as some hydrogen product may have escaped the cathodic cell prior to detection. Hydrogen generation in the photoelectrochemical biofuel cell has been experimentally demonstrated with electrons derived from NADH as a sacrificial donor, or with the NAD^+ product being recycled *via* the oxidation of glucose or ethanol.^{3,4} Our previous use of methanol or glucose-6-phosphate as the electron source for electricity generation¹ suggests that the photoelectrochemical biofuel cell is capable of reforming a wide-array of biofuel substrates into hydrogen gas.

Operation of the cell using a solution of ethanol and acetaldehyde, against a platinum cathode under 1 atm of hydrogen, has demonstrated that the photochemical formation of hydrogen proceeds even when the process would be endergonic in the dark ($E_{\text{cell, dark}} \approx -0.18 \text{ V}$).⁴ Thus, some fraction of the incident photon energy can be stored in the hydrogen product during the photochemical reformation process. Moreover, the energy contained in chemical bonds of the initial biofuel itself ultimately represents converted solar energy. Since the photoelectrochemical biofuel cell is able to drive the $\text{NAD(P)}^+/\text{NAD(P)H}$ couple highly

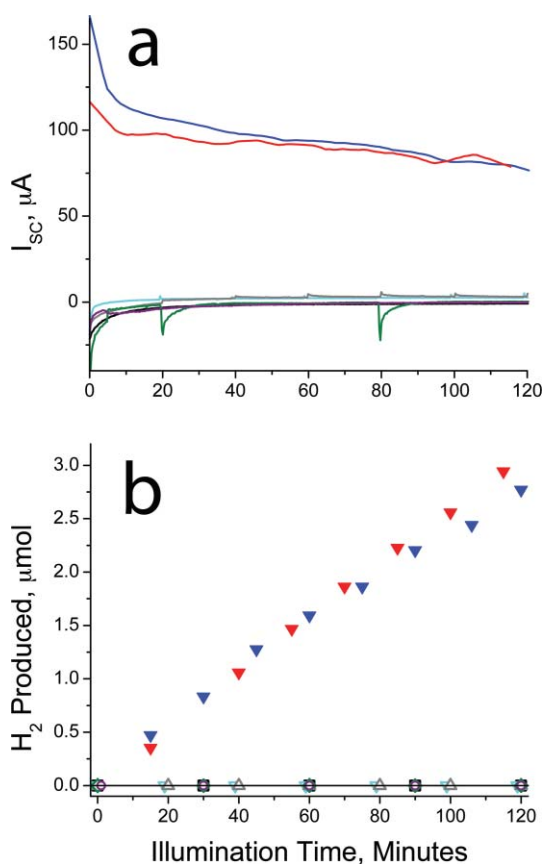


Fig. 5 (a) The short-circuit photocurrent and (b) the hydrogen product detected by gas chromatography, for a porphyrin-sensitized TiO_2 photoanode wired to an anaerobic platinum cathode; both operating in 0.25 M Tris, 0.10 M KCl (pH 8.0) buffer. The anodic solution contained 4 mM NADH (\blacktriangle , \blacktriangledown), or 4 mM NAD^+ /glucose dehydrogenase (GDH)/100 mM glucose (\blacktriangleleft , \blacktriangleright). Controls are shown for the NAD^+ /GDH/glucose solution operated in the absence of light (\square , \square), porphyrin (\blacktriangleleft , \blacktriangleright), glucose (\blacktriangleleft , \blacktriangleright), GDH (\blacktriangleleft , \blacktriangleright) or NAD^+ , GDH, and glucose (\blacktriangleleft , \blacktriangleright). Broadband illumination was provided by a filtered Xe arc lamp ($460 \text{ nm} < \lambda < 1100 \text{ nm}$, $\sim 130 \text{ mW cm}^{-2}$). Data represented in this figure were originally reported in reference 3.

oxidizing,⁴ there is the possibility of oxidizing low-value waste biomass while storing solar energy in a high-value reduced fuel (hydrogen).

Following our preliminary report of hydrogen production at an anaerobic platinum cathode,³ this process was subsequently demonstrated using an [FeFe]-hydrogenase as the cathodic catalyst in the photoelectrochemical biofuel cell.⁵ The selected [FeFe]-hydrogenase, HydA, from *Clostridium acetobutylicum* (*CaHydA*) is a soluble 65.4 kD homolog of the *Clostridium pasteurianum* [FeFe]-hydrogenase CpI (70% identity),³⁹ for which crystal structures have been determined.^{40,41} Mature *CaHydA* contains the [6Fe-6S] H-cluster active site,^{42,43} and is predicted to contain an additional [2Fe-2S] and three [4Fe-4S] accessory clusters based on homology with CpI. *CaHydA* catalyzes the reversible interconversion between protons and molecular hydrogen with a high turnover rate and specificity.^{42,44} Due to inhibition by molecular oxygen, *CaHydA* must be handled under strictly anaerobic conditions to preserve the catalytic activity.^{44,45} In recent years, considerable

attention has been devoted to understanding and addressing the oxygen sensitivity of hydrogenase enzymes.⁴⁵⁻⁵³

In vivo, the accessory iron-sulfur clusters of *CaHydA* likely serve as a pathway for electron transfers between external redox partners and the active site. When non-specifically adsorbed to a carbon electrode *in vitro*, one or more populations of the enzyme are favorably oriented for direct electron transfers between the electrode and the active site, presumably *via* the same accessory iron-sulfur clusters. The electrochemical characterization of *CaHydA* has previously been reported.^{5,52} The interested reader is also referred to many excellent reviews of direct enzyme electrochemistry, especially pertaining to hydrogenase electrodes.^{49,54-58} For the purpose of this discussion, it is sufficient to note that both hydrogenase and platinum behave as reversible catalysts for hydrogen production, operating with little overpotential.^{59,60} The current densities for *CaHydA* electrodes are ~35% of those obtained at platinum.⁵ With sufficient cathodic catalyst present, both platinum and hydrogenase cathodes can maximize the current response of the photoanode. Hence the photocurrent is nearly indistinguishable in the two cases (Fig. 6).

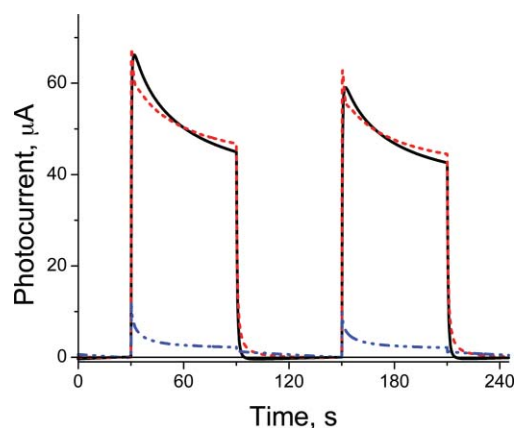


Fig. 6 The short-circuit photocurrent for a porphyrin-sensitized TiO₂ photoanode wired to a carbon felt (---•---•---), carbon felt/*CaHydA* (—), or platinum foil (---) cathode; operating in 0.10 M sodium phosphate (pH 7.0) buffer, with 10 mM NADH in the anodic solution. In each case, the electrochemically active surface area of the cathode was ~3.5 cm². Illumination was provided by a light-emitting diode ($\lambda_{\text{max}} = 520$ nm, peak width at half-height = 50 nm, 3 mW cm⁻²). For the carbon felt/*CaHydA* electrode, an adsorbed hydrogenase film was formed and excess hydrogenase (1.6 U mL⁻¹) was then maintained in the cathodic solution. Data represented in this figure were originally reported in reference 5.

The rate of hydrogen production (*i.e.* current) in the anaerobic photoelectrochemical biofuel cell is a function of the pressure of hydrogen gas above the cathodic solution, an effect demonstrated in Fig. 7. In this experiment the black *I-V* curve was recorded for the photoanode under potentiostatic control in a standard three-electrode configuration. As the potential of the underlying TCO electrode is swept to more negative values, the electron density in this conductor, and in the TiO₂ film, increases. Increased occupancy of sub-bandgap and conduction band states of the TiO₂ film has been correlated with increased rates of charge recombination at the photoanode surface.^{61,62} Charge recombination can occur between conduction band electrons and an oxidized species at the photoanode surface. As the number of conduction band electrons

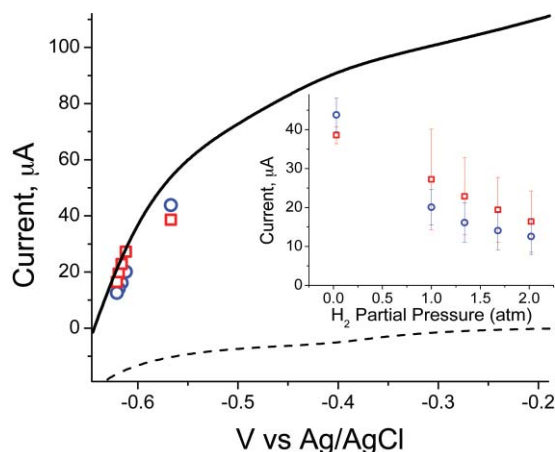


Fig. 7 Data demonstrating the effect of hydrogen ‘back-pressure’ on the photoelectrochemical biofuel cell performance. A current–voltage profile ($v = 5$ mV s⁻¹) was obtained for a porphyrin-sensitized TiO₂ photoanode under illumination ($\lambda = 520$ nm, 3 mW cm⁻²) (—), and in the dark (---), under potentiostatic control with a platinum counter electrode and Ag/AgCl (saturated KCl) reference. Overlaid on the *I-V* profile is the short-circuit current obtained for the photoanode wired to a carbon felt/*CaHydA* (□), or platinum (○) cathode in a two-electrode configuration, under 520 nm illumination (3 mW cm⁻²) with the pressure of H₂ above the cathodic solution stepped to higher values. The inset shows the raw hydrogen ‘back-pressure’ data before being converted to *V* vs. Ag/AgCl by the Nernst equation. The conditions of the experiment are the same as those in Fig. 6. Data represented in this figure were originally reported in reference 5.

increases, so too does the probability of charge recombination. At a sufficiently negative potential, corresponding to the quasi-Fermi level of the TiO₂ under illumination, the current goes to zero. This potential defines a limit for the cathodic redox couples that are accessible in the photoelectrochemical biofuel cell under a given illumination regime.

Fig. 7 also contains data points measured in a two-electrode configuration for the photoelectrochemical biofuel cell operating at short circuit with either an anaerobic platinum or hydrogenase cathode under varying partial pressures of hydrogen gas. The good agreement between data obtained under potentiostatic control and at short-circuit in the photoelectrochemical biofuel cell confirms that both platinum and hydrogenase are reversible catalysts operating at the formal potential of the solution. Increasing the partial pressure of hydrogen shifts the formal potential of the H⁺/H₂ redox couple to more negative values, having the same effect as applying a more negative bias to the photoanode in isolation. Moreover, even at low hydrogen partial pressures, hydrogen production in the photoelectrochemical biofuel cell requires the photoanode to operate near the ohmic tail of the *I-V* curve (far left of curve). Consequently, the accumulation of the hydrogen product has a deleterious influence on the overall rate of hydrogen production. The impact of the position of hydrogen production on the *I-V* curve of the photoanode is also evident in the low IPCE values observed under anaerobic conditions,⁴ relative to those when operating for electricity generation under aerobic conditions (Fig. 4). Overall, the data in Fig. 7 demonstrate that the photoelectrochemical biofuel cell is able to pressurize hydrogen in excess of two atmospheres. The data also suggest that a redesign of the photoanode with a sensitizer dye/semiconductor pair that

could operate at more negative potentials could substantially improve the rate of hydrogen production.

Influence of the anodic redox mediator

The use of NAD(P)H as the anodic redox mediator in the photoelectrochemical biofuel cell has important implications for the performance. This is especially true at the low potentials required for hydrogen production. To better understand the role played by the anodic redox mediator, the performance of the cell was compared when using NADH or 1,4-hydroquinone as a sacrificial electron donor in the anodic solution.⁴ The operation of a dye-sensitized photoanode from an aqueous solution of hydroquinone has been reported in the literature.⁶³⁻⁶⁵ For our initial comparison, the photocurrent response of a porphyrin-sensitized TiO₂ photoanode was monitored as a function of the NADH or 1,4-hydroquinone concentration, with the photoanode poised at 0 V vs. SCE. In both cases, the photocurrent was essentially saturated in the presence of 10 mM of the sacrificial electron donor (Fig. 8). The maximum photocurrent with 1,4-hydroquinone was approximately 25% of that achieved with NADH.

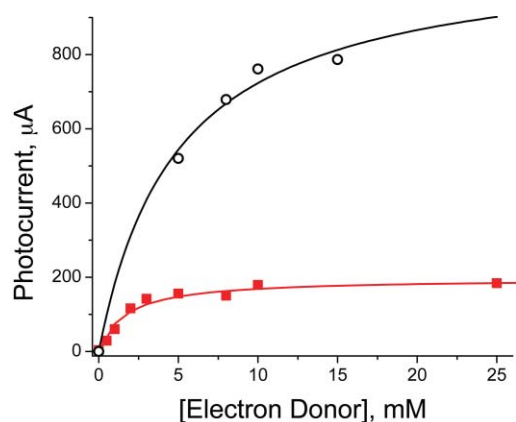


Fig. 8 Photocurrent for a porphyrin-sensitized photoanode, operating at 0 V vs. SCE, as a function of the concentration of the sacrificial electron donor: NADH (○), or 1,4-hydroquinone (■). For NADH, the photoanode operated in 0.25 M Tris, 0.1 M KCl (pH 8.0) buffer. For hydroquinone, the photoanode operated in 0.1 M KCl, 25 mM each of citrate, phosphate, borate (pH 6.0) buffer. Broadband illumination (460 nm < λ < 1100 nm, ~ 30 mW cm⁻²) was provided by a filtered Xe arc lamp. Data represented in this figure were originally reported in reference 4.

As shown in Fig. 9, the NADH and 1,4-hydroquinone electron donors were further tested with increasing concentrations of the oxidized form of the redox couple (NAD⁺ or 1,4-benzoquinone, respectively) present in the anodic solution. If the oxidized redox mediator participates in electron recombination reactions at the photoanode surface, then the photocurrent would be expected to decrease with increasing concentrations of the oxidized species. With NADH as the electron donor, an increased concentration of NAD⁺ had little effect on the current. With hydroquinone as the electron donor, the current decreased exponentially with increasing concentrations of benzoquinone. Additionally, Fig. 10 displays the photocurrent for the photoanode operating with the TCO electrode poised at different potentials under potentiostatic control, with either NADH or 1,4-hydroquinone used

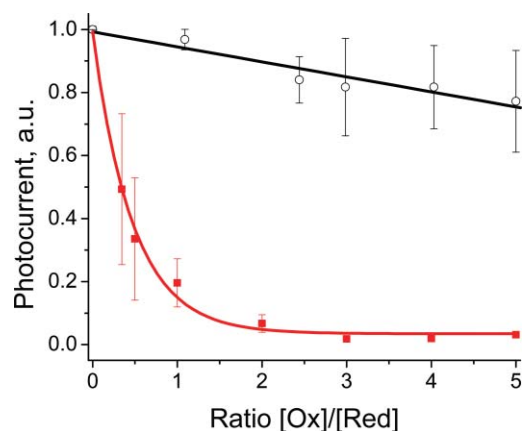


Fig. 9 Photocurrent for a porphyrin-sensitized TiO₂ photoanode, operating at 0 V vs. SCE with NAD⁺/NADH (○) or benzoquinone/hydroquinone (■), as a function of the [Oxidized]/[Reduced] ratio for the sacrificial electron donor in the anodic solution. The conditions of the experiment are generally the same as those in Fig. 8. For the present data, the [Reduced] was held constant at 10 mM, while the [Oxidized] was varied from 0 to 50 mM. The data are the average of three replicates, with error bars representing one standard deviation. Data represented in this figure were originally reported in reference 4.

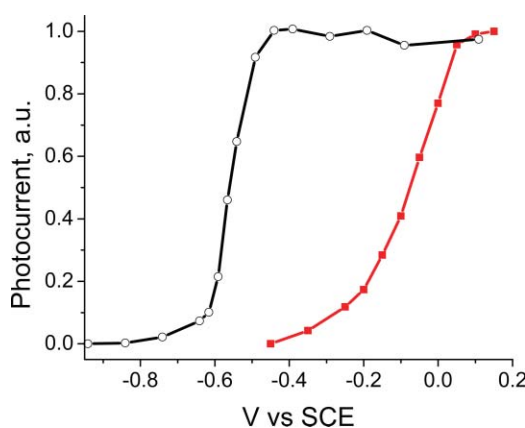


Fig. 10 Photocurrent for a porphyrin-sensitized TiO₂ photoanode operating under potentiostatic control, with a platinum counter electrode and Ag/AgCl (saturated KCl) reference. The photocurrent was recorded after 1 minute of illumination at each potential step using NADH (○) or hydroquinone (■) as the sacrificial electron donor. The experimental conditions are the same as those reported in Fig. 8, with a 10 mM concentration of either NADH or 1,4-hydroquinone in the anodic solution. Data represented in this figure were originally reported in reference 4.

as a sacrificial electron donor. As is the case for Fig. 7, at a sufficiently negative potential, charge recombination dominates the performance and the photocurrent falls to zero. The point of zero current determines the most reducing cathodic redox couple accessible to the photoanode. This value is almost 400 mV more negative when using NADH as compared to 1,4-hydroquinone. In Figs. 8, 9, and 10 the anodic solution was buffered at pH 8 for work with NADH, and at pH 6 for work with 1,4-hydroquinone, due to the different pH optima for these redox mediators. Recalling that the potential of the TiO₂ conduction band shifts negative by 59 mV for each unit increase in pH, the two pH unit increase when working with NADH can account for no more than a 120 mV difference in the point of zero current. Hence, Fig. 10 reveals that

the photoanode is capable of operating at lower potentials when using the NAD^+/NADH couple as the anodic redox mediator.

The preceding data indicate that both the photocurrent (Fig. 8) and photovoltage (Fig. 10) decrease when operating the photoelectrochemical biofuel cell with the benzoquinone/hydroquinone redox couple. Further, the cell performance is quite dependent upon the ratio of oxidized to reduced quinone in the anodic solution (Fig. 9). These observations are consistent with facile charge recombination between injected electrons and oxidized quinone species, but not oxidized NAD species. In biology, both NAD(P)H and hydroquinone operate as two electron carriers. However, NAD(P) redox chemistry occurs by a concerted two-electron/one-proton (*i.e.* hydride) transfer, while quinone redox chemistry can occur as two discrete one-electron steps. In the photoelectrochemical biofuel cell, both electron donation to the oxidized porphyrin radical cation and charge recombination to the oxidized redox mediator are one-electron processes. Mechanistic consideration of the one-electron redox chemistry of NAD(P)H and hydroquinone provides insight regarding charge recombination in the photoelectrochemical biofuel cell.

The single-electron oxidation of NADH has been reported to occur at 0.93 V vs. NHE.⁶⁶ The $\text{NADH}^{+\cdot}$ radical cation product is highly acidic ($\text{p}K_{\text{a}} \sim -4$) and spontaneously deprotonates to form the neutral NAD^{\cdot} radical.⁶⁷ In turn, the NAD^{\cdot} radical is highly reducing and undergoes a single-electron oxidation at potentials positive of -0.92 V vs. NHE.⁶⁶ Due to instability of the NAD^{\cdot} radical, the intermediate can decay by the following: (1) disproportionation of two NAD^{\cdot} radicals to form one NADH and one NAD^+ molecule, (2) dimerization followed by oxidation of the dimer, (3) electron donation to a second porphyrin radical cation, or (4) direct electron donation to the TiO_2 conduction band or TCO electrode.^{67,68} The low reduction potential for the $\text{NAD}^+/\text{NAD}^{\cdot}$ transition imposes a large activation barrier for charge recombination *via* the single-electron reduction of NAD^+ in solution. Further, the high acidity of the $\text{NADH}^{+\cdot}$ radical cation disfavors the one-electron/one-proton reduction of NAD^{\cdot} to NADH . Consequently, the oxidized NAD species are not suitable electron acceptors for charge recombination at the photoanode surface.

In comparison, for 1,4-hydroquinone ($\text{p}K_{\text{a}1} = 9.9$, $\text{p}K_{\text{a}2} = 11.4$)^{69,70} in a buffered pH 6.0 solution, the single-electron oxidation occurs at 0.58 V vs. NHE.⁷¹ Since the doubly-protonated semiquinone radical ($\text{QH}_2^{\cdot+}$) has an estimated $\text{p}K_{\text{a}} \approx -1$,^{72,73} and the singly-protonated semiquinone radical (QH^{\cdot}) has a $\text{p}K_{\text{a}}$ of 4.1,⁷¹ the one-electron oxidation of 1,4-hydroquinone primarily leads to the formation of the semiquinone radical anion ($\text{Q}^{\cdot-}$) under the indicated solution conditions. At pH 6.0, the semiquinone radical anion can subsequently undergo a single-electron oxidation ($E_{\text{m}} = 0.10$ V vs. NHE) to yield the final 1,4-benzoquinone product.⁷¹ Once again, instability of the semiquinone intermediate allows for the disproportionation of two semiquinones to form hydroquinone and benzoquinone, with the equilibrium strongly disfavoring the semiquinone in aqueous solution near neutral pH.⁷¹⁻⁷⁴ Based upon these considerations, both the semiquinone and quinone oxidation products are thermodynamically poised to accept electrons from either the TiO_2 conduction band or exposed regions of the TCO substrate.

These thermodynamic and kinetic properties of the NAD^+/NADH and benzoquinone/hydroquinone redox media-

tors highlight favorable aspects of using the NAD^+/NADH couple in the photoelectrochemical biofuel cell. An initial observation is that the NAD^{\cdot} intermediate is sufficiently reducing to donate an electron directly to either the TiO_2 conduction band or to exposed regions of the TCO substrate. This process has not been experimentally verified, and would be in competition with the rapid disproportionation of NAD^{\cdot} and $\text{NADH}^{+\cdot}$ radicals.⁶⁸ Nevertheless, the possibility of a secondary dark electron transfer to the electrode cannot be discounted. Such a process could allow up to two electrons to transverse the external circuit per absorbed photon, thus offering the intriguing possibility of obtaining a quantum yield greater than unity. In contrast, with hydroquinone as the electron donor, the oxidized quinone intermediates are not sufficiently reducing to donate directly an electron to either the TiO_2 conduction band or to the TCO electrode when producing hydrogen. A second point is that NAD^+ and NAD^{\cdot} are unfavorable acceptors for charge recombination reactions. Consequently, with NADH as the anodic mediator, charge recombination to solution⁷⁵ is essentially eliminated, although charge recombination with oxidized sensitizer dyes^{16,17,76} remains a potential source of inefficiency. In contrast, the oxidized quinone species are suitable acceptors for charge recombination. This recombination process is the most likely explanation for the different performance observed with NADH and hydroquinone in Figs. 8, 9 and 10.

Design strategies

The data in Figs. 7 and 10 reveal that operation of the photoanode at the negative potentials required for hydrogen production limits the quantum efficiency of the photochemical process. Using the $\text{NAD(P)}^+/\text{NAD(P)H}$ redox couple, a large activation energy precludes electron recombination to oxidized NAD(P) species as a loss mechanism. Despite this irreversible oxidation at the photoanode surface, the ultimate NAD(P)^+ product is readily reduced by dehydrogenase enzymes in the anodic solution. This rectifying behavior of the $\text{NAD(P)}^+/\text{NAD(P)H}$ electron relay is an important factor in the successful operation of the photoelectrochemical biofuel cell for hydrogen production. In broad strokes, the kinetics with this mediator are reminiscent of the behavior of the I_3^-/I^- redox couple in traditional DSSCs, in which I^- oxidation is kinetically facile relative to the reduction of oxidized iodine species at the semiconductor/dye/electrolyte interface.⁷⁷ The decreased performance of the photoelectrochemical biofuel cell operating with the benzoquinone/hydroquinone relay is then analogous to the poor performance of traditional DSSCs operating with more reversible redox mediators, such as the ferrocenium/ferrocene couple.⁷⁷

However, the advantages of using the $\text{NAD(P)}^+/\text{NAD(P)H}$ redox mediator are balanced against the high overpotential required for NAD(P)H oxidation in the photoelectrochemical biofuel cell. Thermodynamically, the $\text{NAD(P)}^+/\text{NAD(P)H}$ couple operates as a two-electron mediator with a formal potential of -0.35 V vs. NHE at pH 8.0. Nonetheless, in order to oxidize NAD(P)H *via* two stepwise one-electron transfers, the dye radical cation must operate near 1 V vs. NHE. Consequently, much of the 1.9 eV free base-porphyrin excitation energy serves to supply the overpotential to make NAD(P)H oxidation proceed at a sufficiently rapid rate. This requirement for a highly oxidizing sensitizer dye constrains

modification of the semiconductor/sensitizer dye pair used in the photoelectrochemical biofuel cell.

An intriguing approach towards improving the cell performance would be to modify the photoanode such that electrons are shuttled from the biofuel to the porphyrin radical cation at close to the thermodynamic potential of the NAD(P)⁺/NAD(P)H redox couple (−0.35 V vs. NHE at pH 8). For this purpose, the dehydrogenase enzyme active site could be wired directly to the porphyrin radical cation,^{78,79} eliminating the need for the NAD(P) electron relay. Alternatively, a second redox enzyme (such as diaphorase)⁸⁰ could be wired to the porphyrin radical cation, mediating electron transfers from NAD(P)H. In both of these cases, the enzymatic oxidation of biomass could occur as a concerted multi-electron process operating near the thermodynamic potential of the NAD(P)⁺/NAD(P)H couple, with redox cofactors within the enzyme stabilizing the intermediates that would inevitably form when interfaced with a one-electron photochemical oxidant.

Such modification of the photoelectrochemical biofuel cell would allow considerable flexibility in the choice of a semiconductor/sensitizer dye pair. In particular, for the 5-(4-carboxyphenyl)-10,15,20-tris(4-methylphenyl)porphyrin used as the sensitizer in the work described, the P⁺/P transition occurs at 1.23 V vs. NHE. Coupled with a 1.9 eV excitation energy, this places the P⁺/P* transition of the first excited-singlet state of the dye at −0.67 V vs. NHE, only slightly negative of the TiO₂ conduction band at pH 8.0 (~−0.63 V vs. NHE).³ In turn, the TiO₂ conduction band is only modestly more reducing than the H⁺/H₂ redox couple, contributing to the decreased performance of the cell under hydrogen backpressure (Fig. 7). However, if NAD(P)H could be oxidized closer to −0.35 V vs. NHE, then highly reducing semiconductor/sensitizer dye pairs could be explored; such as naphthalocyanines⁸¹ in conjunction with semiconductors such as SrTiO₃ or ZrO₂-doped TiO₂.^{32,82–84} The outcomes of this modification would be enhanced driving force for hydrogen production and a decreased likelihood of charge recombination at a given partial pressure of hydrogen. Further, with the dye radical cation needing to operate only modestly positive of −0.35 V vs. NHE, considerably less excitation-energy would be required to inject electrons into an *n*-type semiconductor at a sufficiently reducing potential to produce hydrogen with a good yield. Consequently, far-red light absorbers could be studied that make better utilization of the solar spectrum, possibly increasing the energy conversion efficiency of the device.^{19,85}

At present, the energy conversion efficiency of the un-optimized photoelectrochemical biofuel cell is understandably low, given the large overpotential for NAD(P)H oxidation, the high probability of charge recombination as hydrogen accumulates above the cathodic solution, and the high energy content of the initial biofuel substrate. Further, the *in vitro* enzyme catalysts in the photoelectrochemical biofuel cell have demonstrated good stability in our laboratory;¹ the long-term (*t* > 48 h) stability of these enzymes has not been investigated. Nevertheless, the fact that the energy stored in the biofuel ultimately represents solar energy converted *via* natural photosynthesis, and the versatility of the photoelectrochemical biofuel cell to oxidize a variety of biomass substrates,¹ leaves open the possibility of photochemically reforming low-value waste materials into a high-value reduced fuel. However, as currently demonstrated, there is only a modest energy enhancement during the oxidation of biofuels, such as

ethanol, with the concomitant production of a more reduced fuel such as hydrogen. Therefore, a second approach to improving the overall cell performance would be to extract electrons from a less energy-rich substrate, such as *via* the oxidation of water to molecular oxygen.^{86,87}

Part of the initial motivation for testing the benzoquinone/hydroquinone redox relay in the photoelectrochemical biofuel cell was the hope of coupling the photoanode to the natural water-oxidizing enzyme, photosystem II, in a hybrid, dual-photosystem device. Such a situation has been previously reported,⁸⁸ with photosystem II particles immobilized at the surface of a Ru-polypyridyl dye-sensitized TiO₂ photoanode, and an electrical connection between the two photosystems established *via* a soluble benzoquinone/hydroquinone electron relay. The dissimilar spectral coverage of the Ru-based dye and the photosystem II chlorophylls allowed these dual photosystems to be placed in optical series, increasing the utilization of incident solar photons. Nonetheless, this system was only demonstrated to operate with the photoanode poised at a modestly oxidizing potential (0.2 V vs. SCE), and the immobilization of PSII was required to achieve sufficiently high local concentrations of hydroquinone at the photoanode surface.⁸⁸ Our data suggest that charge recombination would significantly diminish the performance of such a device if wired to a low potential cathode for the photochemical splitting of water to O₂ and H₂. In contrast, hydrogen production has been reported for a dye-sensitized photoanode wired to a platinum cathode, using hydroquinone as a sacrificial electron donor.⁸⁹ In that work, the hydrogen product was not quantified and the photocurrent observed with hydroquinone was substantially less than with iodide as the electron donor. Nonetheless, the report of hydrogen production in a DSSC from hydroquinone suggests that control of the interfacial dynamics to minimize the access of oxidized species in solution to the TiO₂ surface and underlying TCO conductor is a possible means of minimizing the charge recombination reactions that were observed in our work.^{17,77,90}

One design strategy for the production of a high-value reduced fuel from water would involve dual photosystems, tuned to operate at reducing and oxidizing potentials, respectively. The reducing photosystem could be designed as described above, such as with a naphthalocyanine dye and Zr-doped TiO₂ semiconductor. The oxidizing photosystem could be designed with a higher-potential SnO₂ semiconductor, a highly oxidizing dye,⁹¹ and an appropriate water oxidation catalyst.^{92,93} Interfacing these two photosystems using an appropriate redox relay, such as the I₃[−]/I[−] couple, could result in a dual photosystem device capable of photochemical fuel production with electrons derived from water as a substrate.^{15,94–96} The ramifications of such a device could be relevant to addressing societal energy concerns.^{19,97–99}

Conclusions

The photoelectrochemical biofuel cell couples the photochemical formation of a charge-separated state to the enzyme-catalyzed oxidation of a biomass-derived substrate and the production of a reduced fuel. Alternatively, the photochemical step can be coupled to a high potential cathode for electricity generation. The energy to drive these processes is provided both by incident photons and by solar energy stored in the chemical bonds of the biomass-derived substrate. Operation of the photoelectrochemical biofuel cell with

a platinum cathode demonstrates that the transition between electricity generation and hydrogen formation can be controlled by the presence of oxygen in the cathodic solution. Comparison of the performance using either NAD(P)⁺/NAD(P)H or benzoquinone/hydroquinone as the anodic redox mediator demonstrates the influence of charge recombination in the photoelectrochemical biofuel cell, and highlights the suitability of the NAD(P)⁺/NAD(P)H couple for operation with a low-potential cathode. Appropriate redesign of the photoelectrochemical biofuel cell could in principle allow high rates of photochemical fuel production using either low-value, waste biomass or water as the anodic electron donor.

References

- 1 L. de la Garza, G. Jeong, P. A. Liddell, T. Sotomura, T. A. Moore, A. L. Moore and D. Gust, *J. Phys. Chem. B*, 2003, **107**, 10252–10260.
- 2 A. Brune, G. Jeong, P. A. Liddell, T. Sotomura, T. A. Moore, A. L. Moore and D. Gust, *Langmuir*, 2004, **20**, 8366–8371.
- 3 M. Hambourger, A. Brune, D. Gust, A. L. Moore and T. A. Moore, *Photochem. Photobiol.*, 2005, **81**, 1015–1020.
- 4 M. Hambourger, P. A. Liddell, D. Gust, A. L. Moore and T. A. Moore, *Photochem. Photobiol. Sci.*, 2007, **6**, 431–437.
- 5 M. Hambourger, M. Gervaldo, D. Svedruzic, P. W. King, D. Gust, M. Ghirardi, A. L. Moore and T. A. Moore, *J. Am. Chem. Soc.*, 2008, **130**, 2015–2022.
- 6 E. Katz, A. N. Shipway and I. Willner, in *Handbook of Fuel Cells - Fundamentals, Technology and Applications*, eds. W. Vielstich, H. A. Gasteiger and A. Lamm, John Wiley and Sons, Ltd, London, 2003, vol. 1, p. 355.
- 7 S. C. Barton, J. Gallaway and P. Atanassov, *Chem. Rev.*, 2004, **104**, 4867–4886.
- 8 R. A. Bullen, T. C. Arnot, J. B. Lakeman and F. C. Walsh, *Biosens. Bioelectron.*, 2006, **21**, 2015–2045.
- 9 F. Davis and S. P. J. Higson, *Biosens. Bioelectron.*, 2007, **22**, 1224–1235.
- 10 M. J. Cooney, V. Svoboda, C. Lau, G. Martin and S. D. Minteer, *Energy Environ. Sci.*, 2008, **1**, 320–337.
- 11 J. A. Cracknell, K. A. Vincent and F. A. Armstrong, *Chem. Rev.*, 2008, **108**, 2439–2461.
- 12 M. J. Moehlenbrock and S. D. Minteer, *Chem. Soc. Rev.*, 2008, **37**, 1188–1196.
- 13 I. Willner, Y. -M. Yan, B. Willner and R. Tel-Vered, *Fuel Cells*, 2009, **9**, 7–24.
- 14 A. Hagfeldt and M. Grätzel, *Chem. Rev.*, 1995, **95**, 49–68.
- 15 M. Grätzel, *Nature*, 2001, **414**, 338–344.
- 16 M. Grätzel, *Inorg. Chem.*, 2005, **44**, 6841–6851.
- 17 J. R. Durrant, S. A. Haque and E. Palomares, *Chem. Commun.*, 2006, 3279–3289.
- 18 S. Ardo and G. J. Meyer, *Chem. Soc. Rev.*, 2009, **38**, 115–164.
- 19 M. Hambourger, G. F. Moore, D. M. Kramer, D. Gust, A. L. Moore and T. A. Moore, *Chem. Soc. Rev.*, 2009, **38**, 25–35.
- 20 N. Mano, F. Mao and A. Heller, *J. Am. Chem. Soc.*, 2003, **125**, 6588–6594.
- 21 A. Heller, *Phys. Chem. Chem. Phys.*, 2004, **6**, 209–216.
- 22 B. O'Regan and M. Grätzel, *Nature*, 1991, **353**, 737–739.
- 23 M. Borgström, E. Blart, G. Boschloo, E. Mukhtar, A. Hagfeldt, L. Hammarström and F. Odobel, *J. Phys. Chem. B*, 2005, **109**, 22928–22934.
- 24 J. B. Asbury, E. Hao, Y. Wang and T. Lian, *J. Phys. Chem. B*, 2000, **104**, 11957–11964.
- 25 J. B. Asbury, E. Hao, Y. Wang, H. N. Ghosh and T. Lian, *J. Phys. Chem. B*, 2001, **105**, 4545–4557.
- 26 N. A. Anderson and T. Lian, *Coord. Chem. Rev.*, 2004, **248**, 1231–1246.
- 27 S. A. Haque, S. Handa, K. Peter, E. Palomares, M. Thelakkat and J. R. Durrant, *Angew. Chem., Int. Ed.*, 2005, **44**, 5740–5744.
- 28 M. K. Nazeeruddin, F. D. Angelis, S. Fantacci, A. Selloni, G. Viscardi, P. Liska, S. Ito, B. Takeru and M. Grätzel, *J. Am. Chem. Soc.*, 2005, **127**, 16835–16847.
- 29 G. Rothenberger, D. Fitzmaurice and M. Grätzel, *J. Phys. Chem.*, 1992, **96**, 5983–5986.
- 30 G. Redmond and D. Fitzmaurice, *J. Phys. Chem.*, 1993, **97**, 1426–1430.
- 31 L. A. Lyon and J. T. Hupp, *J. Phys. Chem. B*, 1999, **103**, 4623–4628.
- 32 H. P. Maruska and A. K. Ghosh, *Sol. Energy*, 1978, **20**, 443–458.
- 33 I. Bedja, S. Hotchandani and P. V. Kamat, *J. Phys. Chem.*, 1994, **98**, 4133–4140.
- 34 D. F. Watson, A. Marton, A. M. Stux and G. J. Meyer, *J. Phys. Chem. B*, 2004, **108**, 11680–11688.
- 35 Y. Tachibana, S. A. Haque, I. P. Mercer, J. R. Durrant and D. R. Klug, *J. Phys. Chem. B*, 2000, **104**, 1198–1205.
- 36 A. J. Bard and L. R. Faulkner, *Electrochemical methods: fundamentals and applications*, 2nd edn., John Wiley and Sons, Inc., 2001.
- 37 R. A. Alberty, *Arch. Biochem. Biophys.*, 2001, **389**, 94–109.
- 38 G. W. Huber, S. Iborra and A. Corma, *Chem. Rev.*, 2006, **106**, 4044–4098.
- 39 P. W. King, M. C. Posewitz, M. L. Ghirardi and M. Seibert, *J. Bacteriol.*, 2006, **188**, 2163–2172.
- 40 J. W. Peters, W. N. Lanzilotta, B. J. Lemon and L. C. Seefeldt, *Science*, 1998, **282**, 1853–1858.
- 41 A. S. Pandey, T. V. Harris, L. J. Giles, J. W. Peters and R. K. Szilagy, *J. Am. Chem. Soc.*, 2008, **130**, 4533–4540.
- 42 L. Girbal, G. von Abendroth, M. Winkler, P. M. C. Benton, I. Meynial-Salles, C. Croux, J. W. Peters, T. Happe and P. Soucaille, *Appl. Environ. Microbiol.*, 2005, **71**, 2777–2781.
- 43 S. E. McGlynn, S. S. Ruebush, A. Naumov, L. E. Nagy, A. Dubini, P. W. King, J. B. Broderick, M. C. Posewitz and J. W. Peters, *JBIC, J. Biol. Inorg. Chem.*, 2007, **12**, 443–447.
- 44 M. W. Adams and L. E. Mortenson, *J. Biol. Chem.*, 1984, **259**, 7045–7055.
- 45 M. L. Ghirardi, M. C. Posewitz, P.-C. Maness, A. Dubini, J. Yu and M. Seibert, *Annu. Rev. Plant Biol.*, 2007, **58**, 71–91.
- 46 T. Burgdorf, O. Lenz, T. Buhrke, E. von der Linden, A. K. Jones, S. P. J. Albracht and B. Friedrich, *J. Mol. Microbiol. Biotechnol.*, 2005, **10**, 181–196.
- 47 S. C. E. Tosatto, S. Toppo, D. Carbonera, G. M. Giacometti and P. Costantini, *Int. J. Hydrogen Energy*, 2008, **33**, 570–578.
- 48 J. A. Cracknell, K. A. Vincent, M. Ludwig, O. Lenz, B. Friedrich and F. A. Armstrong, *J. Am. Chem. Soc.*, 2008, **130**, 424–425.
- 49 K. A. Vincent, A. Parkin and F. A. Armstrong, *Chem. Rev.*, 2007, **107**, 4366–4413.
- 50 G. Goldet, A. F. Wait, J. A. Cracknell, K. A. Vincent, M. Ludwig, O. Lenz, B. Friedrich and F. A. Armstrong, *J. Am. Chem. Soc.*, 2008, **130**, 11106–11113.
- 51 A. Parkin, G. Goldet, C. Cavazza, J. C. Fontecilla-Camps and F. A. Armstrong, *J. Am. Chem. Soc.*, 2008, **130**, 13410–13416.
- 52 C. Baffert, M. Demuez, L. Cournac, B. Burlat, B. Guigliarelli, P. Bertrand, L. Girbal and C. Léger, *Angew. Chem., Int. Ed.*, 2008, **47**, 2052–2054.
- 53 E. Reisner, J. C. Fontecilla-Camps and F. A. Armstrong, *Chem. Commun.*, 2009, 550–552.
- 54 F. A. Armstrong, J. N. Butts and A. Sucheta, *Methods Enzymol.*, 1993, **227**, 479–500.
- 55 F. A. Armstrong, H. A. Heering and J. Hirst, *Chem. Soc. Rev.*, 1997, **26**, 169–179.
- 56 J. Hirst, *Biochim. Biophys. Acta, Bioenerg.*, 2006, **1757**, 225–239.
- 57 C. Léger and P. Bertrand, *Chem. Rev.*, 2008, **108**, 2379–2438.
- 58 F. A. Armstrong, N. A. Belsey, J. A. Cracknell, G. Goldet, A. Parkin, E. Reisner, K. A. Vincent and A. F. Wait, *Chem. Soc. Rev.*, 2009, **38**, 36–51.
- 59 A. K. Jones, E. Sillery, S. P. J. Albracht and F. A. Armstrong, *Chem. Commun.*, 2002, 866–867.
- 60 A. A. Karyakin, S. V. Morozov, E. E. Karyakina, N. A. Zorin, V. V. Pereygin and S. Cosnier, *Biochem. Soc. Trans.*, 2005, **33**, 73–75.
- 61 S. A. Haque, Y. Tachibana, D. R. Klug and J. R. Durrant, *J. Phys. Chem. B*, 1998, **102**, 1745–1749.
- 62 S. A. Haque, Y. Tachibana, R. L. Willis, J. E. Moser, M. Grätzel, D. R. Klug and J. R. Durrant, *J. Phys. Chem. B*, 2000, **104**, 538–547.
- 63 N. Vlachopoulos, P. Liska, A. J. McEvoy and M. Grätzel, *Surf. Sci.*, 1987, **189–190**, 823–831.
- 64 N. Vlachopoulos, P. Liska, J. Augustynski and M. Grätzel, *J. Am. Chem. Soc.*, 1988, **110**, 1216–1220.
- 65 M. Gervaldo, F. Fungo, E. N. Durantini, J. J. Silber, L. Sereno and L. Otero, *J. Phys. Chem. B*, 2005, **109**, 20953–20962.
- 66 B. W. Carlson, L. L. Miller, P. Neta and J. Grodkowski, *J. Am. Chem. Soc.*, 1984, **106**, 7233–7239.
- 67 F. M. Martens and J. W. Verhoeven, *Recl. Trav. Chim. Pays-Bas*, 1981, **100**, 228–236.

- 68 J. Moiroux and P. J. Elving, *J. Am. Chem. Soc.*, 1980, **102**, 6533–6538.
- 69 C. A. Bishop and L. K. Tong, *J. Am. Chem. Soc.*, 1965, **87**, 501–505.
- 70 S. I. Bailey and L. M. Ritchie, *Electrochim. Acta*, 1985, **30**, 3–12.
- 71 Y. A. Ilan, G. Czapski and D. Meisel, *Biochim. Biophys. Acta, Bioenerg.*, 1976, **430**, 209–224.
- 72 E. Laviron, *J. Electroanal. Chem. Interfacial Electrochem.*, 1984, **169**, 29–46.
- 73 R. A. Binstead, M. E. McGuire, A. Dovletoglou, W. K. Seok, L. E. Roecker and T. J. Meyer, *J. Am. Chem. Soc.*, 1992, **114**, 173–186.
- 74 V. A. Roginsky, L. M. Pisarenko, W. Bors and C. Michel, *J. Chem. Soc., Perkin Trans. 2*, 1999, 871–876.
- 75 S. Y. Huang, G. Schlichthörl, A. J. Nozik, M. Grätzel and A. J. Frank, *J. Phys. Chem. B*, 1997, **101**, 2576–2582.
- 76 J. R. Durrant, S. A. Haque and E. Palomares, *Coord. Chem. Rev.*, 2004, **248**, 1247–1257.
- 77 B. A. Gregg, F. Pichot, S. Ferrere and C. L. Fields, *J. Phys. Chem. B*, 2001, **105**, 1422–1429.
- 78 I. Willner and E. Katz, *Angew. Chem., Int. Ed.*, 2000, **39**, 1180–1218.
- 79 I. Willner and B. Willner, *Coord. Chem. Rev.*, 2003, **245**, 139–151.
- 80 G. T. R. Palmore, H. Bertschy, S. H. Bergens and G. M. Whitesides, *J. Electroanal. Chem.*, 1998, **443**, 155–161.
- 81 X. Y. Li, N. J. Long, J. N. Clifford, C. J. Campbell and J. R. Durrant, *New J. Chem.*, 2002, **26**, 1076–1080.
- 82 J. M. Bolts and M. S. Wrighton, *J. Phys. Chem.*, 1976, **80**, 2641–2645.
- 83 F. Lenzmann, J. Krueger, S. Burnside, K. Brooks, M. Grätzel, D. Gal, S. Rühle and D. Cahen, *J. Phys. Chem. B*, 2001, **105**, 6347–6352.
- 84 M. Dürr, S. Rosselli, A. Yasuda and G. Nelles, *J. Phys. Chem. B*, 2006, **110**, 21899–21902.
- 85 M. C. Hanna and A. J. Nozik, *J. Appl. Phys.*, 2006, **100**, 074510.
- 86 A. J. Bard and M. A. Fox, *Acc. Chem. Res.*, 1995, **28**, 141–145.
- 87 C. Herrero, B. Lassalle-Kaiser, W. Leibl, A. W. Rutherford and A. Aukauloo, *Coord. Chem. Rev.*, 2008, **252**, 456–468.
- 88 K. K. Rao, D. O. Hall, N. Vlachopoulos, M. Grätzel, M. C. W. Evans and M. Seibert, *J. Photochem. Photobiol., B*, 1990, **5**, 379–389.
- 89 L. A. Gallagher, S. A. Serron, X. Wen, B. J. Hornstein, D. M. Dattelbaum, J. R. Schoonover and T. J. Meyer, *Inorg. Chem.*, 2005, **44**, 2089–2097.
- 90 L. Kavan and M. Grätzel, *Electrochim. Acta*, 1995, **40**, 643–652.
- 91 G. F. Moore, M. Hambourger, M. Gervaldo, O. G. Poluektov, T. Rajh, D. Gust, T. A. Moore and A. L. Moore, *J. Am. Chem. Soc.*, 2008, **130**, 10466–10467.
- 92 W. J. Youngblood, S.-H. A. Lee, Y. Kobayashi, E. A. Hernandez-Pagan, P. G. Hoertz, T. A. Moore, A. L. Moore, D. Gust and T. E. Mallouk, *J. Am. Chem. Soc.*, 2009, **131**, 926–927.
- 93 M. W. Kanan and D. G. Nocera, *Science*, 2008, **321**, 1072–1075.
- 94 M. Grätzel, *Cattech*, 1999, **3**, 3–17.
- 95 A. Duret and M. Grätzel, *J. Phys. Chem. B*, 2005, **109**, 17184–17191.
- 96 M. Grätzel, *Chem. Lett.*, 2005, **34**, 8–13.
- 97 N. S. Lewis and D. G. Nocera, *Proc. Natl. Acad. Sci. U. S. A.*, 2006, **103**, 15729–15735.
- 98 P. V. Kamat, *J. Phys. Chem. C*, 2007, **111**, 2834–2860.
- 99 W. Lubitz, E. J. Reijerse and J. Messinger, *Energy Environ. Sci.*, 2008, **1**, 15–31.

Hydrogen storage in liquid organic heterocycles

Robert H. Crabtree

Received 3rd April 2008, Accepted 13th May 2008

First published as an Advance Article on the web 11th June 2008

DOI: 10.1039/b805644g

Hydrogen storage in liquid organic heterocycles is feasible thermodynamically and is attractive in terms of simplicity, safety, scalability, heat management and economy, but extensive catalyst development is needed to bring it to fruition.

In his 1908 book, *Worlds in the Making*, Svante Arrhenius¹ expanded on his 1896 prediction that industrial CO₂ production would eventually raise average global temperature. Doubling atmospheric CO₂ would, he believed, cause a 4 °C rise, a value within the presently accepted range. Perhaps because he was writing from a cool northern city, however, he felt this rise would be a good thing.

We often hear lamentations that the coal stored up in the earth is wasted by the present generation without any thought of the future... We may find a kind of consolation that here, as in every other case, there is good mixed with the evil. By the influence of the increasing percentage of carbonic acid in the atmosphere, we may hope to enjoy ages with more equable and better climates, especially as regards the colder regions of the earth, ages when the earth will bring forth more abundant crops than at present, for the benefit of a rapidly propagating mankind.^{1a}

Few informed individuals still retain this optimistic view of climate change, now much more often considered deeply problematic.² Average energy consumption for the planet as a whole has been estimated at 2 kW h per person,³ more than 80% based on fossil fuel, leading to an injection of *ca.* 10¹³ kg of CO₂ per year into the atmosphere.

Efforts to alleviate CO₂ production confront several problems. Costs are obvious, prompt and local while benefits are putative, delayed and global. It can be little wonder that the research

budgets in this field are dwarfed by those for health and defense. As the reality of the situation sinks in and climate disruption becomes more obvious, climate change and alternative energy may well become the dominant scientific problems of the century.

While a number of technical solutions appear plausible in principle, the challenge of applying them on the required global scale is daunting. For instance, to take just one likely scenario, in a world based on nuclear power, transport would require either light, highly efficient storage batteries or else some transportable fuel that can be safely stored on board. In either case the principle is the same—electrical energy is stored in chemical form.

Taking a global view, transport is an increasingly energy-intensive area, particularly with China and India rapidly industrializing. Hydrogen has been suggested as a possible energy carrier using an internal combustion engine (ICE) or fuel cell for the motive power. Efficiency in an ICE is limited by the physics of the Carnot cycle to approximately 25% while fuel cells escape from this limitation and can have efficiencies above 50%.⁴ H₂ is currently generated mainly from fossil fuel with release of CO₂, so the relatively widespread demonstration transport vehicles, usually advertised as ‘green’, do not yet achieve the stated goal. Both nuclear-to-H₂ and solar-to-H₂ schemes have been proposed to remedy this defect. Assuming H₂ can be generated efficiently by a CO₂-free route or with CO₂ sequestration, very hard problems in themselves,^{5–7} we would next need a method for hydrogen storage in vehicles.

Numerous reports have treated this problem^{3,4,7,8} so it will only be necessary to summarize the major prior H₂ storage approaches. These are physical: (i) high pressure (HP) tanks; (ii) cryogenic methods; or chemical: (iii) reversible absorption in metal or main group hydrides; (iv) reversible absorption on solids; and (v) storage in the form of metals that can liberate H₂ from H₂O. Current plans for future vehicles employ one of three approaches, either (i), (ii) or (iii).

For a fuel-efficient automobile, 4–8 kg of H₂ need to be stored to match current consumer needs and expectations.^{3,4} High pressure tanks are heavy and voluminous and may pose practical problems. Just this month (Feb 2008) a major interstate highway in the writer’s state was closed down for the whole day as a result of an otherwise minor mishap without gas release involving a commercial vehicle carrying high pressure H₂. Nevertheless, this is a cheap and readily reversible storage method and it is available today.

Given the low critical temperature, 33 K, cryogenic storage requires very low temperatures, implying a large energy loss from

Yale University, Chemistry Department, 225 Prospect Street, P.O. Box 208107, New Haven, CT 06520-8107, USA. E-mail: robert.crabtree@yale.edu



Robert H. Crabtree

Educated at Oxford and Sussex Universities and CNRS Natural Products Institute in Paris. Now, a Professor of Chemistry at Yale, he works extensively on catalysis, both organometallic and bioinorganic. Appointed Dow lecturer at Berkeley, Sabatier Lecturer at Toulouse, and will be Osborn Lecturer at Strasbourg and Mond Lecturer in the UK. He has been awarded ACS and RSC prizes for organometallic chemistry.

the liquefaction step. Apart from the weight penalty of the cooling module, this method is not ideal for vehicles used only intermittently because energy input is constantly required to maintain cooling.

Chemical methods are advantageous in binding H_2 at ambient temperature and pressure but can suffer from lack of complete and easy reversibility. The H_2 release enthalpies that appear to be most appropriate for automobile H_2 storage lie in the range 15–25 kJ mol^{-1} and correspond to release temperatures in the range of 0–100 $^{\circ}\text{C}$. Carbon-based solids⁹ such as single walled nanotubes¹⁰ (SWNTs) or microporous metal–organic frameworks¹¹ have shown attractive performance in room temperature hydrogen absorption but the performance still needs to be much improved before practical application can be envisaged. Metal hydrides^{12,13} such as LaNi_5 , Mg_2Ni or MgH_2 have also been very extensively studied. Although they have many attractive properties, the fact that they tend to employ relatively high atomic weight elements means that few such metal hydrides are close to meeting the very ambitious criteria set by the US Department of Energy (DOE): 9% hydrogen by weight by 2015. For comparison, one H stored per C atom leads to a gravimetric capacity of 7.1% but LaNi_5H_6 stores only 1.37%.

This gravimetric criterion has focused attention on the light atoms of the Periodic Table, notably Li and B and on compounds that hold more than one H per non-hydrogen atom. One compound that fulfils both points is BH_3NH_3 (ammonia–borane, or AB)¹⁴ and related materials.¹⁵ From its molecular weight and polarity, AB would be a gas except for the strong proton–hydride interactions present in the solid (m pt, 109 $^{\circ}\text{C}$).¹⁶ If it were to lose all its H_2 (19.6% theoretical capacity) it would form boron nitride, an unpromising material for the regeneration step needed for any storage/release cycle.

Thermal H_2 release from BH_3NH_3 is straightforward, and catalytic methods can also be successfully applied. Acid-catalyzed, as well as transition metal-catalyzed release have recently been reported.¹⁴ Catalytic AB dehydrogenation can give $\text{BH}_3\text{NH}_2\text{BH}_2\text{NH}_3$, $(\text{H}_2\text{NBH}_2)_n$ ($n = 3, 5$), $(\text{HBNH})_3$ or $(\text{HBNH})_n$ polymer. The regeneration step is not at all straightforward, however.¹⁷

A related strategy based on light element salts involves borohydrides,^{18,19} amidoborates²⁰ or aluminohydrides. For example, Zuetel and coworkers have investigated LiBH_4 , a hydride salt containing 18 mass% of hydrogen. Hydrogen desorption was catalyzed with SiO_2 and 13.5 mass% of hydrogen was liberated over the range 200–350 $^{\circ}\text{C}$; LiBH_4 regeneration proved challenging, however.²¹ Bogdanovic and Schwickardi¹⁹ demonstrated reversible hydrogen storage with Ti-doped NaAlH_4 , where the Ti acts as the catalyst. The LiBH_4 – LiNH_2 system in which the principal phase present is $\text{Li}_4\text{BH}_4(\text{NH}_2)_3\text{F}$, has also been proposed.²²

Perhaps not sufficiently considered in current approaches is scalability. Any new technology would have to be applied on a vast scale to make any impact on global climate. Assuming a material having a 10% gravimetric capacity, 10^2 kg of material would plausibly be needed for each of an assumed 10^9 vehicles worldwide for a total of 10^{11} kg of storage material. On this basis, elements that are not available on this scale may be unrealistic candidates. According to the US Geological Survey Mineral Resources Program,²³ the 2007 world production values for

selected elements are: La, $< 1.6 \times 10^6$ kg; B, 9×10^8 kg; Ni, 1.6×10^9 kg; Mg, 4×10^9 kg; Li, 2.5×10^{10} kg. In other cases, the element or elements may be available in quantity but the challenges for production of such vast quantities of absorbent may have been underestimated. This does not detract from the scientific value of work on such materials, of course, particularly where new principles emerge.

Liquid storage materials and heat management strategy

Whatever the storage material, liquids have significant engineering advantages over solids. They can be readily pumped not just for distribution and delivery but also within the vehicle during operation. This means that instead of heating the whole storage tank, only a small aliquot would be pumped into the catalytic dehydrogenation chamber for heating to reaction temperature at any given time. This is also a safety consideration in a collision, where it would be undesirable to have a large mass of hot, reactive—perhaps even pyrophoric—material present in the vehicles involved. Once dehydrogenated, the spent storage material would pass back into the fuel tank and a partition would move across the tank to allow the spent material that is being pumped in to displace, but not mix with, the fresh material that is being pumped out. At the fuel station, the spent material would be off-loaded and the fresh material substituted in a similar manner. Trucks that deliver fresh material to the fuel stations would return the spent material for recharging with hydrogen. The liquid strategy also employs a simple, light fuel tank, as today, not a heavy duty tank capable of taking high pressure and temperature as would be needed if the whole storage bed had to be heated.

The properties of hydrogen make it most suitable for handling within commercial facilities by trained personnel. A liquid storage material thus has the further advantage that there would be no free hydrogen in the public sphere. H_2 has an exceptionally high diffusivity, leading to an enhanced risk from leaks. It can cause embrittlement of metals, generating greater potential for leaks and complicating the engineering. A hydrogen flame is essentially invisible thus presenting greater dangers than a flame from other fuels. As an illustration, a standard method of detecting H_2 flames is to advance cautiously with a piece of paper in an outstretched hand, the flame being located when the piece of paper begins to burn.

An even more compelling argument for the liquid strategy is its heat management benefits. When any storage material is hydrogenated, large amounts of heat are necessarily generated. If this happens in a solid bed of storage material, the exotherm will require dissipation by cooling while the vehicle stands at the fuelling station. Not only is this an energy loss to the global energy balance of the strategy, but it means filling the vehicle will be prolonged, and incompatible with the level of patience usually encountered among the driving public, as well as detracting from the profitability of the fuel station. If cooling is applied *via* refrigeration to speed the filling process, the energy input required would further degrade the energy balance of the system as a whole. This contrasts with the liquid strategy in which filling the vehicle takes no more time than today and involves no exotherm. If the hydrogenation step occurs in a commercial facility on a very

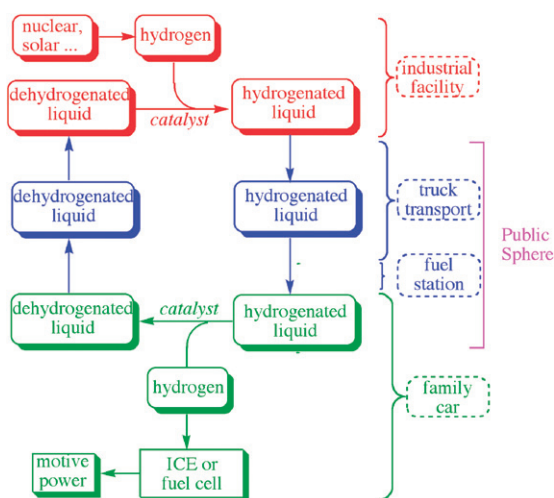


Fig. 1 The liquid strategy showing how the presence of free hydrogen is avoided in the public sphere. The exotherm of rehydrogenation of the spent storage material can also be more efficiently recovered if produced in a central facility on a large scale.

large scale, as in the liquid strategy, then the exotherm is produced in one place, where it can be at least partially recovered, rather than in fuel stations throughout the city where it will typically be lost. Fig. 1 illustrates the liquid strategy in more detail.

Organic heterocycle strategy

The possibility of storage of hydrogen in organic compounds has been widely excluded from consideration because reversible, low temperature H_2 release has not been thought feasible. For example, according to a standard review of the field.³

The second important criterion is reversibility of hydrogen uptake and release. This criterion excludes all covalent carbon hydrogen compounds as hydrogen is only released from carbon hydrogen compounds if they are heated to temperatures above 800 °C or if the carbon is oxidized.

While this was a plausible argument based on much of the data available at the time (2004), this analysis does not consider the twin possibilities of catalytic H_2 release and of chemical modification of the “carbon hydrogen compounds” to favor low temperature H_2 release.

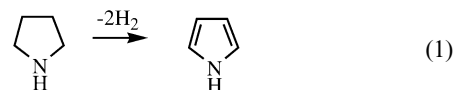
Catalysis was first considered for alkane–arene pairs, such as decalin–naphthalene, but the endothermicity of the release step is such that elevated temperatures are required for the thermodynamics to become favorable. Saito and coworkers²⁴ proposed ‘liquid film state’ conditions, a nonequilibrium technique which allows much higher hydrogen production rates than in a batch reaction. Similarly, a pulse-spray mode reactor has been adopted by Ichikawa and coworkers.²⁵ The highest rate, an impressive 3800 mmol g⁻¹ Pt min⁻¹, was obtained in the dehydrogenation of cyclohexane over Pt/alumite heated at 375 °C with a cyclohexane feed of 190 mmol min⁻¹ with 3.5 mmol pulses at 1.0 s intervals. A bimetallic Pt–Rh catalyst showed higher activity than a simple Pt catalyst on the same support.

The release temperatures are still rather high and it would be useful to lower the endothermicity of release and thus bring down the equilibrium release temperature.

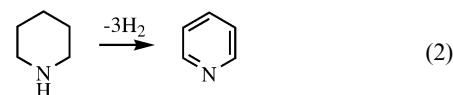
Taking the cyclohexane–benzene pair as a model, the endothermicity of H_2 release is such that a temperature of ca. 600 K is required to bring the reaction to a ΔG value of zero. At this point the unfavorable enthalpy is exactly compensated by the favorable entropy of H_2 release. We refer to this temperature as T_d , the point at which $\Delta G = 0$. Intermediate dehydrogenation products (e.g. cyclohexene) that do not benefit from the aromaticity of benzene are even more strongly disfavored than the final arene. The overall reaction could still be accessible if these intermediates were sufficiently stabilized by binding to the catalyst. Even in very endothermic cases, product formation is experimentally possible, however. For example, alkane dehydrogenation to alkenes and free H_2 has been observed with numerous homogeneous catalysts by us and others even at temperatures of 90–150 °C. These reactions are driven by reflux of the alkane, because the H_2 is swept out of the solvent and the equilibrium continually displaced.²⁶

The organic heterocycle H_2 storage strategy, first proposed by Alan Cooper and Guido Pez at Air Products, appeared in a series of key patents.^{27,28} Our later, but independent computational work on this problem, largely in collaboration with Eric Clot and Odile Eisenstein,²⁹ identified some general trends for design of the heterocycles to favor low temperature H_2 release. In summary, the storage step involves catalytic hydrogenation of an aromatic heterocycle to give the corresponding hydrogenated product. Release is effected by heating the hydrogenated form in the presence of a catalyst. Both directions must therefore be viable, implying that the endothermicity of the dehydrogenation has to be moderate. This endothermicity translates into a temperature T_d at which $\Delta G = 0$ and the results are therefore discussed in terms of T_d .

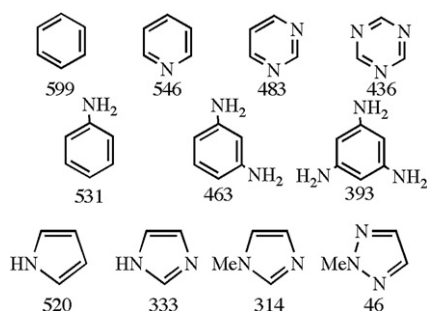
The all-carbon systems (e.g., cyclohexane–benzene) have a T_d that is far too high but introduction of nitrogen atoms into the organic ring dramatically favors the thermodynamics of H_2 release: in extreme cases, T_d can now go below 50 K. The most important design consideration for a low T_d is a move to a 5-membered ring, when aromatic stabilization can be achieved after cleavage of only four C–H bonds (eqn (1)), not six as for cyclohexane–benzene, always provided a NH or NR is present in the 1-position to permit aromaticity. Cyclopentane–cyclopentadiene shows no such advantage.



Incorporation of N into a six-membered ring also favors dehydrogenation because the N–H bond that is now broken is weaker than the C–H bond it replaced. In addition, C–H bonds adjacent to a N atom are also weakened relative to a C–H bond in a pure carbocycle. Nitrogen substituents are also effective.



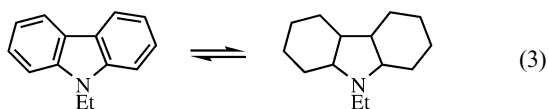
The thermodynamic data calculated {DFT(B3PW91)} by Eric Clot and Odile Eisenstein allow useful structure-activity trends to



Scheme 1 Thermodynamic hydrogen release temperatures (temperature {K} at which $\Delta G = 0$) for selected model compounds by DFT(B3PW91) calculations of Clot and Eisenstein.²²

be identified. Scheme 1 shows the T_d values for a number of key cases. The most effective way of lowering T_d is moving to a 5-membered ring, with incorporation of N-substituents and N ring atoms in a 1,3-arrangement being somewhat less effective strategies. As an aside, the data also suggest that the long known resistance of certain azoles (e.g., imidazole) to hydrogenation is the result of thermodynamic rather than purely kinetic factors.

In their patent, Pez and coworkers²⁸ demonstrate reversible hydrogenation–dehydrogenation of heterocyclic liquids. For example, N-ethyl carbazole is hydrogenated with 72 atm H_2 and a Pd catalyst at 160 °C to form a mixture of isomers of the fully hydrogenated species (eqn (3)). Dehydrogenation gave pure H_2 with Ru at 50–197 °C and at least 5 cycles can be run without HSM degradation.



The carbazole fulfils some of the thermodynamic requirements of Scheme 1 in that the nitrogen is a substituent to two rings and a member of the central 5-membered ring.

In this vision, a nitrogen-containing organic liquid is preferred as a hydrogen storage material (HSM) on several counts. Both C and N are available in very large amounts, with 2007 world production figures for nitrogen²³ of 1.2×10^{11} kg and just counting carbon in the form of coal, 5×10^{14} kg (World Coal Institute).³⁰ The material must not only be readily available but also be distributed economically to users. The Sallan Foundation³¹ estimates the infrastructure costs of the distribution system for petroleum based transport fuels at several hundred billion dollars. A liquid organic HSM can plausibly be distributed *via* the existing gasoline infrastructure with minimal modification, saving vast capital costs. Ideally the HSM would be minimally volatile, minimally toxic, and biodegradable.

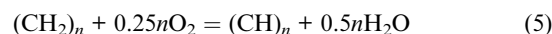
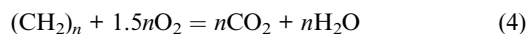
One advantage of the heterocyclic liquid strategy is that the liquid can in principle be repurified when necessary, so that the inevitable non-regenerable fraction of the HSM does not build up on the vehicle—a weight and capacity penalty. For this step, vacuum distillation may be desirable and if so, the components will need to have appreciable volatility.

Efficiency of HSM regeneration will be a key point because any shortfall would raise purification costs and require HSM to

be made up with newly manufactured material with a consequent economic penalty. Catalysts that can meet the severe selectivity and activity requirements must be further developed. Since it is not yet clear which HSM to choose, the HSM and the catalyst will have to be optimized together.

Limitations

Gravimetric capacity for typical HSMs of the type proposed are in the range from 6 to 8%, not as good as BH_3NH_3 . To meet the more aggressive DOE goals, more than one H would need to be stored per heavy atom, for example $C(CH_2NH_2)_4-C(CN)_4$ has an 11.7% capacity. The volumetric capacity for typical heterocycles is also satisfactory, although in energy terms not as good as gasoline, because only some of the hydrogen atoms of the HSM end up as H_2O and all the carbon remains uncombusted. The situation for gasoline, denoted $(CH_2)_n$, undergoing complete combustion *versus* the same $(CH_2)_n$, but now acting as an HSM with the hydrogen released ultimately undergoing oxidation with air, can be represented as follows.



In general terms, the exothermicity of a combustion reaction of H_2 or of a hydrocarbon is simply proportional to the amount of O_2 consumed. Comparison of the O_2 used in the two equations above suggests that the energy content of an organic HSM is *ca.* 17% of the value that the same material would have if completely combusted as a normal fuel. Of course, complete combustion would form CO_2 , contrary to the requirement for carbon dioxide abatement.

Design of the HSM requires attention to numerous points including (i) toxicity; (ii) thermal stability against undesired decomposition pathways; (iii) safety in accidental release such as in automobile collisions; (iv) biodegradability; (v) thermodynamic tendency to liberate H_2 ; (vi) kinetic facility for reversible H_2 release; (vii) cheap manufacture on a 10^{11} kg scale. Points (i)–(vii) severely restrict the types of materials that can be used, not only for the liquid organic strategy but for all others as well.

Azaheterocycles can be of low toxicity, 1-decyl pyridinium chloride is used as a mouthwash in almost all common formulations and is thus in intimate contact with humans on a daily basis as well as being released into the environment on a large scale. Thermal decomposition is a serious issue and work will be needed to understand the thermolysis pathways of candidate HSMs and find ways to guard against them by suitable design. Liquid organic HSMs can be of low volatility and have a high flash point, minimizing accidental release problems, and they may be biodegradable, particularly in their hydrogenated form, thanks to their heteroatom content. Quantitative structure-activity relationships (QSAR), now being developed both for toxicity and for biodegradation of N-heterocycles.³²

A HSM that readily releases H_2 is of necessity hard to hydrogenate. ‘Virtual H_2 storage’ could avoid this step by using the electrical power source not to produce free H_2 but to directly reduce the HSM electrocatalytically, but precedent is lacking. Likewise, a direct fuel cell could allow the conversion of the fresh

HSM to motive power without H₂ production. With air as the oxidant, the driving force of eqn (5) would be greatly enhanced and the high T_d problem circumvented.

Conclusion

The liquid heterocycle strategy is worth greater emphasis because it has a number of advantages of simplicity, safety, scalability, heat management, and economy. Catalyst development is needed for further progress, however, since catalytic heterocycle dehydrogenation is a neglected topic.

Acknowledgements

I thank Eric Clot and Odile Eisenstein for their many insightful contributions to this and other problems of mutual interest, Peter Hall (Strathclyde) for the direct fuel cell idea, the referees for useful suggestions and DOE and NSF for funding our catalysis work.

References

- 1 S. Arrhenius, *Worlds in the Making*, (transl. by H. Borns), Harper Bros., London & New York, 1908; p. 62.
- 2 "Climate Change 2007", Fourth IPCC Assessment Report, <http://www.ipcc.ch/ipccreports/index.htm>.
- 3 A. Zuetzel, *Naturwissenschaften*, 2004, **91**, 157–172.
- 4 L. Sclapbach and A. Zuetzel, *Nature*, 2001, **414**, 353.
- 5 J. A. Turner, *Science*, 2004, **305**, 972.
- 6 R. F. Service, *Science*, 2004, **305**, 962.
- 7 W. Grochala and P. P. Edwards, *Chem. Rev.*, 2004, **104**, 1283.
- 8 A. W. C. van den Berg and C. O. Areán, *Chem. Commun.*, 2008, **6**, 668–681.
- 9 (a) Z. Yang, Y. Xia and R. Mokaya, *J. Am. Chem. Soc.*, 2007, **129**, 1673; (b) H. M. Cheng, Q. H. Yang and C. Liu, *Carbon*, 2001, **39**, 1447.
- 10 H. G. Schimmel, G. J. Kearley and M. G. Nijkamp, *Chem.–Eur. J.*, 2003, **9**, 4764.
- 11 N. L. Rosi, J. Eckert, M. Eddaoudi, D. T. Vodak, J. Kim, M. O'Keeffe and O. M. Yaghi, *Science*, 2003, **300**, 1127.
- 12 C. M. Jensen and K. J. Gross, *Appl. Phys. A: Mater. Sci. Process.*, 2001, **72**, 213.
- 13 S. I. Orimo, Y. Nakamori, J. R. Eliseo, A. Zuetzel and C. M. Jensen, *Chem. Rev.*, 2007, **107**, 4111.
- 14 (a) R. J. Keaton, J. M. Blacquiere and R. T. Baker, *J. Am. Chem. Soc.*, 2007, **129**, 1844; (b) F. H. Stephens, R. T. Baker, M. H. Matus, D. J. Grant and D. A. Dixon, *Angew. Chem., Int. Ed.*, 2007, **46**, 746.
- 15 D. A. Dixon and M. Gutowski, *J. Phys. Chem. A*, 2005, **109**, 5129.
- 16 W. T. Klooster, T. F. Koetzle, P. E. M. Siegbahn, T. B. Richardson and R. H. Crabtree, *J. Am. Chem. Soc.*, 1999, **121**, 6337.
- 17 S. Hausdorf, F. Baitalow, G. Wolf and F. O. R. L. Mertens, *Int. J. Hydrogen Energy*, 2008, **33**, 608.
- 18 Y. Nakamori and S. Orimo, *J. Alloys Compd.*, 2004, **370**, 271.
- 19 B. Bogdanovic and M. Schwickardi, *J. Alloys Compd.*, 1997, **253**, 1.
- 20 Z. Xiong, C. K. Yong, G. Wu, P. Chen, W. Shaw, A. Karkamkar, T. Autrey, M. O. Jones, S. R. Johnson, P. P. Edwards and W. I. F. David, *Nat. Mater.*, 2008, **7**, 138.
- 21 A. Zuetzel, P. Wenger, S. Rentsch, P. Sudan, Ph. Mauron and Ch. Emmenegger, *J. Power Sources*, 2003, **118**, 1.
- 22 (a) F. E. Pinkerton, G. P. Meisner, M. S. Meyer, M. P. Baloghand and M. D. Kundrat, *J. Phys. Chem. B*, 2005, **109**, 6; (b) M. Aoki, K. Miwa, T. Noritake, G. Kitahara, Y. Nakamori, S. Orimo and S. Towata, *Appl. Phys. A: Mater. Sci. Process.*, 2005, **80**, 1409.
- 23 US Geological Survey, Washington, DC, USA, <http://minerals.usgs.gov/>.
- 24 N. Meng, S. Shinoda and Y. Saito, *Int. J. Hydrogen Energy*, 1997, **22**, 361.
- 25 N. Kariya, A. Fukuoka, T. Utagawa, M. Sakuramoto, Y. Goto and M. Ichikawa, *Appl. Catal., A*, 2003, **247**, 247.
- 26 (a) K. Krogh-Jespersen, M. Czerw, N. Summa, K. B. Renkema, P. D. Achord and A. S. Goldman, *J. Am. Chem. Soc.*, 2002, **124**, 11404; (b) T. Aoki and R. H. Crabtree, *Organometallics*, 1993, **12**, 294.
- 27 G. P. Pez, A. R. Scott, A. C. Cooper and H. Cheng, *US Pat.*, 7101530, September 5, 2006 and prior patents cited.
- 28 G. P. Pez, A. R. Scott, A. C. Cooper, H. Cheng, F. C. Wilhelm and A. H. Abdourazak, *US Pat.*, (7351395), 2008.
- 29 E. Clot, O. Eisenstein and R. H. Crabtree, *Chem. Commun.*, 2007, **22**, 2231–2233.
- 30 World Coal Institute, London, UK, <http://www.worldcoal.org/>.
- 31 Sallan Foundation, New York City, USA, <http://www.sallan.org/newviews/archives/2007/05/000617.php>.
- 32 (a) J. Chen, Y. Liao, Y. Zhao, L. Wang, G. Lu and T. Zhao, *Bull. Environ. Contam. Toxicol.*, 1996, **57**, 77; (b) B. Philipp, M. Hoff, F. Germa, B. Schink, D. Beimborn and V. Mersch-Sundermann, *Environ. Sci. Technol.*, 2007, **41**, 1390.



Comparing Photosynthetic and Photovoltaic Efficiencies and Recognizing the Potential for Improvement

Robert E. Blankenship, *et al.*

Science **332**, 805 (2011);

DOI: 10.1126/science.1200165

This copy is for your personal, non-commercial use only.

If you wish to distribute this article to others, you can order high-quality copies for your colleagues, clients, or customers by [clicking here](#).

Permission to republish or repurpose articles or portions of articles can be obtained by following the guidelines [here](#).

The following resources related to this article are available online at www.sciencemag.org (this information is current as of May 12, 2011):

Updated information and services, including high-resolution figures, can be found in the online version of this article at:

<http://www.sciencemag.org/content/332/6031/805.full.html>

Supporting Online Material can be found at:

<http://www.sciencemag.org/content/suppl/2011/05/12/332.6031.805.DC1.html>

This article **cites 53 articles**, 12 of which can be accessed free:

<http://www.sciencemag.org/content/332/6031/805.full.html#ref-list-1>

This article appears in the following **subject collections**:

Chemistry

<http://www.sciencemag.org/cgi/collection/chemistry>

Comparing Photosynthetic and Photovoltaic Efficiencies and Recognizing the Potential for Improvement

Robert E. Blankenship,^{1*} David M. Tiede,^{2*} James Barber,³ Gary W. Brudvig,⁴ Graham Fleming,⁵ Maria Ghirardi,⁶ M. R. Gunner,⁷ Wolfgang Junge,⁸ David M. Kramer,⁹ Anastasios Melis,¹⁰ Thomas A. Moore,¹¹ Christopher C. Moser,¹² Daniel G. Nocera,¹³ Arthur J. Nozik,¹⁴ Donald R. Ort,¹⁵ William W. Parson,¹⁶ Roger C. Prince,¹⁷ Richard T. Sayre¹⁸

Comparing photosynthetic and photovoltaic efficiencies is not a simple issue. Although both processes harvest the energy in sunlight, they operate in distinctly different ways and produce different types of products: biomass or chemical fuels in the case of natural photosynthesis and nonstored electrical current in the case of photovoltaics. In order to find common ground for evaluating energy-conversion efficiency, we compare natural photosynthesis with present technologies for photovoltaic-driven electrolysis of water to produce hydrogen. Photovoltaic-driven electrolysis is the more efficient process when measured on an annual basis, yet short-term yields for photosynthetic conversion under optimal conditions come within a factor of 2 or 3 of the photovoltaic benchmark. We consider opportunities in which the frontiers of synthetic biology might be used to enhance natural photosynthesis for improved solar energy conversion efficiency.

Sunlight is the most abundant and sustainable source of energy available to humanity. Earth receives solar energy at the rate of approximately 120,000 TW (1 TW = 10^{12} W) in a highly reliable and distributed fashion. This vastly exceeds the current annual worldwide

energy consumption rate of ~15 TW and any conceivable future needs in this century (1–3). However, sunlight is dilute; the yearly averaged solar power striking the Earth's surface is about 170 W per square meter, which varies depending on geographical location (4). Devising methods by which to efficiently capture and store this energy for societal use is one of the great challenges of our age. There is general agreement that no one approach is capable of solving our energy needs for the future and that a mix of sustainable technologies will be required (5).

There is considerable confusion, especially in the popular press, about how to compare the efficiency of solar energy capture in photovoltaic devices with a corresponding characteristic of photosynthetic organisms. The problem hinges on the different assumptions and conditions underlying the definition of efficiency in each case (6, 7). To facilitate direct comparisons between photosynthetic and photovoltaic (PV) systems, we provide consistent definitions and examine the major factors that define the efficiencies of both processes—first considering current technology, then looking forward to possible strategies for improvements. In all cases, we consider the efficiency of harvesting the entire solar spectrum as a basis for comparison.

We focus exclusively here on conversion efficiency. However, the total integrated cost of the systems, including land, water, capital, operations and maintenance, waste disposal, transmission, transportation and storage, as well as risks from manufacturing and possible interac-

tions with the food supply and climate change, must also be considered. Therefore, the technology with the highest efficiency may not necessarily be the best choice to implement in a given situation. Ultimately, a comparison of solar energy options must come from the perspective of a complete life-cycle assessment in order to evaluate the full suite of energy inputs, infrastructure and renewal requirements, and environmental factors, including greenhouse gas balance. This is a critical and active area of research for both photosynthetic and PV systems (8, 9), but currently there is little consistency in the methods used. Differences in assumptions about efficiency terms, life-cycle inventory components, and systems boundaries create large variations in the metadata generated from the many concomitant efforts.

Comparing Photosynthetic and Photovoltaic Efficiencies

Efficiency is a concept that is deceptively simple yet can be elusive for comparisons between such different systems as living organisms and photovoltaic cells. The solar conversion efficiency of a PV device can be directly measured with high accuracy and is usually quoted by researchers and manufacturers in terms of power: electrical power out (W/cm^2) divided by incident solar irradiance (W/cm^2) measured over the entire solar spectrum. This instantaneous metric, measured at peak solar intensity, does not include energy storage and transmission. In contrast, natural photosynthesis stores energy in the chemical bonds of its molecular products and uses much of this energy to sustain and replicate the organism, typically over a defined growing season.

A more direct comparison of PV and photosynthetic solar energy conversion efficiencies would consider a process in which PV also stores energy in chemical bonds. Application of PV-derived energy to electrolysis of water is a good choice for this purpose: Existing commercial electrolyzers afford accurate efficiency benchmarks, and the free energy needed in order to split H_2O into H_2 and O_2 ($\Delta G^\circ = 1.23$ eV) is essentially equal to the free energy change associated with photosynthesis [$\Delta G^\circ = 1.24$ eV for $\text{CO}_2 + \text{H}_2\text{O}$ to $(\text{CH}_2\text{O}) + \text{O}_2$, where (CH_2O) is shorthand for carbohydrate].

The power conversion efficiency of present commercial single-junction (single photosystem) silicon solar cell modules is typically $18 \pm 2\%$ (10). This value pertains to peak solar intensity ($1 \text{ kW}/\text{m}^2$), with an AM1.5 spectral distribution or solar zenith angle of 48.2° (sunlight passing through 1.5 atmospheres). The efficiency of a PV module changes during the day and throughout the year because of the changing solar zenith angle, and the PV efficiency averaged over a 1-year cycle is about 95% of the maximum AM1.5 value. Modern commercial electrolyzers have efficiencies as high as 80% [based

¹Departments of Biology and Chemistry, Washington University in St. Louis, St. Louis, MO 63130, USA. ²Chemical Sciences and Engineering Division, Argonne National Laboratory, Argonne, IL 60439, USA. ³Division of Molecular Biosciences, Imperial College London, London SW7 2AZ, UK; Department of Material Sciences and Engineering, Polytechnic of Turin, 10129 Turin, Italy. ⁴Department of Chemistry, Yale University, New Haven, CT 06520–8107, USA. ⁵Department of Chemistry, University of California, Berkeley, and Physical Biosciences Division, Lawrence Berkeley National Laboratory, Berkeley, CA 94720, USA. ⁶Biosciences Center, National Renewable Energy Laboratory, Golden, CO 80401, USA. ⁷Department of Physics, City College of New York, New York, NY 10031, USA. ⁸Division of Biophysics, University of Osnabrück, D-49069 Osnabrück, Germany. ⁹Biochemistry and Molecular Biology and DOE-Plant Research Laboratory, Michigan State University, East Lansing, MI 48824, USA. ¹⁰Department of Plant and Microbial Biology, University of California, Berkeley, CA 94720–3102, USA. ¹¹Department of Chemistry and Biochemistry, Arizona State University, Tempe, AZ 85287–1604, USA. ¹²Department of Biochemistry and Biophysics, University of Pennsylvania, Philadelphia, PA 19104, USA. ¹³Department of Chemistry, Massachusetts Institute of Technology, Cambridge, MA 02139–4307, USA. ¹⁴National Renewable Energy Laboratory, Golden, CO 80401, USA; Department of Chemistry and Biochemistry, University of Colorado, Boulder, CO 80309, USA. ¹⁵U.S. Department of Agriculture/Agricultural Research Service, Photosynthesis Research Unit, University of Illinois, Urbana, IL 61801, USA. ¹⁶Department of Biochemistry, University of Washington, Seattle, WA 98195, USA. ¹⁷ExxonMobil Biomedical Sciences, Annandale, NJ 08801, USA. ¹⁸Donald Danforth Plant Science Center, St. Louis, MO 63132, USA.

*To whom correspondence should be addressed. E-mail: blankenship@wustl.edu (R.E.B.); tiede@anl.gov (D.M.T.)

on heat of combustion of H_2 to H_2O in liquid form at atmospheric pressure and 25°C , standard temperature and pressure (STP) conditions]. Thus, an annual averaged efficiency for solar water splitting by PV-driven electrolysis would be about $(0.18) \times (0.95) \times (0.8) \sim 14\%$ (11). This assumes that there is no mismatch between the photovoltage generated by the PV array and the voltage required for electrolysis. Present Si PV modules arranged in electrical series would suffer mismatch losses as high as 20 to 30%, bringing the overall H_2O splitting efficiency down to ~ 10 to 11%. This constitutes the first benchmark to compare with the efficiency of photosynthetic fuel production. As discussed below, ongoing research is providing opportunities to construct PV devices with considerably higher efficiencies.

Several different measures of efficiency have been used in describing natural photosynthesis. The quantum efficiency is the percentage of absorbed photons that give rise to stable photoproducts. Photosynthetic organisms typically can operate at nearly 100% quantum efficiency under optimum conditions (12). For comparison with PV electrolysis over an annual cycle, the energy efficiency of photosynthesis is a more useful parameter and is defined as the energy content (heat of combustion of glucose to CO_2 and liquid H_2O at STP) of the biomass that can be harvested annually divided by the annual solar irradiance over the same area. Using this definition, solar energy conversion efficiencies for crop plants in both temperate and tropical zones typically do not exceed 1% (7, 13), a value that falls far below the benchmark for PV-driven electrolysis. Higher 3% annual yields are reported for microalgae grown in bioreactors (14).

Short-term (rapid growth phase) efficiencies measured during the growing season are higher, reaching 3.5% for C3 and 4.3% for C4 plants (7), and perhaps 5 to 7% for microalgae in bubbled bioreactors (15). These efficiencies are measured in the absence of restrictions imposed by plant life-cycle regulation or by light and gas exchange limitations in the case of algae. Even so, these values fall below theoretical limits and ultimately limit the net annual productivity. Most natural photosynthetic systems store solar energy only during a growing season; efficiencies measured during that period must therefore be reduced accordingly to make valid comparisons on an annual basis, although the extent of reduction depends

on the type of crop and the environmental conditions.

Theoretical Limits to Solar Energy Conversion

Both PV and natural photosynthetic systems obey the same fundamental laws of thermodynamics, which impose firm upper bounds on efficiency. There is an extensive literature on each process dating back over 50 years, and although the formulations differ substantially, the overall conclusions are similar. Following pioneering studies by Duysens (16), many au-

(UV) to nearly 1200 nm in the near-infrared (near-IR).

Thermodynamics furthermore dictates that not all the energy in each absorbed photon can be captured for productive use. Figure 2 shows the relevant energy diagrams. In photosynthetic organisms, absorption initially creates an excited state of chlorophyll or an accessory pigment. Although photons with blue wavelengths may be efficiently absorbed, ultrafast internal conversion processes relax higher excited states through release of heat to the energy of the lowest (red-most) absorption band. Similarly, conventional semiconductor-based PV cells can absorb photons with energy equal to or greater than the band-gap separating the valence-band from the conduction-band, but any photon energy in excess of the bandgap is lost as heat. Thus, both systems have a threshold energy that defines attainable light absorption, conversion efficiency, and energy storage capabilities.

When these considerations are included in a more detailed thermodynamic analysis using the entire solar spectrum, a single-junction PV system has a maximal instantaneous power conversion efficiency of $\sim 32\%$ at one-sun intensity and an AM1.5 spectral distribution, the so-called Shockley-Queisser limit (18). The Shockley-Queisser treatment is the isothermal equivalent of the Carnot cycle and assumes that all processes are reversible (no overpotentials, no dissipative losses), with the consequence that extracting chemical or electrical work from the system would be infinitely slow.

In a realistic photoelectrolysis cell based on a single-threshold semiconductor photoelectrode (in direct contact with water) that generates hydrogen and oxygen at finite rates, the overvoltage would be finite. At unconcentrated solar intensities, the current density is relatively low ($< 35 \text{ mA cm}^{-2}$), so that an overvoltage of $\sim 0.15 \text{ V}$ is a reasonable assumption; this would decrease the maximum Shockley-Queisser efficiency for a photoelectrolysis cell to $\sim 24\%$ (19).

A theoretical limit of $\sim 12\%$ for the efficiency of photosynthetic glucose production from CO_2 and water (based on free energy) can be calculated by considering the chlorophyll band-edge absorption and the two-photosystem structure of oxygenic photosynthesis (6, 13). Taking into account the known losses in light harvesting, overpotentials, and respiration, the maximum limit to photosynthetic efficiency is reduced to 4.6 and 6.0% for C3 and C4 plants, respectively (7). Short-term (rapid-growth phase) conversion

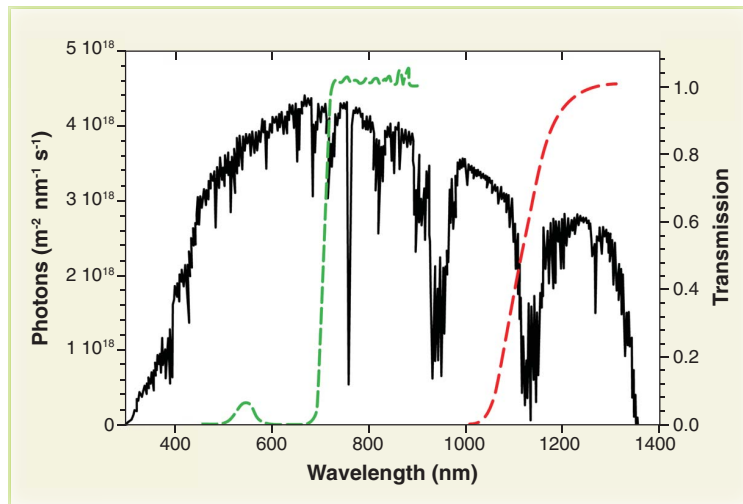


Fig. 1. The photon flux spectrum of solar radiation reaching Earth's surface (plotted in black) (66) and the transmission spectra of a natural photosynthetic organism, the cyanobacterium *Synechocystis* PCC 6803 (green dot-dashed line) and of crystalline silicon [red dashed line, redrawn with permission from (67)]. The transmission spectra show that both the cyanobacteria and silicon absorb almost all photons at shorter wavelengths above the threshold energy but transmit photons at longer wavelengths below the threshold energy. The cyanobacterial sample has a window of transmission in the green region of the spectrum that causes the culture to appear green. The cyanobacterial sample had an absorbance of 3.4 at 678 nm and was digitally corrected for scattering.

thors have examined the thermodynamics of photosynthesis, most recently Knox and Parson (17). Shockley and Queisser pioneered studies on the maximal efficiency of PV cells (18); a recent analysis by Hanna and Nozik considers multiple-junction cells and other modern developments (19).

The first step in each system's energy conversion process is light absorption, which is governed by quantum mechanics. Figure 1 shows a reference solar spectrum at the surface of the Earth, with transmission spectra of a cyanobacterium and a silicon cell superimposed. The radiant energy intercepted by the chlorophyll, carotenoids, and other accessory pigments in oxygenic photosynthetic organisms is usually limited to the visible region of the spectrum (400 to 700 nm). Photosynthetic organisms thus access only $\sim 50\%$ of the incident solar energy (7, 20, 21). The silicon cell has a broader absorption range, extending from the ultraviolet

efficiencies come within 70 to 75% of meeting these limits. The passive diffusion of CO₂ at atmospheric concentration will set a conversion limit for fixation in both photosynthesis and artificial devices. Indeed, dense stands of rapidly photosynthesizing crops such as corn or soybean can lower CO₂ levels within the canopy 50 parts per million (ppm) or more below ambient (22), suggesting that CO₂ delivery affects the rate of carbon fixation. Given these constraints, opportunities to enhance photosynthetic productivity lie in the development of plant and microalgal systems that achieve sustained CO₂ fixation at yields close to the theoretical limits. Further productivity gains in both photosynthetic and PV systems could potentially be realized by designing systems that reset the limits to energy conversion as described below.

Improved System Design Raising Theoretical Limits

A key opportunity for raising the efficiency ceiling in PV systems lies in replacing single-junction devices with tandem cells optimized for water oxidation and hydrogen production. This approach could give efficiencies approaching 40% (free energy basis) as overvoltages approach zero (19, 23). Further increases in PV efficiencies might be obtained by devices that use the blue and near-UV region of the solar spectrum more effectively or capture the energy of the sub-bandgap IR photons. Prospects under study include hot-carrier

solar cells, intermediate-band solar cells, multi-junction tandem architectures, and absorbing media that generate multiple charge carriers per absorbed photon. In these cases, the theoretical thermodynamic limit set by the second law reaches 66% at one-sun intensity (24, 25), with corresponding increases in the yield of electrochemical products.

Turning to photosynthesis, one straightforward strategy for improving the efficiency limit would involve tuning the light-absorbing pigments to extend the range of solar light absorption (26). A related, substantial source of inefficiency arises from nature's use of two photochemical systems connected in series to generate the electric potential difference required to split water and reduce nicotinamide adenine dinucleotide phosphate (NADP⁺). The effective bandgaps (absorption thresholds) of the two photosystems are similar. In practical terms, this means that the two photosystems compete for the same regions of the solar spectrum, cutting the energy efficiency nearly in half compared with what might be achieved if the bandgaps were different and optimized to use different regions of the spectrum (19, 27).

Photosynthesis is unique in its capacity to produce a diverse array of complex organic compounds (leading to replication of the organism) through light-driven CO₂ reduction. There is no PV device that can deliver comparably selective carbon-fixation photochemistry, nor of course can PV devices replicate themselves. Although

it can be argued that self-replication represents a real advantage for natural photosynthesis, it is also clear that the structure and function of the photosynthetic apparatus are limited by the need to operate within a living organism, for which they were tailored by evolution. The comparatively low efficiency of natural photosynthesis may result partly from the "legacy biochemistry" photosynthetic organisms inherited from earlier non-photosynthetic organisms that used biochemical pathways with redox cofactors not optimally matched for photochemical processes (28). Some factors that limit the efficiency of natural photosynthetic systems are intrinsic to the basic structure and organization of the photosynthetic apparatus and would require a major re-engineering to improve, whereas other improvements may be attained by more straightforward adjustments in the structure of the organisms or the growth conditions. Although this approach may seem daunting, agricultural breeding has been steadily achieving these goals for millennia, albeit primarily for food production, and typically not necessarily for high-efficiency energy storage. Because we have only just started breeding or engineering plants and algae for fuels production, it is likely that substantial improvements are feasible.

Photosynthetic organisms in the wild are selected through evolution for reproductive success, not for high biomass production in plant monocultures in which competition for resources (including light) is, in many cases, a disadvantage (29). Likewise, crop plants have been bred for various properties of the harvestable product but not for overall photosynthetic efficiency, while being nurtured by intensive agricultural practices that use substantial inputs of fossil fuels. Consequently, photosynthetic rates are often limited or down-regulated even below the theoretical limits imposed by the slowest reactions of CO₂ fixation and electron transport, leading to strategic down-regulation of productivity. This problem could be alleviated with breeding or engineering, even without radical changes to the photosynthetic apparatus (7, 30). An interesting example of the importance of regulatory strategy is the acclimation of plants to higher CO₂ levels. In principle, the recent increase in atmospheric CO₂ levels should alleviate limitations of photosynthesis at the enzyme ribulose-bisphosphate carboxylase-oxygenase (RuBisCO); however, these gains may not be realized in plants that evolved to use the lower CO₂ levels that prevailed before the industrial revolution (31). This lack of acclimation to current and future CO₂ levels, which results in kinetic mismatches among the component processes of photosynthesis, is an obvious target for plant breeding and engineering. Further, cellular growth and maintenance of the organism can also be viewed as a loss of at least 30% of the stored energy (7). Part of this energy is used to synthesize large quantities of RuBisCO to compensate for the enzyme's relatively low catalytic rate constant.

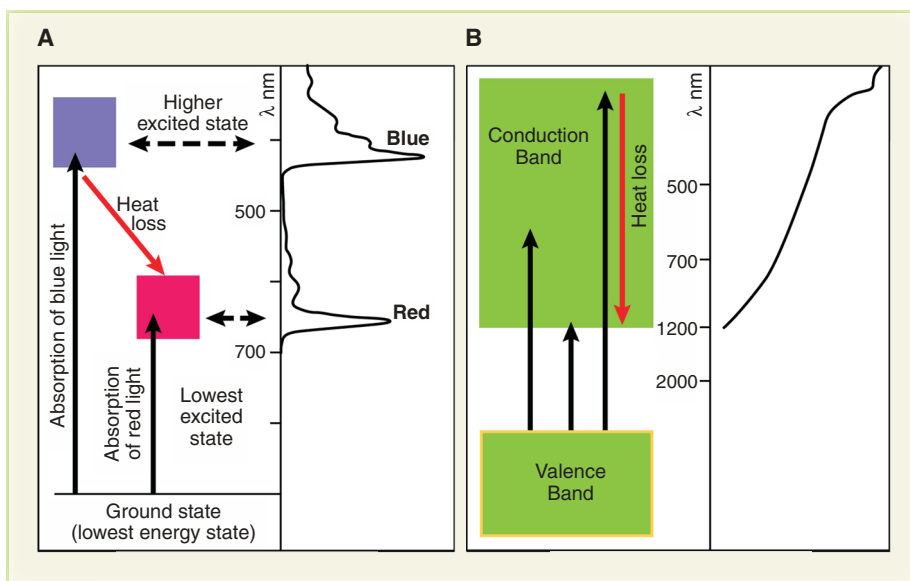


Fig. 2. Comparison of the threshold properties of photosynthetic and silicon-based PV systems. **(A)** Energy-level diagram for chlorophyll *a*, the major pigment found in most oxygenic photosynthetic organisms. The excited state is populated by blue light absorption and rapidly relaxes through heat loss to the energy level accessed by red light absorption, which is the effective threshold for energy storage. An absorption spectrum for chlorophyll *a* is shown for comparison. **(B)** Energy-level diagram for crystalline silicon, which is characteristic of the band structure of a semiconductor. The threshold absorption energy just bridges the bandgap (middle black arrow). Photons with a range of higher energies can still be absorbed, but their energy in excess of the bandgap is lost as heat before it can be stored. An absorption spectrum of silicon is shown for comparison (67).

Another instance of inefficiency in natural photosynthesis occurs when RuBisCO fixes the competitive substrate O_2 instead of CO_2 , initiating the energy-intensive recovery process of photorespiration (32). Photorespiration can consume up to 25% of the initially stored energy (7). Some cyanobacteria, algae, and plants have evolved CO_2 -concentration processes that largely circumvent photorespiration (33, 34). However, these processes also entail an energetic cost that prevents realization of the entire advantage. In C4 photosynthesis, CO_2 is initially fixed into compounds with four carbon atoms (hence, the term “C4”) and subsequently released at high concentrations near RuBisCO, where it competes more effectively with O_2 and reduces the oxygenation reaction substantially (35, 36). Efforts are currently underway to introduce C4 photosynthesis or other carbon-concentrating systems into higher plants where they are currently lacking (35). If successful, these efforts may not only increase maximal photosynthetic rates and efficiencies directly but could reduce the large investment of energy and nutrients that C3 plants make in the synthesis of RuBisCO.

The amount of photorespiration can also potentially be reduced by engineering improved versions of RuBisCO with higher specificity for CO_2 over O_2 , although this has proven difficult (36). A promising approach is the insertion of the *Escherichia coli* pathway for glycolate catabolism into *Arabidopsis* chloroplasts, introducing a bypass of the normal photorespiratory pathway by converting glycolate to glycerate directly in the chloroplast (7, 37). Additionally, natural variants of RuBisCO that are better suited to current and anticipated CO_2 levels may be useful (38). Photorespiration also might be virtually eliminated by using flue gases from fossil fuel- or biomass-burning installations (such as power plants) as input gases for microalgal-based photobioreactor systems (39). These flue gases typically comprise ~10% CO_2 , a concentration sufficient to suppress photorespiration almost completely.

All natural photosynthetic organisms contain light-gathering antenna systems, in which specialized pigments (typically several hundred) collect energy and transfer it to a reaction center where photochemistry takes place (6, 40). With so many pigments absorbing light, full sunlight rapidly exceeds the capacity of the photosynthetic apparatus to process the influx of energy. In leaves in full sun, up to 80% of the absorbed energy must be dissipated or risk causing serious damage to the system (41). Plants have evolved a variety of mechanisms for dealing with this excess energy, including non-photochemical quenching pathways to prevent damage (42) and repair mechanisms if damage to reaction center proteins has occurred (43). However, the consequence is that surface cells exposed to the most light dissipate much of the available energy, whereas cells in lower layers remain starved for light. This overly aggressive capture of light may have an evolutionary advantage (for example,

by shading competitors), but it decreases the overall efficiency of energy storage.

To address this issue, research efforts are underway in microorganisms to reduce the size of the antenna system (44, 45). Truncated light-harvesting antennas can simultaneously reduce the problem of saturation at the surface and reduce shading deep in the water column, permitting more uniform illumination of the culture. In crop plants, modifying plant architecture can allow more light to pass to lower levels of the canopy, although lowering the chlorophyll con-

the amount of solar energy that can potentially be stored (26, 47, 48). Reducing the size of the antenna as discussed above might make it possible to expand the absorption spectrum without increasing saturation effects.

Synthetic Biology

The techniques of synthetic biology (49) may allow a more radical redesign of the photosynthetic apparatus for both bioenergy and food production applications. As mentioned above, the two photosystems required for oxygenic photo-

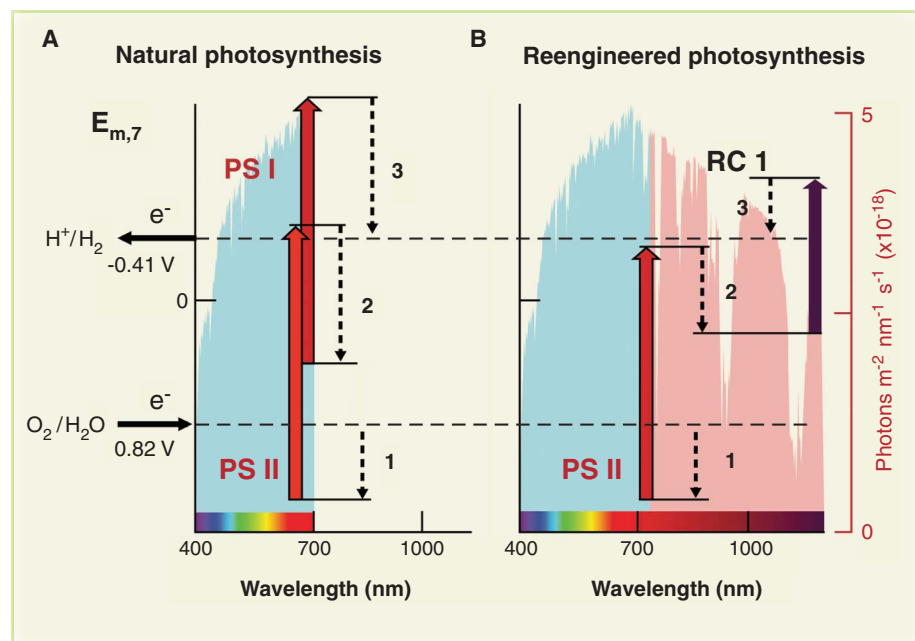


Fig. 3. (A) Photoelectrochemical energy capture diagram for photosynthesis and **(B)** photosynthesis reengineered following the thermodynamic principles in (19) for improved efficiency. The lengths of the upward arrows mark the initial photoinduced ground-to-excited-state electrochemical energy change of the reaction center primary donor chlorophylls. The position of the arrows along the wavelength axis is fixed by their length and is approximately at the red-most absorption edge of these chlorophylls. In (A), the vertical positions of the bases of the upward arrows reflect the approximate reduction potentials for the radical cation of the primary donor chlorophylls of photosystem I and photosystem II. In (B), the vertical and horizontal positions of the upward arrows are optimized for photosystems operating in tandem and providing 800 mV of overpotential to drive a chemical reaction having ΔG^0 of 1.23 eV that converts solar energy to electrochemical potential. The lengths of the downward dashed arrows indicate intrinsic free-energy losses associated with charge separation and electron transfer between photosystem II and reaction center I (arrow 2) and the overpotential necessary to drive the chemical oxidation-reduction reactions (arrows 1 and 3). In (A), electron transfer between the photosystems (dashed arrow 2) is associated with an energy-conserving ATP-coupling site. The background shows the portion of incident solar photons captured in each case. In (B) reengineered photosynthesis, photosystem I is replaced by a new reaction center, RC1, with farther-red-absorbing pigments. This increases the efficiency of photosynthesis by approximately doubling the solar photon capture and, using this biological version of a tandem cell, better matching the solar spectrum to the electrochemical work. For this illustration, reaction centers using chlorophyll *d* and bacteriochlorophyll *b* would be optimal for driving the redox catalysis.

tent may be a more robust way to promote light energy distribution and canopy photosynthetic efficiency (46).

As noted earlier, plants and algae are generally restricted to absorbing visible light. Some species of cyanobacteria possess variants of chlorophyll that absorb further into the near-IR (740- to 750-nm wavelength range), increasing

synthesis compete for the same wavelengths of light, reducing overall photochemical efficiency. An ambitious modification would be to maintain the two photosystems but engineer one of them to use the bacteriochlorophylls found in many anoxygenic photosynthetic organisms, which have absorption maxima that extend out to ~1100 nm. Figure 3 presents a schematic il-

lustration of a radically redesigned system in which the two photosystems have complementary optical spectra, conferring pseudotandem photocell function. The extent to which true tandem-cell efficiency were achieved would depend on the success of directing energy transfer from antennas absorbing 400- to 730-nm and 730- to ~1100-nm photons to different reaction centers. Wiring each antenna to the appropriate reaction center could potentially take advantage of structures in which exciton coupling or quantum coherence effects direct energy flow more efficiently (50). An optimum configuration could mimic a two-junction tandem photovoltaic cell (19).

Substantial improvements can be envisaged even within the context of the two-photosystem architecture of current oxygenic photosynthesis. As discussed earlier, for example, the carbon fixation process is currently limited by photorespiration associated with the low substrate selectivity of RuBisCO. Although RuBisCO is found in all oxygenic photosynthetic organisms, it might nonetheless be possible to introduce a different carbon-fixation cycle in place of the Calvin-Benson cycle (51, 52). Most of the known alternative cycles are highly O₂ sensitive and are probably unsuitable for organisms that live in the presence of oxygen. However, the hydroxypropionate cycle found in filamentous anoxygenic phototrophs is not O₂-sensitive (53). An alternative is to forego production of reduced carbon storage products and produce H₂ by reduction of H⁺. This process can be accomplished by using hydrogenase enzymes (54) or platinum nanoparticles (55) that are tethered to photosystem I. Because most hydrogenase enzymes are destroyed by O₂, re-engineering this system to be less O₂-sensitive is an important objective (56, 57). In addition, a range of promising, O₂-tolerant transition metal catalysts are being developed (58). An intermediate enzymatic approach that is under investigation would treat CO₂ as an electron acceptor but reduce it only to the level of formate by using the enzyme formate dehydrogenase (59). The production of either hydrogen or formate may at the same time reduce the problem of light saturation because these systems have intrinsically very high capacity and could be capable of processing the electrons delivered by the reaction centers at a much higher rate than that of the RuBisCO-based C3 carbon-fixation cycle.

Outlook

We have sought here to make the most consistent comparison possible between the fundamental solar energy storage efficiencies of photovoltaic and photosynthetic systems. In this context, the efficiency advantage clearly goes to photovoltaic systems. However, there is clearly need to apply both in the service of sustainable energy conversion for the future. Approaches in which photovoltaics are coupled to redox chemistry in photoelectrochemical cells and even living organisms (60, 61) also hold promise for solar fuels production. Numerous points of inefficiency in the natural system are amenable to improvement by using genetic engineering and more aggressive techniques of synthetic biology.

References and Notes

References and Notes

- M. I. Hoffert *et al.*, *Science* **298**, 981 (2002).
- N. S. Lewis, D. G. Nocera, *Proc. Natl. Acad. Sci. U.S.A.* **103**, 15729 (2006).
- J. Barber, *Chem. Soc. Rev.* **38**, 185 (2009).
- World Energy Council, www.worldenergy.org/publications/survey_of_energy_resources_2007/solar/720.asp (2007).
- Committee on America's Future, *America's Energy Future: Technology and Transformation: Summary Edition* (National Academy Press, Washington, DC, 2009).
- R. E. Blankenship, *Molecular Mechanisms of Photosynthesis*, Blackwell Science, Oxford, UK (2002).
- X.-G. Zhu, S. P. Long, D. R. Ort, *Annu. Rev. Plant Biol.* **61**, 235 (2010).
- S. C. Davis, K. J. Anderson-Teixeira, E. H. Delucia, *Trends Plant Sci.* **14**, 140 (2009).
- A. F. Sherwani, J. A. Usmani, *Renew. Sustain. Energy Rev.* **14**, 540 (2010).
- M. A. Green, K. Emery, Y. Hishikawa, W. Warta, *Prog. Photovolt. Res. Appl.* **18**, 144 (2010).
- M. Topic, K. Brecl, J. Sites, Performance assessment of PV modules relationship between STC rating and field performance, in *Conference Record of the 2006 IEEE 4th World Conference on Photovoltaic Energy Conversion, vol. 1 and 2* (IEEE, New York 2006), pp. 2141–2144.
- C. A. Wraight, R. K. Clayton, *Biochim. Biophys. Acta* **333**, 246 (1974).
- D. A. Walker, *J. Appl. Physiol.* **21**, 509 (2009).
- R. H. Wijffels, M. J. Barbosa, *Science* **329**, 796 (2010).
- M. Janssen, J. Tramper, L. R. Mur, R. H. Wijffels, *Biotechnol. Bioeng.* **81**, 193 (2003).
- L. N. M. Duysens, *Brookhaven Symp. Biol.* **11**, 10 (1959).
- R. S. Knox, W. W. Parson, *Biochim. Biophys. Acta* **1767**, 1189 (2007).
- W. Shockley, H. J. Queisser, *J. Appl. Phys.* **32**, 510 (1961).
- M. C. Hanna, A. J. Nozik, *J. Appl. Phys.* **100**, 74510 (2006).
- The 400- to 700-nm spectral range is commonly referred to as photosynthetically active radiation (PAR). This spectral range applies to organisms that carry out oxygenic photosynthesis, in which H₂O is oxidized to O₂ and CO₂ is reduced to sugars. There are also numerous anoxygenic (non-O₂-evolving) phototrophs that use bacteriochlorophyll *b* absorbing out to ~1100 nm (62). These organisms primarily drive cyclic electron transfer reactions and only secondarily oxidize reduced substrates such as H₂S.
- J. R. Bolton, D. O. Hall, *Annu. Rev. Energy* **4**, 353 (1979).
- N. Buchmann, J. R. Ehleringer, *Agric. For. Meteorol.* **89**, 45 (1998).
- J. Genovesse, K. Harg, M. Paster, J. Turner, Current (2009) state of the art hydrogen production cost estimate using water electrolysis. NREL/BK-6A1-46676, www.hydrogen.energy.gov/pdfs/46676.pdf (2009).
- N. S. Lewis, G. Crabtree, A. J. Nozik, M. R. Wasielewski, P. Alivisatos, *Basic research needs for solar energy utilization* (U.S. Department of Energy, Office of Basic Energy Sciences, Washington, DC, 2005).
- M. Green, *Third Generation Photovoltaics* (Springer-Verlag, Berlin, 2003).
- M. Chen, R. E. Blankenship, *Trends Plant Sci.*, published online 12 April 2011.
- Two coupled photosystems (large integral membrane pigment-protein complexes) connected in series are needed to carry out the complete oxygenic photosynthetic process. Photosystem II oxidizes H₂O and produces O₂ and a weak reductant, whereas photosystem I oxidizes a weak reductant and reduces NADP⁺ to NADPH, which along with adenosine 5'-triphosphate (ATP) provides the free energy for the Calvin-Benson carbon fixation cycle. The theoretical minimum quantum requirement (the inverse of the quantum yield) for the complete photosynthetic process leading to production of one molecule of O₂ is 8 because each photosystem transfers one electron per photon absorbed, and the oxidation of H₂O to O₂ is a four-electron process. Experimental

- values for quantum requirements for O₂ evolution under optimal laboratory conditions are 9 to 10 (63–65).
- D. Gust, D. Kramer, A. Moore, T. A. Moore, W. Vermaas, *MRS Bull.* **33**, 383 (2008).
- N. P. R. Anten, *Ann. Bot. (Lond.)* **95**, 495 (2005).
- C. A. Raines, *Photosynth. Res.* **75**, 1 (2003).
- S. P. Long, X.-G. Zhu, S. L. Naidu, D. R. Ort, *Plant Cell Environ.* **29**, 315 (2006).
- C. H. Foyer, A. J. Bloom, G. Queval, G. Noctor, *Annu. Rev. Plant Biol.* **60**, 455 (2009).
- M. Giordano, J. Beardall, J. A. Raven, *Annu. Rev. Plant Biol.* **56**, 99 (2005).
- M. R. Badger, G. D. Price, *J. Exp. Bot.* **54**, 609 (2003).
- J. M. Hibberd, S. Covshoff, *Annu. Rev. Plant Biol.* **61**, 181 (2010).
- R. J. Spreitzer, M. E. Salvucci, *Annu. Rev. Plant Biol.* **53**, 449 (2002).
- R. Kebeish *et al.*, *Nat. Biotechnol.* **25**, 593 (2007).
- X.-G. Zhu, A. R. Portis Jr., S. P. Long, *Plant Cell Environ.* **27**, 155 (2004).
- R. T. Sayre, *Bioscience* **60**, 722 (2010).
- B. R. Green, W. W. Parson, Eds., *Light-Harvesting Antennas in Photosynthesis, vol. 13* (Kluwer, Dordrecht, Netherlands, 2003).
- A. Melis, *Plant Sci.* **177**, 272 (2009).
- N. R. Baker, *Annu. Rev. Plant Biol.* **59**, 89 (2008).
- W. Sakamoto, *Annu. Rev. Plant Biol.* **57**, 599 (2006).
- J. H. Mussgnug *et al.*, *Plant Biotechnol. J.* **5**, 802 (2007).
- M. Mitra, A. Melis, *Opt. Express* **16**, 21807 (2008).
- D. R. Ort, X. G. Zhu, A. Melis, *Plant Physiol.* **155**, 79 (2011).
- H. Miyashita *et al.*, *Nature* **383**, 402 (1996).
- M. Chen *et al.*, *Science* **329**, 1318 (2010).
- D. F. Savage, J. Way, P. A. Silver, *ACS Chem. Biol.* **3**, 13 (2008).
- G. S. Engel *et al.*, *Nature* **446**, 782 (2007).
- R. K. Thauer, *Science* **318**, 1732 (2007).
- A. Bar-Even, E. Noor, N. E. Lewis, R. Milo, *Proc. Natl. Acad. Sci. U.S.A.* **107**, 8889 (2010).
- J. Zarzycki, V. Brecht, M. Müller, G. Fuchs, *Proc. Natl. Acad. Sci. U.S.A.* **106**, 21317 (2009).
- M. Ihara, H. Nakamoto, T. Kamachi, I. Okura, M. Maeda, *Photochem. Photobiol.* **82**, 1677 (2006).
- L. M. Utschig *et al.*, *J. Phys. Chem. Lett.* **2**, 236 (2011).
- P. M. Vignais, B. Billoud, *Chem. Rev.* **107**, 4206 (2007).
- M. L. Ghirardi *et al.*, *Annu. Rev. Plant Biol.* **58**, 71 (2007).
- J. L. Dempsey, B. S. Brunschwig, J. R. Winkler, H. B. Gray, *Acc. Chem. Res.* **42**, 1995 (2009).
- T. Reda, C. M. Plugge, N. J. Abram, J. Hirst, *Proc. Natl. Acad. Sci. U.S.A.* **105**, 10654 (2008).
- K. P. Nevin, A. E. Woodard, A. E. Franks, Z. M. Summers, D. R. Lovley, *mBio* **1(2)**, e00103 (2010).
- J. J. Kan, L. Hsu, A. C. M. Cheung, M. Pirbazari, K. H. Nealon, *Environ. Sci. Technol.* **45**, 1139 (2011).
- R. E. Blankenship, M. T. Madigan, C. E. Bauer, Eds., *Anoxygenic Photosynthetic Bacteria* (Kluwer Academic Publishing, Dordrecht, Netherlands, 1995).
- R. Emerson, *Annu. Rev. Plant Physiol.* **9**, 1 (1958).
- A. C. Ley, D. C. Mauzerall, *Biochim. Biophys. Acta* **680**, 95 (1982).
- J. B. Skillman, *J. Exp. Bot.* **59**, 1647 (2008).
- A. S. T. M. Standard, G173-03 (2008), Standard tables for reference solar spectral irradiances: Direct normal and hemispherical on 37° tilted surface (10.1520/G0173-03R08), available online: www.astm.org/Standards/G173.htm, <http://rredc.nrel.gov/solar/spectral/am1.5>.
- G. E. Jellison, F. A. Modine, *J. Appl. Phys.* **53**, 3745 (1982).
- This article evolved from presentations and discussions at the workshop "What is the Efficiency of Photosynthesis?" held in May 2009 in Albuquerque, New Mexico, sponsored by the Council on Chemical and Biochemical Sciences of the U.S. Department of Energy, Office of Science, Office of Basic Energy Sciences. The authors thank the members of the Council for their encouragement and assistance in developing this workshop. In addition, the authors are indebted to the agencies responsible for funding their individual research efforts, without which this work would not have been possible.

10.1126/science.1200165

Realizing artificial photosynthesis

Devens Gust,* Thomas A. Moore and Ana L. Moore

Received 9th September 2011, Accepted 12th September 2011

DOI: 10.1039/c1fd00110h

Artificial photosynthesis comprises the design of systems for converting solar energy into useful forms based on the fundamental science underlying natural photosynthesis. There are many approaches to this problem. In this report, the emphasis is on molecule-based systems for photochemical production of fuels using sunlight. A few examples of typical components of artificial photosynthetic systems including antennas, reaction centres, catalysts for fuel production and water oxidation, and units for photoprotection and photoregulation are presented in order to illustrate the current state of the field and point out challenges yet to be fully addressed.

Introduction

“On the arid lands there will spring up industrial colonies without smoke and without smokestacks; forests of glass tubes will extend over the plains and glass buildings will rise everywhere; inside of these will take place the photochemical processes that hitherto have been the guarded secret of the plants, but that will have been mastered by human industry which will know how to make them bear even more abundant fruit than nature, for nature is not in a hurry and mankind is” – Giacomo Ciamician (1912).¹ Realization of Ciamician’s dream, championed over the years by luminaries such as Melvin Calvin^{2–4} and George Porter,⁵ is increasingly urgent as the smokestack emissions threaten the climate worldwide and nations pay the price of vying with one another over dwindling fossil fuel supplies. The attraction is undeniable. Sunlight bathes the earth in energy at a rate 10 000 times greater than that at which humans use technological energy. Solar energy is available everywhere, completely sustainable, and in principle can be converted to forms that meet society’s needs in ways that are environmentally relatively benign. In practice, we are not there yet, but good progress is being made. Here, we will consider the requirements for efficient artificial photosynthesis, explore the current state of the problem, and speculate a bit on future directions. Although the examples of artificial photosynthetic systems referenced below come almost exclusively from our laboratories, thousands of artificial photosynthetic constructs have been reported over the last 30 years or so, and the field has developed due to the combined efforts of many laboratories worldwide. A variety of reviews are available.^{6–14}

What is artificial photosynthesis?

Although sunlight is abundant, light as such is a virtually useless form of energy, and must be changed to some other type. This is the role of photosynthesis: to convert sunlight into biologically useful energy such as electrochemical potential or protonmotive force and store it in fuels such as carbohydrate, lipids, or even hydrogen gas. In the broadest sense, artificial photosynthesis means exploiting the physics and chemistry underlying natural photosynthesis to harvest solar energy

Department of Chemistry and Center for Bio-Inspired Solar Fuel Production, Arizona State University, Tempe, AZ, 85202, USA. E-mail: gust@asu.edu

for technological purposes. The term has been applied to almost any method of and system for converting sunlight to another form of energy. Examples are photovoltaic cells based on inorganic semiconductors for electricity production, dye-sensitized solar cells, photovoltaics based on organic semiconductors, systems for fuel production based on these types of devices, a large variety of devices for direct photochemical conversion of light excitation energy to a fuel using organic or inorganic molecular photocatalysts, natural organisms or their components interfaced to synthetic materials, and combinations of these approaches. For the purposes of this discussion, we will consider artificial photosynthesis to be a process that uses molecular species to store energy from sunlight in a useful fuel. This is what natural photosynthesis does.

Before discussing the process of artificial photosynthesis, it is worth considering why we need solar fuels at all. Commercial photovoltaics, although currently too expensive to compete with fossil fuels in most places, are quite practical and readily available. However, they produce only electricity, and produce it only when illuminated. Because sunlight is available at most for just part of each day and electricity is not readily stored as such, some other form of energy storage is necessary. In addition, solar energy is diffuse. Practical land or air transportation using solar electricity directly is impossible because of the large surface areas that would be required. Energy storage could be mechanical, thermal, in chemical bonds or in batteries, but the very high energy density of hydrocarbon fuels helps explain their dominance in the transportation area. Thus, the preparation of fuels using sunlight is an important research area.

Fuel production requires more than just energy. Generally speaking, a useful fuel can be oxidized with oxygen from the air, with concomitant energy release. Thus, making a fuel requires a source of electrons and a material that can be chemically reduced with these electrons. If artificial photosynthesis is to contribute to filling society's energy needs on a large scale, the electrons must be obtained from water oxidation. This is the source used by green plant, algal and cyanobacterial photosynthesis. Water oxidation produces hydrogen ions, and reduction of these yields hydrogen gas, which is potentially a useful fuel whose oxidation in air regenerates water. The result is a sustainable cycle that is environmentally relatively benign and generates no by-products. Some living organisms produce and/or use hydrogen gas as a fuel. Alternatively, a carbon source such as carbon dioxide from the atmosphere can be reduced to a carbon-based fuel. Combustion of such a fuel regenerates carbon dioxide and water. This sustainable cycle is the one generally used by oxygenic photosynthesis, and is an attractive goal for artificial photosynthesis.

Artificial photosynthetic systems

A typical artificial photosynthetic design for water splitting, based on the natural paradigm, is shown schematically in Fig. 1. The design features four major components.

- *Antenna*. In natural photosynthesis, most of the sunlight is harvested by antenna systems. These are collections of chromophores that absorb light and transfer excitation energy among one another, and eventually to the next component, the reaction centre. Antennas collect light efficiently throughout the portion of the solar spectrum that is used by photosynthesis and deliver excitation energy to the reaction centre at an optimal rate for reaction centre function. Antenna systems are also involved in photoregulation and photoprotection of the photosynthetic apparatus. Artificial antennas can perform all these roles. They are likely to be necessary for artificial photosynthetic systems that can effectively harvest sunlight across the entire spectral range that is potentially useful for fuel production (from about 400 nm out to beyond 1000 nm).

- *Reaction centre*. In a reaction centre, excitation energy drives photoinduced electron transfer to an electron acceptor, thereby generating a charge-separated state

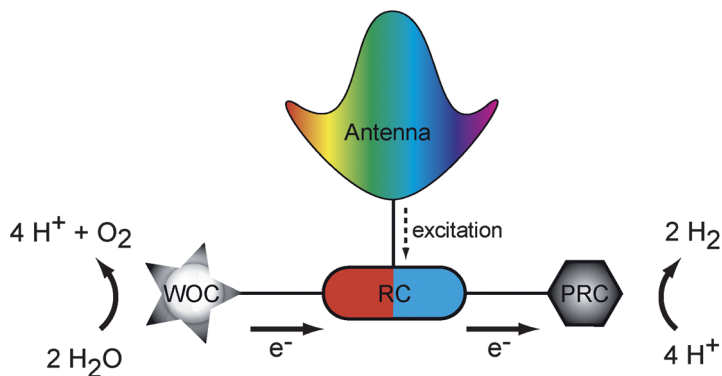


Fig. 1 Schematic representation of an artificial photosynthetic system for water splitting. An antenna absorbs sunlight and transfers excitation energy to a reaction centre (RC) which generates a charge separated state by photoinduced electron transfer. Electrons from the reaction centre enable reduction of hydrogen ions to hydrogen gas at the proton reduction catalyst (PRC). The oxidized reaction centre is regenerated by electrons from the water oxidation catalyst (WOC), which converts water to oxygen gas and hydrogen ions.

that preserves some of the photon energy as electrochemical potential energy. Thus, reaction centres are essentially nanoscale photovoltaic devices. Reaction centres reside in biological membranes and carry out charge separation across the thickness of the membrane. In effect, this places the reducing equivalents resulting from charge separation on one side of the membrane and the oxidizing equivalents on the other. These moieties can then drive fuel production. Artificial reaction centres carry out photoinduced charge separation, as do their natural counterparts. They need not reside in membranes, but they do need to be designed so that the charge separated states live long enough that their oxidizing and reducing power can be transferred to catalysts for fuel production.

- *Fuel production catalyst.* In photosynthesis, the reducing equivalents from the reaction centre are ultimately used to power the organism, and to store energy in the form of carbohydrate, lipid, hydrogen, or some other reduced material. A variety of catalysts (enzymes) are involved. A major challenge in artificial photosynthesis is to devise efficient, inexpensive catalysts for producing hydrogen, hydrocarbons, or other fuels.

- *Water oxidation catalyst.* Oxidizing equivalents from the reaction centre must be used to oxidize water to oxygen gas and hydrogen ions, and in the process rejuvenate the oxidizing side of the reaction centre. In photosynthesis, this is done by an oxygen evolving complex which contains four manganese atoms and a calcium atom at the active site. A structure of the oxygen evolving complex has recently been determined to high resolution by X-ray crystallography,¹⁵ but its mechanism of action whereby four oxidizing equivalents are accumulated and used to oxidize water is not yet well understood. The search for artificial water oxidation catalysts that are useful in artificial photosynthesis is very active.

A functional artificial photosynthetic device

Is it possible to design and prepare devices that functionally mimic the natural photosynthetic process? This can be done, although the systems prepared to date are far from optimal or practical. An example prepared in the laboratory of T. Mallouk is shown schematically in Fig. 2.¹⁶ The system is a photoelectrochemical cell for water splitting. The photoanode, immersed in water, features a nanoparticulate titanium dioxide electrode such as those used in dye sensitized solar cells.¹⁷ The titanium dioxide is a wide band gap semiconductor that does not absorb visible light. Its

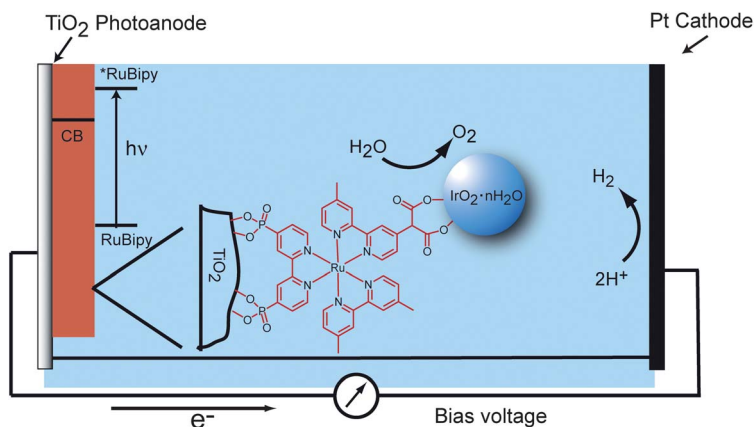


Fig. 2 A photoelectrochemical water splitting cell. The nanoparticulate TiO_2 photoanode is sensitized with a ruthenium complex that also binds an iridium oxide nanoparticle. The excited ruthenium complex injects electrons into the TiO_2 , from whence they travel to the cathode and reduce hydrogen ions to hydrogen gas when a small bias voltage is applied. The oxidized ruthenium complex in turn oxidizes an iridium oxide nanoparticle that serves as a water oxidation catalyst.

mesoscopic nature provides a large surface area exposed to the solution. The electrode surface is coated with a ruthenium-based chromophore that does absorb visible light. Excitation of the ruthenium complex generates an excited state that injects an electron into the TiO_2 , leading to charge separation. Thus, the ruthenium complex and TiO_2 mimic the functions of the natural photosynthetic antenna (light absorption) and reaction centre (photoinduced electron transfer). Oxidizing equivalents on the oxidized ruthenium complex are then transferred to an attached iridium oxide nanoparticle, regenerating the original ruthenium complex. The IrO_2 accumulates the oxidizing equivalents as additional photons are absorbed by the ruthenium complex. It has been known for some time that IrO_2 is a good water oxidation catalyst.¹⁸ In the cell, oxygen is evolved from the nanoparticles when the photoanode is illuminated. The electrons injected into the TiO_2 by the ruthenium complex migrate to an underlying indium tin oxide transparent conductive electrode, and hence to a platinum cathode, where hydrogen ions are reduced to hydrogen gas. Because the open circuit voltage of the cell is only about 1 V, an external bias of a few hundred mV is required to observe oxygen and hydrogen formation.

The device shown in Fig. 2 demonstrates conclusively that artificial photosynthesis can work. It is also an excellent embodiment of the problems that must be overcome if artificial photosynthesis is to become practical for solar energy conversion. The problems arise because none of the components of the system are optimized.

- *Antenna function.* The quantum yield of water splitting is only $\sim 0.9\%$, and the solar conversion efficiency is much smaller. One reason for this is that the ruthenium complex does not absorb light effectively at wavelengths longer than 500–550 nm. Thus, much of the solar spectrum is wasted.

- *Reaction centre function.* Although electron injection from the ruthenium complex into the TiO_2 is efficient, recombination of the resulting charge separated state by migration of an electron back to the oxidized ruthenium complex is rapid ($\tau = 0.37$ ms) compared to the rate of electron transfer from the IrO_2 particle to the oxidized chromophore ($\tau = 2.2$ ms). The rapid charge recombination may also be partially responsible for the fact that a small bias potential must be applied to the cell in order to observe hydrogen production. In addition to this kinetic problem, there is a thermodynamic shortcoming. The conduction band of TiO_2 is not positioned correctly for efficient reduction of hydrogen ions.

- *Proton reduction catalyst.* Platinum is a good catalyst, with low overpotential (activation energy) and rapid turnover for proton reduction to hydrogen gas, but it is a rare and expensive element. Solar fuel production on the scale of human energy usage (~ 15 TW) will not be possible unless cheaper, more abundant catalysts are identified.

- *Water oxidation catalyst.* Although IrO_2 is an effective and stable water oxidation catalyst, it does require significant overpotential, and iridium is the least abundant element on earth. Thus, IrO_2 is not suitable for large scale solar water oxidation systems.

- *Stability.* The ruthenium dye decomposes under irradiation, presumably due to nucleophilic attack on the oxidized dye. Practical solar fuel production systems must have long service lives.

Designing artificial photosynthetic systems

The solar water splitting system described above illustrates most of the major problems faced in designing artificial photosynthetic systems. Natural photosynthesis suggests possible solutions to all of these problems. Below, we will discuss each component of an artificial photosynthesis system, and illustrate some of the important principles that have emerged from the study of both artificial and natural photosynthesis.

Antennas. The chlorophylls found in the reaction centres of organisms that carry out oxygenic photosynthesis typically absorb sunlight at wavelengths shorter than ~ 680 nm. These wavelengths carry about 45% of the solar energy reaching the earth. The ruthenium complexes and porphyrins often used in artificial photosynthesis are generally limited to these or shorter wavelengths. Silicon solar cells, on the other hand, function with light to about 1100 nm, and can absorb about 76% of the total energy of sunlight. Moreover, silicon absorption is well-matched to the theoretical best absorption range for a single junction photochemical solar energy converter.¹⁹ The efficiency of artificial (and natural) photosynthesis is limited by the narrow wavelength range over which light is absorbed. In addition, most chromophores such as chlorophylls, porphyrins and ruthenium complexes do not have high extinction coefficients at all wavelengths within their spectral ranges. How can these problems be addressed?

Photosynthetic organisms achieve efficient absorption of sunlight in the visible and to wavelengths as long as 680 nm in two ways. First, they use antennas containing many chlorophyll molecules to absorb sunlight and deliver it to each reaction centre *via* singlet-singlet energy transfer, thus in effect increasing the absorption cross section of the reaction centre. Secondly, they employ auxiliary chromophores such as carotenoid polyenes, phycoerythrins, and phycocyanins to absorb light in regions where chlorophyll is not a strong absorber and transfer the energy to chlorophylls and eventually to the reaction centre.

Similar strategies can be employed in artificial photosynthesis. An example is molecule **1** (Fig. 3), which consists of a rigid hexaphenylbenzene core that organizes a set of antenna chromophores.²⁰ The two bis(phenylethynyl)anthracene (BPEA) moieties absorb in the blue spectral region around 430–475 nm. The two boron-dipyrromethene (BDPY) chromophores absorb strongly in the 475–530 nm region. The two zinc porphyrins absorb in the 420 nm (Soret band) region, with less intense Q-band absorption in the red region out to about 660 nm. Thus, the three kinds of chromophores together cover the visible spectrum out to about 660 nm. Time resolved spectroscopic studies show that both the BPEA and BDPY excited states transfer singlet excitation energy to the porphyrins with time constants ≤ 15 ps and quantum yields $\geq 96\%$. Energy transfer occurs both by hopping of excitation from one chromophore to another *ortho* to it, and by direct transfer across the central ring of the hexaphenylbenzene. Thus, the auxiliary chromophores are highly

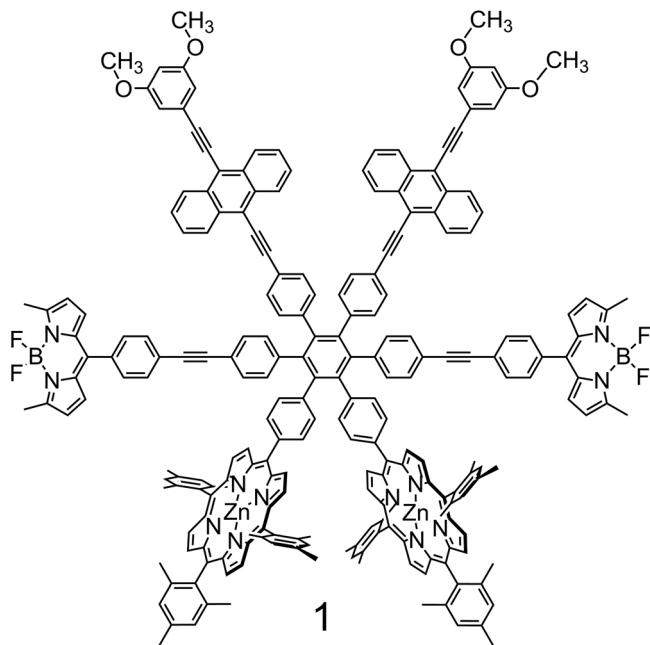


Fig. 3 Artificial photosynthetic antenna **1**, which consists of two bis(phenylethynyl)anthracenes, two borondipyromethenes, and two zinc porphyrins, all organized by a hexaphenylbenzene core.

efficient antennas for the porphyrins. This efficiency was obtained by tuning both the thermodynamics of the various energy transfer steps and the chromophore separations and orientations in accord with the Förster energy transfer theory.^{21,22} Once the excitation energy is localized on the porphyrins, it can be used to initiate photoinduced electron transfer in an artificial reaction centre. In **1**, this has been achieved by self-assembly of a fullerene electron acceptor bearing two pyridine coordination groups to the two zinc porphyrins.²⁰

It was mentioned above that photosynthesis and many artificial photosynthetic systems only absorb light at wavelengths $< \sim 700$ nm, and that this also limits efficiency. One obvious solution to this problem is to use chromophores with absorptions at longer wavelengths. This approach has proven useful in artificial photosynthetic constructs based on both ruthenium complexes and cyclic tetrapyrroles. However, the strategy has limitations with regard to water splitting. Thermodynamically, conversion of water to hydrogen and oxygen requires 1.23 eV. This corresponds to photons at ~ 1000 nm. However, kinetics imposes much more restrictive limits on the process. Separating charge rapidly enough to compete with relaxation of excited states by other mechanisms requires significant thermodynamic driving force, and prevention of rapid charge recombination to yield either the ground state or original excited state necessitates the sacrifice of additional energy. In addition, catalysts for water oxidation and for proton reduction require overpotential (activation energy) in order to function. These energetic considerations require photons of significantly more than 1.2 eV to actually perform water splitting.

One potential strategy for achieving efficient water splitting while still using photons of wavelengths as long as 1000 nm is to design a tandem artificial photosynthetic cell. The tandem arrangement uses two photosystems, and thus two photons to generate the electrochemical potential necessary for water splitting, and has been implemented in systems based on inorganic semiconductors.²³ In such an artificial photosynthetic device, one antenna-artificial reaction centre, absorbing from, say,

400 nm to 700 nm, would be used to generate the redox potential necessary to oxidize water at a catalyst. A second photosystem, electrochemically in series with the first and absorbing in the 700–1000 nm spectral region, would generate the potential necessary to drive catalytic hydrogen ion reduction to hydrogen gas.

Natural oxygenic photosynthetic organisms do in fact use two photosystems operating in series, but the absorption spectra of these photosystems overlap, rather than complement one another, the potentials generated by the two photosystems do not add linearly, and only photons of wavelengths of ~ 680 nm or shorter contribute to photosynthesis. It has been suggested that this apparent inefficiency in the natural system could be addressed by clever synthetic biology.²⁴

Artificial reaction centres. In the reaction centre, excitation energy resulting from light absorption or singlet energy transfer from antennas initiates photoinduced electron transfer to generate a charge-separated state that stores some of the photon energy as electrochemical potential energy. As described by theories originated by Marcus,^{25,26} Hush,^{27,28} and Levich²⁹ and since expanded upon by many researchers, photoinduced electron transfer rates are functions of thermodynamic driving force, solvent and internal reorganization energies, temperature, and the electronic coupling between the initial and final states. The coupling is related to the orbital overlap between donor and acceptor orbitals and therefore the donor–acceptor separation, among other factors. Thus, when designing artificial reaction centres, some relevant factors are the match between the absorption spectrum of the chromophore and the solar spectrum, the energies of the excited state and various charge-separated states, reorganization energies, and the electronic interaction between donor and acceptor. One of the best ways to control this electronic interaction is by covalent linkage of the donor and acceptor. In such situations, the electronic coupling interactions usually occur *via* the chemical bonds of the linkage, rather than simply through the space between moieties. Initial artificial reaction centre research was performed using covalently linked porphyrin–quinone dyads in which the porphyrin excited singlet state donates an electron to the quinone acceptor.^{31,32} However, a relatively large number of donor and acceptor moieties have now been investigated.

Molecular triad **2** (Fig. 4) is an example of an artificial reaction centre.³⁰ It consists of a hexaphenylbenzene bearing two porphyrin electron donor moieties and a fullerene electron acceptor in a macrocyclic arrangement involving a ring of 42 atoms. The two porphyrins are closely spaced, in an arrangement reminiscent of that of the special pair of bacteriochlorophyll molecules in bacterial photosynthetic reaction centres. The molecule is produced by an unusual cyclization reaction that yields mainly a product with C_2 symmetry and *trans*-2 disubstitution at the fullerene. The macrocycle maintains a rigid, highly-constrained structure which in turn establishes a fixed electronic coupling among the components.

Excitation of a porphyrin generates the first excited singlet state $^1\text{P-C}_{60}\text{-P}$. In 2-methyltetrahydrofuran solvent, very rapid photoinduced electron transfer from the porphyrin to the fullerene ($\tau = 1.1$ ps) yields a charge-separated state $\text{P}^+\text{-C}_{60}^-\text{-P}$. The same state is produced by light absorbed by the fullerene moiety ($\tau = 15$ ps). The electron transfer rate constants are much larger than the rates for decay of $^1\text{P-C}_{60}\text{-P}$ and $\text{P-}^1\text{C}_{60}\text{-P}$ by other pathways (2.2 ns and 1.2 ns, respectively), so the quantum yield of charge separation from either excited state is essentially unity. The charge separated state has a lifetime of 2.7 ns. Cyclic voltammetric measurements allow estimation of the energy of $\text{P}^+\text{-C}_{60}^-\text{-P}$ as 1.46 eV. The energies of $^1\text{P-C}_{60}\text{-P}$ and $\text{P-}^1\text{C}_{60}\text{-P}$ are 2.06 eV and 1.71 eV. Thus, the charge-separated state retains a reasonable fraction of the photon energy.

Note that charge recombination in **2** is over 2000 times slower than charge separation. Covalently linked porphyrin–fullerene artificial reaction centres, which have been studied since the mid 1990s,³³ typically demonstrate rapid charge separation and slow recombination relative to many other types of artificial reaction

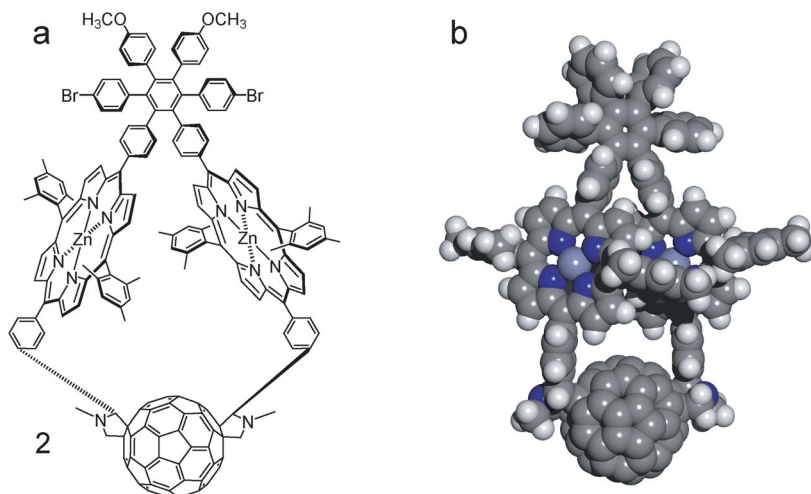


Fig. 4 Triad artificial reaction centre **2**, wherein a hexaphenylbenzene bears two zinc porphyrins which in turn are linked to the same fullerene derivative. (a) Chemical structure. (b) Molecular model in which the bromine and methoxy groups have been replaced by hydrogen in order to facilitate calculations.³⁰

centres due to their small reorganization energies for electron transfer.^{34–36} A small reorganization energy for electron transfer tends to locate the photoinduced electron transfer reaction in a part of the “normal” region of the Marcus rate vs. free-energy-change relationship where electron transfer is rapid, and the charge recombination to the ground state in a part of the “inverted” region where transfer is slow.

Although charge recombination in **2** is slow relative to charge separation, the lifetime of the charge separated state is still rather short relative to the time scales required for molecular diffusion or other processes that might be used to harvest the chemical potential of the charge separated state and use it to make a fuel. Natural reaction centres face the same dilemma: photoinduced charge separation must be rapid to compete with decay of excited states by other pathways, but the electronic coupling necessary for such rapid charge separation also leads to rapid charge recombination. Photosynthetic organisms have solved this problem using a multistep electron transfer strategy. Following the initial photoinduced electron transfer event, the electron is moved through a series of intermediate donor–acceptor moieties before reaching the final acceptor. Each step in this electron transfer cascade is rapid due to relatively strong electronic coupling within each donor–acceptor pair. However, at the end of the process, the electron and hole (which has remained on the original chlorophyll donor or migrated to a nearby moiety) are spatially well separated, the electronic coupling between them is weak, and the lifetime of the state is long.

This multistep electron transfer strategy has been demonstrated in artificial reaction centres since the mid 1980s.^{37–39} A more modern example of its application is molecular triad **3** (Fig. 5).⁴⁰ The molecule consists of a porphyrin light absorber and primary electron donor linked to both a fullerene electron acceptor and a carotenoid secondary donor. Excitation of the porphyrin leads to formation of the first excited singlet state, C⁻¹P-C₆₀. In the absence of photochemistry, this singlet state would decay in about 10 ns (step 1 in Fig. 5b), but in the triad it decays in 32 ps in 2-methyltetrahydrofuran at ambient temperatures to yield the C-P⁺-C₆₀⁻ charge separated state with at quantum yield of essentially unity (step 2). This state can decay to the ground state with a time constant of 3.3 ns (step 3). However, electron transfer from the carotenoid to the porphyrin radical cation (step 4, sometimes

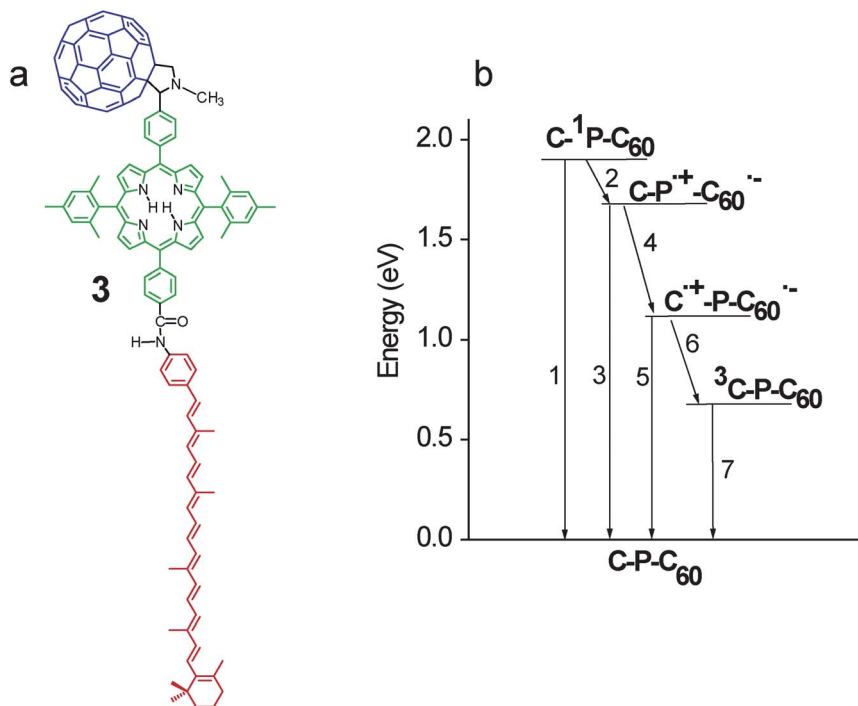


Fig. 5 Carotene–porphyrin–fullerene triad **3**. (a) Structure of the triad. (b) Transient states of the triad and the relevant interconversion pathways. The state energies are estimated from spectroscopic and cyclic voltammetric data. The energy of ^3C in this molecule is not known, but is substantially below that of singlet oxygen at about 1 eV.

referred to as hole transfer) is much faster ($\tau = 125$ ps). This charge shift reaction produces a final $\text{C}^+\text{-P-C}_{60}^-$ charge separated state with an overall quantum yield of 95%, based on light absorbed by the porphyrin. The $\text{C}^+\text{-P-C}_{60}^-$ state stores about 1.0 eV of the photon energy, and has a lifetime of 57 ns. It could in principle decay to either the ground state (step 5) or to yield the carotenoid triplet state, which lies at lower energy than the charge-separated state (step 6). In 2-methyltetrahydrofuran, most of the decay yields the carotenoid triplet, but the partitioning between the two pathways depends upon the solvent and temperature.^{41,42} The $^3\text{C-P-C}_{60}$ has a lifetime of 4.7 μs (step 7) in the absence of oxygen. At low temperatures, the lifetime of $\text{C}^+\text{-P-C}_{60}^-$ increases to several hundred ns. At all temperatures, the lifetime of $\text{C}^+\text{-P-C}_{60}^-$ is very sensitive to small magnetic fields.^{41–43} Magnetic field dependence of the lifetimes of charge-separated states has been observed in photosynthetic reaction centres, and may play a role in the navigation of birds and other animals.⁴¹

Triad **3** illustrates the multistep electron transfer route for obtaining long-lived charge-separated states. Over the last 25 years, many examples of the application of these ideas have been reported, and energetic charge separated states with lifetimes of hundreds of μs or even a few ms have been reported.^{6–14} In principle, such lifetimes allow ample time for harvesting the stored energy by chemical reactions.

Electron transfer reactions can be facilitated by coupling the electron transfer to proton movement. The effect has been observed in porphyrin-quinone triad molecules,^{44,45} and proton coupled electron transfer^{46–48} can be especially useful for coupling the charge-separated states formed by reaction centres to catalysts for water oxidation or fuel generation. For example, the transfer of an electron necessarily increases negative charge on the acceptor and decreases negative charge on the donor. Compensation of this charge by accompanying proton transfer can lower

product energies and activation energies. In photosystem II of oxygenic photosynthesis, a photo-oxidized reaction centre $P680^+$ in turn oxidizes the oxygen-evolving complex, which is the catalyst for water oxidation. A tyrosine residue in the protein is thought to serve as a redox mediator between these two species. The $P680^+$ oxidizes this tyrosine, and during this process, a phenolic proton is transferred to a hydrogen-bonded histidine residue. This change in the protonation state of the tyrosine is thought to facilitate electron transfer by poisoning the redox of the tyrosine between that of $P680^+$ and the manganese cluster in the oxygen evolving complex.

The synthetic system illustrated in Fig. 6 mimics this part of the natural photosynthetic electron flow.⁴⁹ Molecule **4** consists of a porphyrin chromophore and primary electron donor (PF₁₀) linked to a benzimidazole bearing a phenol (BiP). The phenolic proton bound to oxygen is also hydrogen bonded to one of the nitrogen atoms of the benzimidazole. Although in general phenols are difficult to oxidize and show irreversible electrochemical behaviour in cyclic voltammetry, the phenol-benzimidazole moiety of **4** shows quasi-reversible electrochemistry and is oxidized at a potential whereby it can act as an electron donor to the porphyrin radical cation of **4**. Compound **4** is designed such that when adsorbed to a TiO₂ nanoparticle (Fig. 6) and excited with visible light, rapid photoinduced electron transfer occurs from the porphyrin excited singlet state (¹PF₁₀) into the conduction band of the attached semiconductor. The BiP is thermodynamically poised (1.00 V vs. SCE) to quench the resulting high-potential porphyrin radical cation (PF₁₀^{•+}) (1.35 V vs. SCE) via a secondary electron transfer, yielding the final charge separated state (BiP^{•+}-PF₁₀⁻-TiO₂⁻). In EPR experiments, porphyrin excitation with light was found to result in transfer of an electron to the TiO₂ particle, and localization of 95% of the positive charges on the phenol/benzimidazole BiP moiety, in accord with this design. These holes are thermodynamically capable of water oxidation, and constructs similar to **4** may therefore be useful in artificial photosynthetic systems for water splitting.

Fuel production catalyst. The proton reduction catalyst used in the device shown in Fig. 2 is platinum, which is an excellent catalyst that functions at low overpotential. Platinum, however is too rare and expensive for use in very large scale artificial photosynthetic systems for hydrogen production. Living organisms carry out hydrogen production and oxidation using hydrogenase enzymes, which have catalytic sites that contain iron, or iron and nickel atoms. These catalysts function at overpotentials as low as or lower than that of platinum, and some of them have

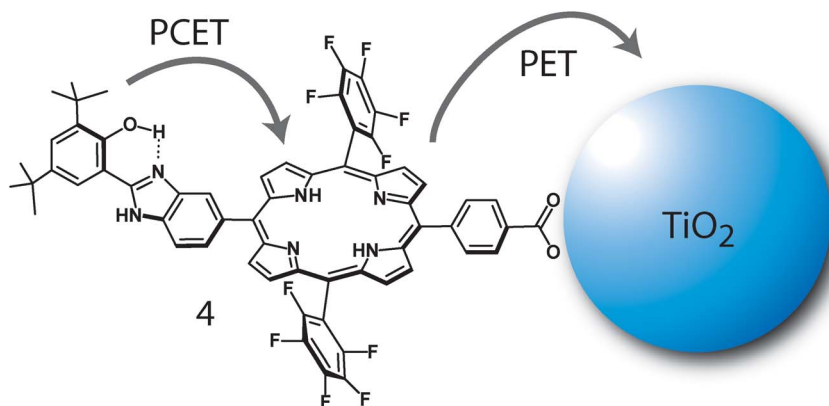


Fig. 6 A synthetic model system for photoinduced electron transfer (PET) and proton coupled electron transfer (PCET) as is observed in photosynthetic water oxidation.

very rapid turnover rates.⁵⁰ Thus, nature has proven that rare metals are not required for active proton reduction catalysts.

It is possible to use hydrogenases directly as catalysts in artificial photosynthesis. An example is shown in Fig. 7.⁵¹ In this photoelectrochemical cell, two electrodes are immersed in a buffer solution. The photoanode is the same type of nanoparticulate TiO_2 electrode used in the water splitting cell shown in Fig. 2. However, the sensitizer is 5-(4-carboxyphenyl)-10,15,20-tris(4-methylphenyl)porphyrin. When the transparent photoanode is illuminated, the porphyrin excited singlet states inject electrons into the TiO_2 , from whence they flow to a cathode consisting of a microporous carbon support to which is adsorbed an [Fe-Fe]-hydrogenase, *CaHydA* from *C. acetobutylicum*. The enzyme is electrically connected to the supporting electrode, and electrons flowing from the TiO_2 photoanode are used by the hydrogenase to produce hydrogen gas, which bubbles off the enzyme-bearing electrode. Meanwhile, the oxidized porphyrin on the photoanode is regenerated by electron donation from nicotinamide adenine dinucleotide in its reduced form (NADH). After two electron donations, NADH is converted to NAD^+ with concomitant release of a hydrogen ion. In this construct, the biofuel NADH provides electrons, a proton and some of the potential energy needed for hydrogen production. The remaining energy necessary to overcome overpotentials and make hydrogen is provided by light. In this cell, platinum cathodes and enzymatic cathodes produced hydrogen at comparable rates.^{51,52}

The NADH is, of course, not a useful biofuel, but if a fuel such as methanol, ethanol or glucose and a suitable dehydrogenase enzyme are added to the photoanode solution of such a cell, the dehydrogenase regenerates NADH by reduction of the coenzyme NAD^+ and oxidizes the biofuel substrate.⁵³ For example, methanol has been oxidized to carbon dioxide in such a cell using a suitable enzyme system.

Hydrogenases are relatively large, complex enzymes, and are sensitive to deactivation by oxygen. Thus, they are not ideal catalysts for artificial photosynthetic

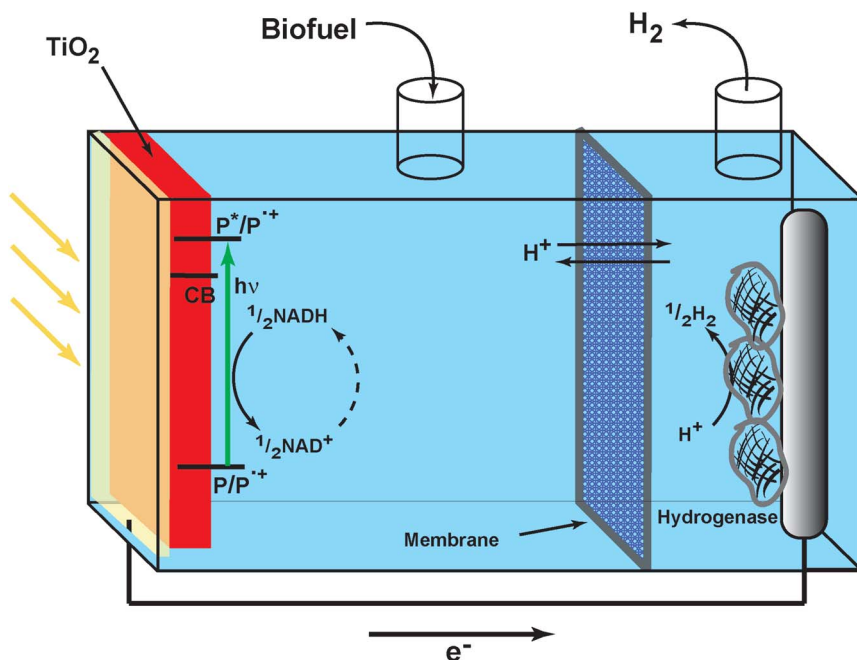


Fig. 7 Photoelectrochemical biofuel cell for producing hydrogen gas from a biofuel. The NADH biofuel shown here can be regenerated through addition of a dehydrogenase enzyme and a more traditional biofuel such as methanol, ethanol or glucose.

hydrogen production. There have been many attempts to produce analogs of the hydrogenase active site and hundreds of these are known, although their activity varies.⁵⁴ A variety of other catalytic materials for hydrogen production are also being investigated, and much progress is being made. However, the *ideal* proton reduction catalyst which uses inexpensive and abundant elements, is stable, and operates with high turnover rate near the thermodynamic potential for the hydrogen production/oxidation redox couple has not yet been discovered.

Water oxidation catalyst. Water oxidation catalysts based on iridium oxide, platinum, ruthenium complexes and other rare and expensive elements sometimes work well, but are not practical for very large-scale use. They may be useful for smaller, specialty applications. Catalysts that use abundant, inexpensive elements are, of course, more desirable. Here again, natural photosynthesis demonstrates that such catalysts are possible. The oxygen evolving complex found in oxygenic photosynthesis includes four manganese atoms and a calcium atom coordinated by the amino acid side chains of the surrounding protein.¹⁵ This complex is clearly a successful catalyst, as it provides the energetic electrons that power nearly all life, has operated successfully for several billion years, and is responsible for the oxygenated atmosphere of the earth. The development of artificial water oxidation catalysts that employ abundant elements is a very active research field, but as yet an inexpensive, robust catalyst that functions with very little overpotential (and is therefore reversible) has yet to be discovered. Cobalt oxide materials appear to be very promising,^{55–57} and preliminary results with manganese^{58,59} and other metal⁶⁰ oxides are intriguing.

Photoprotection. The high energy of visible photons, the photochemical reactivity of biomolecules, and the necessity to perform at least parts of photosynthesis in an oxygenated environment raise questions of stability in both natural and artificial photosynthesis. Indeed, photosynthetic organisms do suffer photodamage, and as a result have developed various photoprotection and repair mechanisms. It seems probable that artificial photosynthetic systems could benefit from photoprotection as well. The research effort devoted to mimicking photoprotection has been small compared to that expended in developing functional artificial photosynthetic reaction centres and catalysts, but some progress has been made. As with the other aspects of artificial photosynthesis discussed above, the natural process can provide useful paradigms.

Much of the photodamage in photosynthesis occurs when the photon flux causes the initial events of photosynthesis to occur more rapidly than later, dark reactions can use the redox potential produced. If the high-energy intermediates resulting from photoinduced electron transfer are not rapidly consumed to further the normal photosynthetic chemistry, they will react with other components of the organism, causing photodamage.

One example is found in reaction centres, where the result of stepwise photoinduced electron transfer is a chlorophyll radical cation and a reduced quinone. In the normal course of events, the reduced quinone leaves the reaction centre and is replaced prior to new photoinduced electron transfer events. However, at high light levels the initial steps of charge separation can recur before replacement of the reduced quinone. Thus, the electron produced by photoinduced electron transfer cannot migrate completely down the redox chain, and instead recombines with the oxidized chlorophyll to generate a chlorophyll triplet state. Chlorophylls, porphyrins and many other chromophore triplet states are excellent sensitizers for production of singlet oxygen from ground-state oxygen by an energy transfer process. If this occurs in the reaction centre, the singlet oxygen attacks lipids and other tissues, causing photodamage.

Photosynthetic organisms limit such photodamage by using carotenoid polyenes as photoprotective agents. The carotenoids rapidly quench chlorophyll triplets by triplet–triplet energy transfer, generating low-energy carotenoid triplet states which cannot sensitize singlet oxygen production and decay to the ground state within

a few μs with the liberation of heat. Carotenoids can also quench singlet oxygen after it has been formed, further limiting tissue damage.

These photoprotective effects of carotenoid polyenes were first mimicked in molecular constructs for artificial photosynthesis some time ago.^{61–66} For example, carotenoporphyrin (C–P) **5** (Fig. 8) features a carotenoid polyene (C) linked to a tetra-arylporphyrin (P) *via* an amide group.⁶³ In deoxygenated toluene solution, excitation of the porphyrin moiety with a laser pulse at 590 nm generates the porphyrin excited singlet state C¹P. Time-resolved fluorescence studies show that this state decays with a time constant of 5.2 ns. One of the products of this decay is the porphyrin triplet state, C³P. In general, porphyrin triplet states are excellent singlet oxygen sensitizers. However, in **5**, transient absorption studies with excitation of the porphyrin at 650 nm show that C³P is converted into the carotenoid triplet state ³C–P by triplet–triplet energy transfer with a time constant smaller than the time resolution of the spectrometer ($\tau < 10$ ns). It may in fact be that the rate constant for triplet energy transfer is greater than that for decay of the porphyrin singlet state. The ³C–P state decays to the ground state with a time constant of 5.7 μs in the absence of oxygen. Because C³P is quenched much more rapidly by energy transfer to the carotenoid than by diffusional quenching by molecular oxygen in oxygenated solutions, this carotenoporphyrin cannot generate singlet oxygen, and is photoprotected. Triplet–triplet energy transfer requires orbital overlap of the chromophores, and the dependence of the transfer rate on the nature of the linkage between the carotene and porphyrin and on the presence or absence of intramolecular motions is strong, as discussed in the articles referenced above.

Another type of photoprotection found in photosynthetic organisms is non-photochemical quenching (NPQ). Under low light conditions, the organism tunes its systems to maximize light absorption and photosynthetic yield. If ambient light levels increase, overdriving of photosynthesis can lead to the build-up of toxic intermediates that destroy vital cellular components. Plants limit such damage by down-regulating the fraction of absorbed light energy available for photosynthesis in the reaction centre as light levels increase.

In cyanobacteria, NPQ is thought to involve orange carotenoid protein (OCP) in the phycobilisome antennas that provide excitation energy for water oxidation.^{67,68} The OCP exists in a thermally stable form that absorbs blue-green light, and has no effect on the singlet excited states of chlorophylls. However, light absorption by the carotenoids of these proteins leads to structural changes, producing a

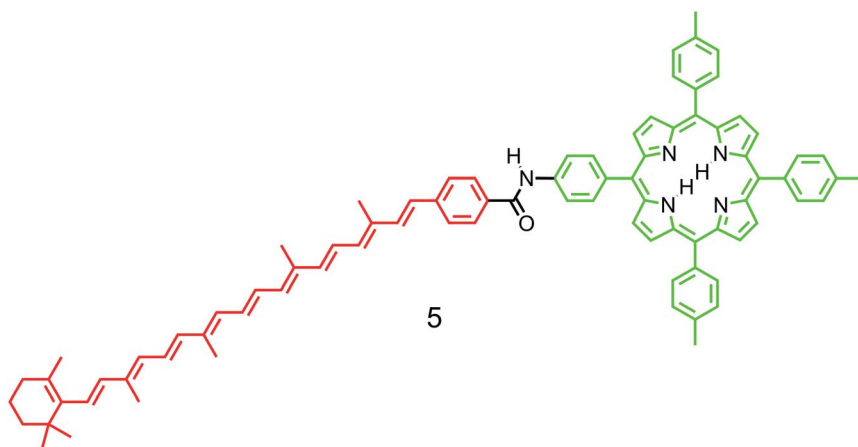


Fig. 8 A covalently linked carotenoporphyrin dyad that demonstrates photoprotection from singlet oxygen damage *via* rapid quenching of the porphyrin triplet state by the carotenoid through triplet–triplet energy transfer.

red-light-absorbing form that can thermally revert to the stable form. This red form of the protein quenches chlorophyll excited singlet states, preventing them from transferring excitation energy to reaction centre chlorophylls where photoinduced electron transfer occurs. The ratio of the two forms of OCP is controlled by the intensity of blue-green light and the temperature, and therefore at high light levels photosynthesis is down regulated.

A synthetic molecule that mimics this process has been reported.⁶⁹ Pentad **6** (Fig. 9a) includes five photochemically active components. The central porphyrin (P) is linked to a fullerene electron acceptor (C₆₀) and two BPEA antennas. In addition, it bears a quinoline-derived dihydroindolizine photochrome (DHI). The closed, spirocyclic form of the photochrome (see **6c**) is the thermodynamically more stable isomer. Thermal isomerization at ambient temperatures favours this form of the molecule, in which the DHI has no effect upon the photochemistry of the rest of the pentad. The open, betaine isomer (BT, see structure **6o**) is generated by photoisomerization initiated by light absorption in the UV and blue light portions of the spectrum. The absorption spectrum of BT and its spatial arrangement relative to the remainder of the molecule are tuned so that it can rapidly quench the excited states of the porphyrin and BPEA antennas by singlet-singlet energy transfer.

The pentad behaves in the following way. At relatively low intensities of white light irradiation of **6** in 2-methyltetrahydrofuran solution, the BPEA moieties absorb in the 430–475 nm region and efficiently ($\Phi = 1.0$) transfer excitation energy to the porphyrin ($\tau = 4.0$ ps) to yield the porphyrin first excited singlet state. The porphyrin excited state, formed by energy transfer or by direct absorption of light, decays by photoinduced electron transfer to the fullerene ($\tau = 2.4$ ns) to yield the P⁺-C₆₀⁻ charge-separated state with a quantum yield of 0.82. The charge separated state has a lifetime of 14.0 ns. Thus, the molecule acts as a typical artificial photosynthetic antenna–reaction centre unit, and the DHI moiety has no influence. As the light intensity is increased, an increasing fraction of the sample is in the betaine form (**6o**). In **6o** the lifetime of the porphyrin first excited singlet state is reduced to 33 ps due to singlet-singlet energy transfer to the BT. This quenching reduces the quantum yield of the P⁺-C₆₀⁻ state to only 1%.

The photochemistry of **6** allows it to act as an adaptive, self-regulating molecular nonlinear transducer that functionally mimics the role of the orange carotenoid protein in cyanobacteria. This is illustrated in Fig. 9b. Along the abscissa are plotted the results of experiments carried out on a solution of **6** in deoxygenated 2-methyltetrahydrofuran. Each point was obtained after 20 s of white light illumination of the solution of **6c** at relative intensities indicated by the open circles. The

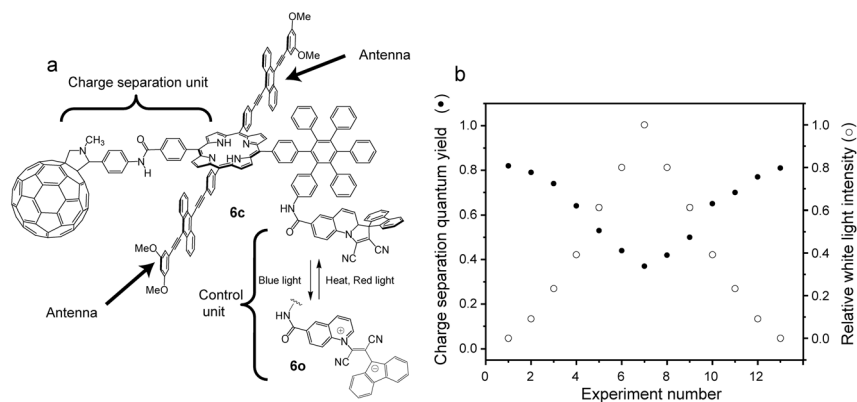


Fig. 9 (a) Self-regulating artificial photosynthetic reaction centre. (b) Quantum yield of charge separation in **6** (solid circles) at different light intensities (open circles).

fluorescence emission from the porphyrin, excited at 480 nm, was immediately measured at each point, and the quantum yield of charge separation was determined (solid circles). Due to the increasing fraction of **6** present in the quenched form **6o** as the light level is increased, the quantum yield of charge separation decreases smoothly as the white light intensity increases, dropping from 82% at low light levels to 37% at the highest levels of white light employed in this particular experiment. When the white light intensity is reduced, the quantum yield rises, eventually returning to its initial value at low light.

Another kind of NPQ is found in green plants. A consequence of photoinduced electron transfer in reaction centres is release of protons into the thylakoid lumen, leading to a pH and charge gradient (membrane potential $\Delta\Psi$) across the photosynthetic membrane. The chemical potential stored in this gradient powers many of the subsequent reactions of energy conversion. At high light levels the lumen pH drops, signalling that electron transfer, which produces reactive high-energy intermediates, is outpacing the fuel-producing reactions that consume the pH gradient. Low pH activates NPQ, which down regulates reaction centre function by converting excitation energy into heat before it can reach the reaction centre and initiate electron transfer. The process by which this occurs is not fully understood, but is known to involve chemical modification of a carotenoid polyene. The modified polyene quenches chlorophyll excited states, possibly by electron and/or energy transfer.^{68,70–75} Recently, the formation of short-lived exciton states has been proposed as a mechanism of NPQ in some natural and artificial antenna systems.^{66,76}

Synthetic hexad **7** (Fig. 10) functionally mimics the role of the antenna system in green plant NPQ.⁷⁷ The molecular hexad comprises five zinc porphyrins and a pH-sensitive dye organized by a hexaphenylbenzene core. When the hexad is dissolved in an organic solvent, the zinc porphyrin antenna moieties absorb light, rapidly exchange excitation energy, and ultimately decay by normal photophysical processes ($\tau = 2.1$ ns). The dye moiety is in the spirocyclic form (see **7c**) which does not absorb light in the visible and has no effect on the porphyrin artificial antenna system. The zinc porphyrin excited state lifetimes are long enough to permit harvesting of the excitation energy for photoinduced charge separation or other work. However, when acid is added, the dye moiety is converted to the open form (in **7o**), which rapidly ($\tau < 40$ ps) quenches all of the porphyrin excited states, converting the excitation energy to heat and rendering the porphyrins kinetically incompetent to readily perform useful photochemistry. The hexad is functionally analogous to NPQ in the antenna, but does not mimic the role of the reaction centre in producing a proton gradient.

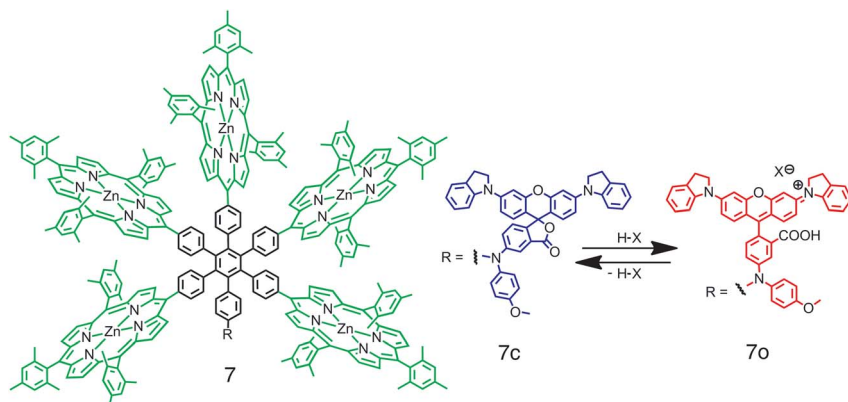


Fig. 10 Acid-regulated artificial photosynthetic antenna. The pH-sensitive dye moiety is converted from the spirocyclic form in **7c** to the open, protonated form in **7o** by addition of an acid H-X. In **7o**, the dye rapidly quenches the excited singlet states of all of the porphyrins.

Device design. Useful artificial photosynthesis requires not only design of suitable components for a fuel production system as discussed above, but also ultimately combining these components in a functional overall system or device. The system must be optimized for sunlight collection, transport of electrons from reaction centres to fuel production catalysts, transport of oxidizing equivalents from reaction centres to water oxidation catalysts, accumulation of oxidation and reduction equivalents for the necessary multielectron processes, separation and removal of products, prevention of charge recombination and other energy wasting reactions, overall efficiency and ultimately stability and cost. Investigating such systems engineering requires complete fuel production devices such as that shown in Fig. 2, and artificial photosynthesis research is only recently reaching the stage of maturity that will permit investigation of these considerations. Thus far, most research has focused mainly on the individual components of a system.

In this connection, there are two extremes in the design spectrum. The first is a modular approach: the development of discrete reaction centres and catalysts, with electrical connections between them made by conventional conductors or semiconductors. The second approach is monolithic, wherein integrated nanoscale devices carry out light absorption and oxidative and reductive catalysis. The modular approach has the advantage that individual components can be optimized in the absence of the other units and easily replaced as better systems are developed. The second approach could offer advantages in terms of materials utilization and expense, but optimization of all parts of a monolithic device concurrently could be difficult. In addition, physical separation of oxygen and a fuel such as hydrogen gas is certainly desirable and could require additional engineering and energetic costs. Of course, hybrid approaches are possible, and may prove most successful. For example, reaction centres that produce high energy excited states or dangerously strong oxidizing equivalents could be integrated with water oxidation catalysts so as to reduce the potential for oxidative damage, while reducing equivalents from these same reaction centres could be transported by conductors to a separate compartment for fuel production. Photosynthesis uses this strategy. In photosystem II, the reaction centre generating oxidation potential and the water oxidation catalytic site are closely coupled in the same enzyme, whereas reductive chemistry for fuel production occurs at more distant sites.

Conclusions

As illustrated by the examples above, artificial photosynthesis has progressed far since the early photochemistry of Ciamician's time. However, much more research is needed before artificial photosynthesis can compete with other technologies for practical energy production. For those working in the field, there are two inescapable facts that guide and inspire. First, fuel production using solar energy must become practical if human society is to prosper and endure while avoiding environmental catastrophe. Secondly, the powering of our biosphere by natural photosynthesis operating at about 130 TW demonstrates that environmentally benign, sustainable solar fuel production at tremendous scale is possible.

D. G. thanks the Center for Bio-Inspired Solar Fuel Production, an Energy Frontier Research Center funded by the U.S. Department of Energy, Office of Science, Office of Basic Energy Sciences under Award Number DE-SC0001016 for support of this work.

References

- 1 G. Ciamician, *Science*, 1912, **36**, 385.
- 2 M. Calvin, *Acc. Chem. Res.*, 1978, **11**, 369.
- 3 M. Calvin, *J. Membr. Sci.*, 1987, **33**, 137.
- 4 M. Calvin, *Photochem. Photobiol.*, 1983, **37**, 349.

- 5 G. Porter, *Nature*, 1980, **288**, 320.
- 6 D. Gust and T. A. Moore, in *The Porphyrin Handbook*, ed. K. M. Kadish, K. M. Smith and R. Guilard, Academic Press, New York, 2000, vol. 8, ch. 57, pp. 153–190.
- 7 T. J. Meyer, *Acc. Chem. Res.*, 1989, **22**, 163.
- 8 N. P. Redmore, I. V. Rubtsov and M. J. Therien, *J. Am. Chem. Soc.*, 2003, **125**, 8769.
- 9 M. R. Wasielewski, *Chem. Rev.*, 1992, **92**, 435.
- 10 D. Gust, T. A. Moore and A. L. Moore, *Acc. Chem. Res.*, 2001, **34**, 40.
- 11 M. Falkenstrom, O. Johansson and L. Hammarstrom, *Inorg. Chim. Acta*, 2007, **360**, 741.
- 12 S. Fukuzumi and H. Imahori, *Electron Transfer in Chemistry*, 2001, **2**, 927.
- 13 L. Flamigni, N. Armaroli, F. Barigelletti, V. Balzani, J.-P. Collin, J.-O. Dalbavie, V. Heitz and J.-P. Sauvage, *J. Phys. Chem. B*, 1997, **101**, 5936.
- 14 D. Gust, T. A. Moore and A. L. Moore, *Acc. Chem. Res.*, 2009, **42**, 1890.
- 15 Y. Umena, K. Kawakami, J. R. Shen and N. Kamiya, *Nature*, 2011, **473**, 55.
- 16 W. J. Youngblood, S.-H. A. Lee, Y. Kobayashi, E. A. Hernandez-Pagan, P. G. Hoertz, T. A. Moore, A. L. Moore, D. Gust and T. E. Mallouk, *J. Am. Chem. Soc.*, 2009, **131**, 926.
- 17 B. O'Regan and M. Grätzel, *Nature*, 1991, **353**, 737.
- 18 A. Harriman, I. J. Pickering, J. M. Thomas and P. A. Christensen, *J. Chem. Soc., Faraday Trans. 1*, 1988, **84**, 2795.
- 19 M. C. Hanna and A. J. Nozik, *J. Appl. Phys.*, 2006, **100**.
- 20 Y. Terazono, G. Kodis, P. A. Liddell, V. Garg, T. A. Moore, A. L. Moore and D. Gust, *J. Phys. Chem. B*, 2009, **113**, 7147.
- 21 T. Förster, *Ann. Phys.*, 1948, **437**, 55.
- 22 T. Förster, *Discuss. Faraday Soc.*, 1959, **27**, 7.
- 23 O. Khaselev and J. A. Turner, *Science*, 1998, **280**, 425.
- 24 R. E. Blankenship, D. M. Tiede, J. Barber, G. W. Brudvig, G. Fleming, M. Ghirardi, M. R. Gunner, W. Junge, D. M. Kramer, A. Melis, T. A. Moore, C. C. Moser, D. G. Nocera, A. J. Nozik, D. R. Ort, W. W. Parson, R. C. Prince and R. T. Sayre, *Science*, 2011, **332**, 805.
- 25 R. A. Marcus and N. Sutin, *Biochim. Biophys. Acta*, 1985, **811**, 265.
- 26 R. A. Marcus, *Can. J. Chem.*, 1959, **37**, 155.
- 27 N. S. Hush and J. Ulstrup, *Some historical notes on chemical charge transfer*, School of Chemistry, The University of Sydney, Australia, 1997.
- 28 N. S. Hush, *Trans. Faraday Soc.*, 1961, **57**, 557.
- 29 V. Levich, *Adv. Electrochem. Electrochem. Eng.*, 1966, **4**, 249.
- 30 V. Garg, G. Kodis, M. Chachisvilis, M. Hambourger, A. L. Moore, T. A. Moore and D. Gust, *J. Am. Chem. Soc.*, 2011, **133**, 2944.
- 31 J. L. Kong and P. A. Loach, in *Frontiers of Biological Energetics: From Electrons to Tissues*, ed. P. L. Dutton and H. Scarpa, Academic Press, New York, 1978, pp. 73–82.
- 32 I. Tabushi, N. Koga and M. Yanagita, *Tetrahedron Lett.*, 1979, **20**, 257.
- 33 P. A. Liddell, J. P. Sumida, A. N. Macpherson, L. Noss, G. R. Seely, K. N. Clark, A. L. Moore, T. A. Moore and D. Gust, *Photochem. Photobiol.*, 1994, **60**, 537.
- 34 D. Kuciauskas, P. A. Liddell, S. Lin, S. Stone, A. L. Moore, T. A. Moore and D. Gust, *J. Phys. Chem. B*, 2000, **104**, 4307.
- 35 H. Imahori, *Org. Biomol. Chem.*, 2004, **2**, 1425.
- 36 D. M. Guldi, *Chem. Soc. Rev.*, 2002, **31**, 22.
- 37 T. A. Moore, D. Gust, P. Mathis, J. C. Mialocq, C. Chachaty, R. V. Bensasson, E. J. Land, D. Doizi, P. A. Liddell, W. R. Lehman, G. A. Nemeth and A. L. Moore, *Nature*, 1984, **307**, 630.
- 38 D. Gust, P. Mathis, A. L. Moore, P. A. Liddell, G. A. Nemeth, W. R. Lehman, T. A. Moore, R. V. Bensasson, E. J. Land and C. Chachaty, *Photochem. Photobiol.*, 1983, **37S**, S46.
- 39 S. Nishitani, N. Kurata, Y. Sakata, S. Misumi, A. Karen, T. Okada and N. Mataga, *J. Am. Chem. Soc.*, 1983, **105**, 7771.
- 40 G. Kodis, P. A. Liddell, A. L. Moore, T. A. Moore and D. Gust, *J. Phys. Org. Chem.*, 2004, **17**, 724.
- 41 K. Maeda, K. B. Henbest, F. Cintolesi, I. Kuprov, C. T. Rodgers, P. A. Liddell, D. Gust, C. R. Timmel and P. J. Hore, *Nature*, 2008, **453**, 387.
- 42 K. Maeda, C. J. Wedge, J. G. Storey, K. B. Henbest, P. A. Liddell, G. Kodis, D. Gust, P. J. Hore and C. R. Timmel, *Chem. Commun.*, 2011, **47**, 6563.
- 43 D. Kuciauskas, P. A. Liddell, A. L. Moore, T. A. Moore and D. Gust, *J. Am. Chem. Soc.*, 1998, **120**, 10880.
- 44 S.-C. Hung, A. N. Macpherson, S. Lin, P. A. Liddell, G. R. Seely, A. L. Moore, T. A. Moore and D. Gust, *J. Am. Chem. Soc.*, 1995, **117**, 1657.
- 45 A. L. Moore, T. A. Moore, D. Gust, S.-C. Hung and A. N. Macpherson, *Photochem. Photobiol.*, 1994, **59S**, 45S.

- 46 J. Stubbe, D. G. Nocera, C. S. Yee and M. C. Y. Chang, *Chem. Rev.*, 2003, **103**, 2167.
- 47 P. Faller, C. Goussias, A. W. Rutherford and S. Un, *Proc. Natl. Acad. Sci. U. S. A.*, 2003, **100**, 8732.
- 48 J. M. Mayer, *Annu. Rev. Phys. Chem.*, 2004, **55**, 363.
- 49 G. F. Moore, M. Hamburger, M. Gervaldo, O. G. Poluektov, T. Rajh, D. Gust, T. A. Moore and A. L. Moore, *J. Am. Chem. Soc.*, 2008, **130**, 10466.
- 50 K. A. Vincent, A. Parkin and F. A. Armstrong, *Chem. Rev.*, 2007, **107**, 4366.
- 51 M. Hamburger, M. Gervaldo, D. Svedruzic, P. W. King, D. Gust, M. Ghirardi, A. L. Moore and T. A. Moore, *J. Am. Chem. Soc.*, 2008, **130**, 2015.
- 52 M. Hamburger, G. Kodis, M. Vaughn, G. F. Moore, D. Gust, A. L. Moore and T. A. Moore, *Dalton Trans.*, 2009, 9979.
- 53 M. Hamburger, A. Brune, D. Gust, A. L. Moore and T. A. Moore, *Photochem. Photobiol.*, 2005, **81**, 1015.
- 54 B. E. Barton, M. T. Olsen and T. B. Rauchfuss, *Curr. Opin. Biotechnol.*, 2010, **21**, 292.
- 55 M. W. Kanan and D. G. Nocera, *Science*, 2008, **321**, 1072.
- 56 F. Jiao and H. Frei, *Angew. Chem., Int. Ed.*, 2009, **48**, 1841.
- 57 Z. Q. Huang, Z. Luo, Y. V. Geletii, J. W. Vickers, Q. S. Yin, D. Wu, Y. Hou, Y. Ding, J. Song, D. G. Musaev, C. L. Hill and T. Q. Lian, *J. Am. Chem. Soc.*, 2011, **133**, 2068.
- 58 F. Jiao and H. Frei, *Chem. Commun.*, 2010, **46**, 2920.
- 59 Y. Gorlin and T. F. Jaramillo, *J. Am. Chem. Soc.*, 2010, **132**, 13612.
- 60 K. Maeda and K. Domen, *J. Phys. Chem. Lett.*, 2010, **1**, 2655.
- 61 R. V. Bensasson, E. J. Land, A. L. Moore, R. L. Crouch, G. Dirks, T. A. Moore and D. Gust, *Nature*, 1981, **290**, 329.
- 62 A. L. Moore, A. M. Joy, R. Tom, D. Gust, T. A. Moore, R. V. Bensasson and E. J. Land, *Science*, 1982, **216**, 982.
- 63 D. Gust, T. A. Moore, A. L. Moore, C. Devadoss, P. A. Liddell, R. M. Hermant, R. A. Nieman, L. J. Demanche, J. M. DeGraziano and I. Gouni, *J. Am. Chem. Soc.*, 1992, **114**, 3590.
- 64 D. Gust, T. A. Moore, A. L. Moore, D. Kuciauskas, P. A. Liddell and B. D. Halbert, *J. Photochem. Photobiol., B*, 1998, **43**, 209.
- 65 G. Kodis, C. Herrero, R. Palacios, E. Mariño-Ochoa, S. L. Gould, L. de la Garza, R. van Grondelle, D. Gust, T. A. Moore, A. L. Moore and J. T. M. Kennis, *J. Phys. Chem. B*, 2004, **108**, 414.
- 66 M. Kloz, S. Pillai, G. Kodis, D. Gust, T. A. Moore, A. L. Moore, R. van Grondelle and J. T. M. Kennis, *J. Am. Chem. Soc.*, 2011, **133**, 7007.
- 67 A. Wilson, G. Ajlani, J. M. Verbavatz, I. Vass, C. A. Kerfeld and D. Kirilovsky, *Plant Cell*, 2006, **18**, 992.
- 68 A. Wilson, C. Punginelli, A. Gall, C. Bonetti, M. Alexandre, J. M. Routaboul, C. A. Kerfeld, R. van Grondelle, B. Robert, J. T. M. Kennis and D. Kirilovsky, *Proc. Natl. Acad. Sci. U. S. A.*, 2008, **105**, 12075.
- 69 S. D. Straight, G. Kodis, Y. Terazono, M. Hamburger, T. A. Moore, A. L. Moore and D. Gust, *Nat. Nanotechnol.*, 2008, **3**, 280.
- 70 P. Horton and A. V. Ruban, *J. Exp. Bot.*, 2004, **56**, 365.
- 71 A. A. Pascal, Z. F. Liu, K. Broess, B. van Oort, H. van Amerongen, C. Wang, P. Horton, B. Robert, W. R. Chang and A. Ruban, *Nature*, 2005, **436**, 134.
- 72 A. V. Ruban, R. Berera, C. Illoia, I. H. M. van Stokkum, J. T. M. Kennis, A. A. Pascal, H. van Amerongen, B. Robert, P. Horton and R. van Grondelle, *Nature*, 2007, **450**, 575.
- 73 N. E. Holt, G. R. Fleming and K. K. Niyogi, *Biochemistry*, 2004, **43**, 8281.
- 74 R. Berera, C. Herrero, L. H. M. van Stokkum, M. Vengris, G. Kodis, R. E. Palacios, H. van Amerongen, R. van Grondelle, D. Gust, T. A. Moore, A. L. Moore and J. T. M. Kennis, *Proc. Natl. Acad. Sci. U. S. A.*, 2006, **103**, 5343.
- 75 C. Kulheim, J. Agren and S. Jansson, *Science*, 2002, **297**, 91.
- 76 P. N. Liao, S. Pillai, D. Gust, T. A. Moore, A. L. Moore and P. J. Walla, *J. Phys. Chem. A*, 2011, **115**, 4082.
- 77 Y. Terazono, G. Kodis, K. Bhushan, J. Zaks, C. Madden, A. L. Moore, T. A. Moore, G. R. Fleming and D. Gust, *J. Am. Chem. Soc.*, 2011, **133**, 2916.

A bioinspired redox relay that mimics radical interactions of the Tyr–His pairs of photosystem II

Jackson D. Megiatto Jr[†], Dalvin D. Méndez-Hernández¹, Marely E. Tejada-Ferrari¹, Anne-Lucie Teillout^{1,3}, Manuel J. Llansola-Portolés¹, Gerdenis Kodis¹, Oleg G. Poluektov², Tijana Rajh², Vladimiro Mujica¹, Thomas L. Groy¹, Devens Gust¹, Thomas A. Moore¹ and Ana L. Moore^{1*}

In water-oxidizing photosynthetic organisms, light absorption generates a powerfully oxidizing chlorophyll complex (P680⁺) in the photosystem II reaction centre. This is reduced via an electron transfer pathway from the manganese-containing water-oxidizing catalyst, which includes an electron transfer relay comprising a tyrosine (Tyr)–histidine (His) pair that features a hydrogen bond between a phenol group and an imidazole group. By rapidly reducing P680⁺, the relay is thought to mitigate recombination reactions, thereby ensuring a high quantum yield of water oxidation. Here, we show that an artificial reaction centre that features a benzimidazole–phenol model of the Tyr–His pair mimics both the short-internal hydrogen bond in photosystem II and, using electron paramagnetic resonance spectroscopy, the thermal relaxation that accompanies proton-coupled electron transfer. Although this artificial system is much less complex than the natural one, theory suggests that it captures the essential features that are important in the function of the relay.

Photosystem II (PSII), the enzyme that uses sunlight to oxidize water to molecular oxygen, contains two redox-active tyrosines called tyrosine Z (Tyr_Z) and tyrosine D (Tyr_D), which are located in positions related by approximately two-fold rotational symmetry in the D1 and D2 core proteins, respectively^{1–3}. According to the recently determined PSII crystal structure³, Tyr_D is located in a relatively hydrophobic domain with its phenolic proton forming a short hydrogen bond with the imidazole nitrogen atom of a nearby histidine, D2-His189. In contrast, Tyr_Z is in a more hydrophilic environment, forming an even shorter hydrogen bond with the corresponding D1-His190. Photo-oxidation of both tyrosines during PSII activity is coupled to the transfer of their phenolic protons, most likely to their respective hydrogen-bonded histidine partners. The resulting neutral tyrosyl radicals Tyr_Z[•] and Tyr_D[•] have different functional roles in the enzyme. Tyr_Z[•] is directly involved in the water oxidation process, whereas Tyr_D[•] is not^{4–10}.

Because of the extraordinarily long lifetime (several hours under some conditions) of the Tyr_D[•] radical, it has been possible to study it using a number of techniques^{11–15}. Using high-field electron paramagnetic resonance (EPR), Faller and colleagues demonstrated¹⁵ that oxidation of Tyr_D in OEC-depleted PSII reaction centres occurs through a high-energy radical intermediate that can be trapped at 1.8 K. The initial radical formed at 1.8 K relaxes at 77 K to yield a phenoxyl radical with a longer hydrogen bond to the histidine.

Designing synthetic models able to mimic intricate protein/radical interactions that ultimately allow the generation of highly energetic but long-lived radicals through proton-coupled electron transfer reactions (PCET) is a challenging step in the development of artificial photosynthetic devices¹⁶ and could lead to a deeper understanding of the more complex natural system¹⁷. A bioinspired organic/inorganic hybrid system, **triad-1**, consisting of approximately three to four dyads of benzimidazole–phenol porphyrin

moieties (BiP–PF₁₀) attached to a nanoparticle of TiO₂, has been constructed. Although it is not structurally a triad, it functions as such. Excitation of the porphyrin is followed by electron transfer to the nanoparticle, and a second electron transfer from BiP to the porphyrin radical cation ensues. The second electron transfer is coupled to an associated proton transfer process to yield a final charge-separated state characterized by an electron in the semiconducting TiO₂ nanoparticle, a benzimidazolium cation and a neutral phenoxyl radical that is thermodynamically competent to oxidize water¹⁸ (Fig. 1).

Using EPR spectroscopy, we provide evidence that the formation of the phenoxyl radical species in **triad-1** at 13 K results in an energetic intermediate radical state, which at 100 K undergoes a change that can be interpreted in terms of solvation and conformational reorganization to yield a relatively more stable phenoxyl radical. This relaxation mimics that observed for the D2-Tyr_D–His189 pair in PSII¹⁵ and suggests a key role of PCET in mediating electron transfer between natural and artificial reaction centres and water-oxidizing catalysts.

Results

The formation of a charge-separated state in **triad-1** is unambiguously verified by the X-band (9.5 GHz) EPR spectrum (Supplementary Fig. 1), which shows an axially symmetric signal with $g_{\parallel} = 1.961$ and $g_{\perp} = 1.989$, corresponding to electrons in the TiO₂ interior, and an isotropic signal at $g = 2.0043$ that corresponds to holes localized on the organic part of the construct. Importantly, this spectrum clearly indicates an approximately equal number of injected electrons in the TiO₂ nanoparticles and holes in the organic moiety, confirming that excitation of the porphyrin (PF₁₀) is followed by charge separation via electron transfer from PF₁₀ to the semiconductor^{19,20}. The EPR signals observed with **dyad-2** (see structure in Fig. 4), which lacks the primary electron

¹Department of Chemistry and Biochemistry, Arizona State University, Tempe, Arizona 85287-1604, USA, ²NanoBio Interface Group, Center for Nanoscale Materials and Chemical Sciences and Engineering Division, Argonne National Laboratory Argonne, Illinois 60439, USA, ³Laboratoire de Chimie Physique, Groupe d'Electrochimie et de Photoelectrochimie, UMR 8000, CNRS, Université Paris-Sud, Batiment 350, 91405 Orsay Cedex, France; [†]Present address: Institute of Chemistry, Campinas State University (UNICAMP), PO Box 6154, Campinas, SP, 13084-861, Brazil. *e-mail: amoores@asu.edu

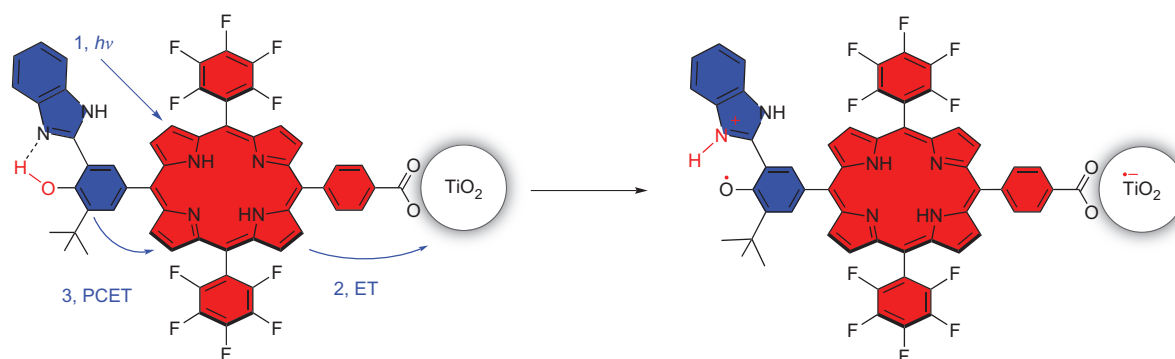


Figure 1 | Bioinspired triad-1 consisting of three covalently linked redox subunits. Upon irradiation (1, $h\nu$), the system is able to undergo a primary electron transfer reaction (2, ET) and a proton-coupled electron transfer (3, PCET) reaction.

acceptor (TiO_2), is $\sim 1\%$ of the signal obtained with **triad-1** (Supplementary Fig. 2).

Following the initial charge separation, a secondary electron transfer from the phenol moiety of BiP to $\text{PF}_{10}^{\bullet+}$ is expected to form a phenoxyl radical. Evidence for such a process comes from transient absorption studies with a molecular triad system, where in place of the TiO_2 nanoparticle of **triad-1**, a high-potential tetracyano porphyrin was used as the primary electron acceptor¹⁸.

Any change in the local environment of the initially formed phenoxyl radical of **triad-1** on annealing can be determined from high-resolution, temperature-dependent EPR measurements by following the change of the g -tensor component oriented along the phenolic C–O bond (g_x). For phenoxyl radicals, a spin–orbit coupling interaction between the unpaired electron in the singly occupied molecular orbital (SOMO) and the non-bonding electron pairs of the oxygen atom induces a magnetic moment, which results in a deviation of the g_x component of the g -tensor from the free electron g -value ($g_e = 2.0023$). Hydrogen bonding with the lone pair of the oxygen atom in the oxygen-centred radicals and/or delocalization of the unpaired spin density are known to decrease this deviation, yielding radicals with lower g_x values^{21,22}.

When a suspension of **triad-1** in acetonitrile at 13 K is irradiated with a 532 nm laser, the high-resolution D-band (130 GHz) EPR spectrum (Fig. 2, purple trace) is dominated by the resolved g

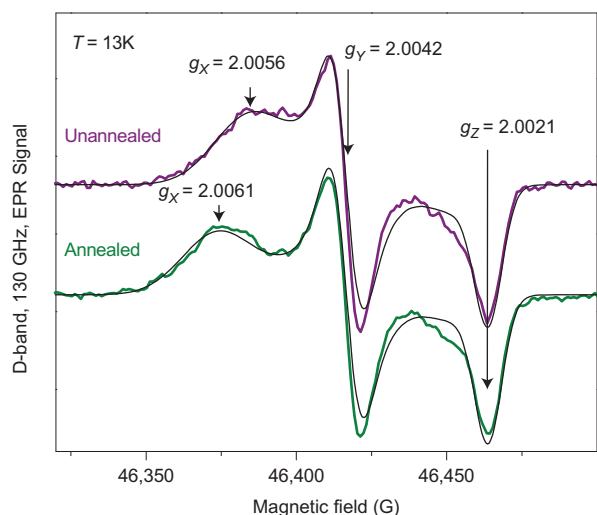


Figure 2 | Photoinduced D-band (130 GHz) EPR spectra of an acetonitrile suspension of **triad-1** recorded at 13 K. Purple: immediately after sample illumination in the cavity of the spectrometer. Green: after the illuminated sample has been annealed at 100 K in the dark for 10 min and cooled back to 13 K. Black: theoretical simulation (see Methods).

anisotropic coupling tensors ($g_x = 2.0056$; $g_y = 2.0042$; $g_z = 2.0021$). Annealing the sample at 100 K in the dark for 10 min and returning to 13 K (see Methods) results in a significant increase in the g_x value from 2.0056 to 2.0061, while the other two g -tensor components remain unchanged (Fig. 2, green trace). These observations clearly indicate the thermally activated conversion of the initially formed phenoxyl radical species to another in which structural and solvent reorganization have taken place^{23–29}. This temperature dependence of the g_x values was not observed in a construct related to **triad-1** in which the benzimidazole was the linker between PF_{10} and the phenol group²⁰ and has not been reported in any other BiP system or artificial system that mimics PSII.

Extensive theoretical and experimental EPR investigations of proteins and model compounds have established that the g_x values for non-interacting tyrosyl and phenoxyl radicals in nonpolar environments are larger than 2.0080, whereas those radicals engaged in hydrogen bonds range from 2.0064 to 2.0075 (refs 23,28). A protonated phenoxyl radical can be understood as an extreme case where one of the oxygen lone pairs is engaged in a covalent bond with the proton. A very low g_x value is therefore expected for such a radical. From density functional theory (DFT) calculations, the g_x value for a protonated phenoxyl radical in a BiP model compound has been estimated to be as low as 2.004 (refs 23,25).

The g_x values determined at low temperature (2.0056) and after annealing and returning to 13 K (2.0061) for the phenoxyl radicals in **triad-1** are lower than those reported in the literature for such radicals interacting exclusively through hydrogen bonds^{20,23–28}, suggesting spin delocalization between the phenoxyl radical and the high-potential porphyrin (*vide infra*), but are significantly higher than the g_x value calculated for a protonated phenoxyl radical (2.004)²⁵. The fact that the g_x values are higher than that of the protonated phenoxyl radical strongly indicates that both phenoxyl radicals detected in the present study are formally neutral radicals. This supports the hypothesis that the oxidation of the phenol in **triad-1** occurs with transfer of the phenolic proton to the benzimidazole group, even at 13 K.

Spin delocalization over the porphyrin core in the radical of **triad-1** is supported by DFT calculations on the organic component of **triad-1** (Supplementary Fig. 4), which reveal non-negligible spin density over the porphyrin moiety. Data from electrochemical experiments in acetonitrile on the methyl ester derivative of the organic component of **triad-1** (**dyad-2**, chemical structure in Fig. 4) corroborate delocalization of the spin and cationic charge of the phenolic radical onto the porphyrin. The first porphyrin oxidation in **dyad-2** occurs at a much higher potential (about 1.65 V, versus saturated calomel electrode (SCE)) than that of a porphyrin model compound lacking the BiP group (1.29 V versus SCE), whereas the phenol oxidation potential is roughly the same

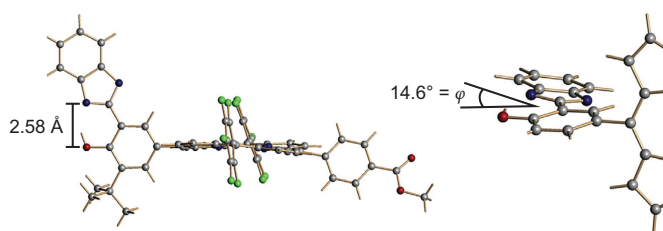


Figure 3 | Crystal structure of *dyad-2*. Carbon is shown in grey, oxygen in red, nitrogen in blue and fluorine in green. On the right, a partial structure of *dyad-2* is shown where the *t*-butyl group *ortho* to the phenol and part of the porphyrin have been deleted to better visualize the dihedral angle between the phenol and imidazole groups.

(1.00 V versus SCE) in *dyad-2* and in a BiP model compound lacking the porphyrin group (1.04 V versus SCE) (Supplementary Table 3). Because in *dyad-2* the phenol electrochemical oxidation occurs at ~ 1 V, and formation of the porphyrin radical cation is the second electrochemical oxidation, the increase of the porphyrin oxidation potential from 1.29 V to 1.65 V is clear evidence that the hole of the BiP residue is partially delocalized over the porphyrin core, making it harder to oxidize.

Formation of a neutral phenoxyl radical in *triad-1* at 13 K, where nuclear motions are restricted, implies that very little energy, probably only zero-point motion, is required for the proton to move to a new potential minimum during oxidation of the phenol residue. This finding indicates that the BiP group is well-oriented to form a strong intramolecular hydrogen bond, which creates a coordinate for proton motion that facilitates its transfer, even at very low temperatures^{13,23,24,30–33}. Structural investigation of *dyad-2* confirms the formation of a strong intramolecular hydrogen bond. The crystal structure of *dyad-2* (Fig. 3, CCDC deposition no. 949079) reveals that the phenol and benzimidazole moieties are nearly coplanar with a dihedral angle of 14.6° , which is significantly smaller than those between 29° and 33° observed for similar systems in the absence of intramolecular hydrogen bonds²³. This relatively small dihedral angle between the two hydrogen-bonded partners in *dyad-2* results in a short O...N distance of 2.58 Å, indicating the presence of a strong electrostatic interaction between the phenolic proton and the lone pair of the nitrogen atom on the BiP³⁴.

The strong hydrogen bond in *dyad-2* is also observed in solution. The ¹H NMR spectrum of *dyad-2* in chloroform (Fig. 4) shows the presence of a sharp signal at 14.23 ppm, which is unambiguously attributed to the phenolic proton³⁵. Such a downfield shift from the usual 5–6 ppm region indicates that the phenolic proton is relatively far from the shielding effects of the electrons on the oxygen atom, and the sharpness of the peak is strong evidence that the phenolic proton is not exchanging on the NMR timescale, which is ensured by the strong intramolecular hydrogen bond^{28,34}. The ¹H NMR spectra in more polar media (deuterated acetonitrile, –OH resonance at 14.47 ppm; deuterated acetone, –OH resonance at 14.58 ppm) lead to similar conclusions.

Furthermore, when comparing the ¹H NMR spectrum of *dyad-2* in deuterated acetonitrile with that of a simple BiP model²⁰, the –OH resonance in *dyad-2* is found 0.8 ppm further downfield. This is evidence for a stronger hydrogen bond in *dyad-2*. We propose that the strong electron-withdrawing effect of the fluorinated porphyrin bonded to the phenol residue renders the phenolic group significantly more acidic, reducing its pK_a to a value closer to that of the benzimidazolium ion. This inductive effect promotes a better match of the proton affinities of the two hydrogen-bond partners in *dyad-2*, hence accounting for the observed strong hydrogen bond³⁰. Turning to the distal proton of the benzimidazole group, its NMR resonance in *dyad-2* is shifted downfield from 9.88 ppm in the nonpolar chloroform to 11.09 ppm in acetonitrile and to

12.43 ppm in acetone (Fig. 4), indicating increasing hydrogen bond formation with the solvent.

Discussion

As mentioned already, the high g_x values for the phenoxyl radicals of *triad-1* (2.0056 and 2.0061) compared to that of a protonated phenoxyl radical (2.004) provide clear evidence that the electron transfer from the phenol to the radical cation of the porphyrin in *triad-1* occurs with transfer of the phenolic proton to the benzimidazole group. The presence of a strong hydrogen bond between the phenol and the benzimidazole moiety leads to the possibility that the electron and proton transfer reactions occur through a single step in a concerted mechanism. The concerted mechanism is supported by thermodynamic considerations. Electrochemical investigation in acetonitrile (Supplementary Table 3) reveals that a porphyrin model compound lacking the BiP group shows a standard potential of 1.29 V (versus SCE), while a non-hydrogen bonded phenol model has an oxidation potential of 1.36 V (versus SCE, irreversible). Therefore, the photogenerated fluorinated porphyrin radical cation (PF₁₀^{•+}) should not be thermodynamically competent to oxidize the phenol residue in *triad-1* without transfer of the proton to the benzimidazole moiety, rendering the stepwise electron transfer followed by proton transfer (ET-PT) mechanism unlikely although it cannot be absolutely excluded with the present information¹⁸. A proton transfer followed by electron transfer (PT-ET) stepwise mechanism is also unlikely in the case of *triad-1*, as the benzimidazolium cation ($pK_a \approx 7$) is a stronger acid than the phenol group ($pK_a \approx 27$) in acetonitrile^{30,36}, even after taking into consideration the inductive effect of the electron-deficient PF₁₀ on the phenol^{36,37}.

The observation that both electron and proton transfer processes occur at 13 K strongly suggests that either the proton tunnels from a site near the phenolic oxygen to one near the imidazole nitrogen or its zero-point energy is higher than the proton transfer barrier^{28,33}. Although tunnelling usually has a distinct kinetic isotope effect (KIE) signature, a negligible KIE was observed in electrochemical experiments with *dyad-2* (1.0 ± 0.2) (Supplementary Fig. 8). Theory predicts that under certain circumstances a vanishingly small KIE would be observed for PCET reactions involving proton tunnelling³⁸. Additional electrochemical measurements with model systems and theoretical calculation are being conducted to clarify this issue.

Focusing on the temperature-induced relaxation process observed in the EPR experiments, DFT calculations were performed in an effort to elucidate the cause(s) responsible for the thermal relaxation of the phenoxyl radicals initially generated upon illumination of *triad-1* at 13 K. Following literature methodology²⁵, the g -values for different structures of the radical cation of the organic component of *triad-1* were calculated (Supplementary Fig. 5 and Table 1).

The calculated g_x value for structure **A**^{•+} (Fig. 5) is consistent with the experimental g_x value at 13 K. The main features of **A**^{•+} are that the phenolic proton resides on the benzimidazole group, the benzimidazole distal proton is hydrogen-bonded with a water molecule, and a second water molecule is hydrogen-bonded to the phenoxyl oxygen. These features are consistent with the tentative conclusion that the PCET process at the BiP moiety occurs in a concerted single step and the observation that the distal proton is hydrogen-bonded with solvent molecules. At 13 K, neither solvent molecule has enough energy to reorganize, resulting in a high-energy state with a g_x of 2.0056.

On warming the solution to 100 K, the energy available for solvent reorganization increases and hydrogen bond formation involving the solvent and the newly formed N–H site is possible, resulting in structure **B**^{•+}. Compared to **A**^{•+}, **B**^{•+} (which has a new bifurcated hydrogen bond with a water molecule) shows an increase in both

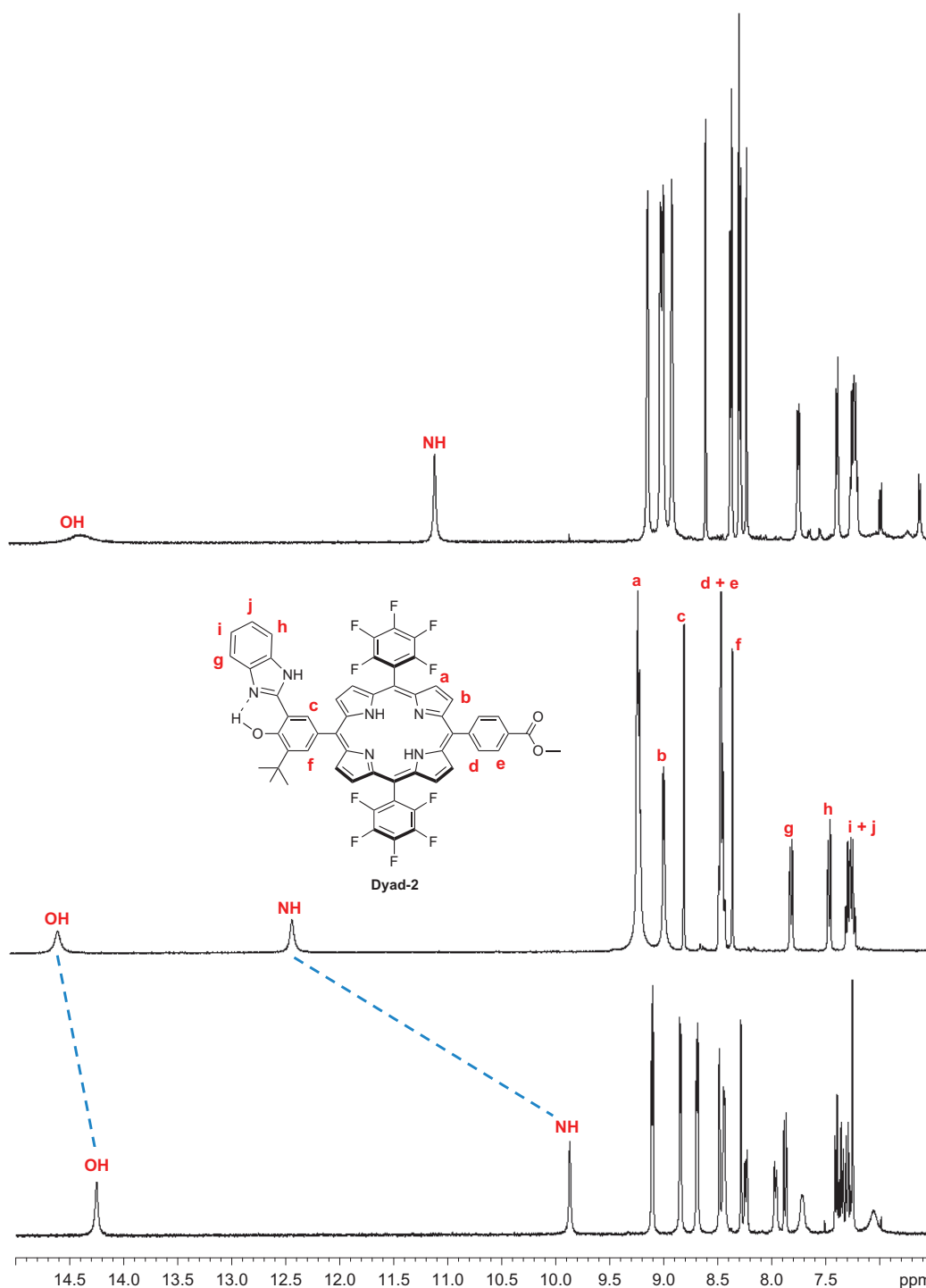


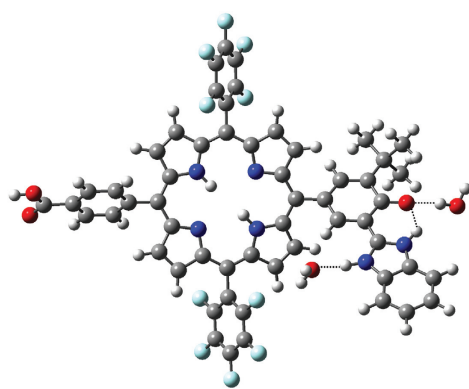
Figure 4 | Partial ¹H NMR spectra of **dyad-2**. The spectra were obtained at 298 K, 500 MHz, in three different deuterated solvents: acetonitrile (top), acetone (middle) and chloroform (bottom).

the BiP dihedral angle and in the O–H and O–N distances, which would result in an increase of the g_x value. Indeed, the calculated g_x value for \mathbf{B}^{*+} is in agreement with the g_x value observed after annealing at 100 K, indicating that \mathbf{B}^{*+} or similar structures are plausible (Supplementary Table 1). Calculations performed using acetonitrile as the hydrogen-bonding solvent yielded similar results (Supplementary Fig. 5 and Table 1).

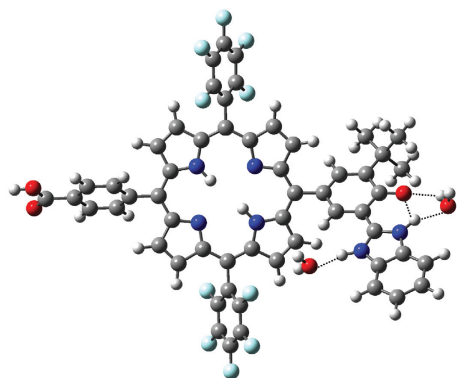
The inclusion of explicit solvent molecules in a continuum model for the calculated g values results in a better match to the values observed experimentally in the case of *o*-semiquinones in protic solvents^{39,40}. In our model, the water molecule around the proximal

N–H bond of \mathbf{B}^{*+} is acting as a hydrogen bond acceptor with the newly formed N–H and as a hydrogen bond donor to the phenoxyl oxygen. Interestingly, this water molecule is positioned similarly to the water molecule hydrogen-bonded to Tyr_D[•] proposed for the multiple proton pathway mechanism of Barry and colleagues for the reduction of Tyr_D[•] to Tyr_D^{29,41,42}. We also note that several ordered water molecules are present around Tyr_Z His 190 in the water-oxidizing branch of PSII³.

In summary, a hybrid construct comprising approximately three to four molecular dyads attached to a semiconductor nanoparticle has been found to model the functional and structural aspects of



Structure A⁺
 Calculated $g_x = 2.0052$
 BiP dihedral $\varphi = 1.82^\circ$
 O–H distance = 1.88 Å
 O–N distance = 2.62 Å



Structure B⁺
 Calculated $g_x = 2.0060$
 BiP dihedral $\varphi = 7.12^\circ$
 O–H distance = 2.14 Å
 O–N distance = 2.72 Å

Figure 5 | Calculated structures of the radical cation of the organic component of triad-1. Structure A⁺ before thermal relaxation and structure B⁺ after thermal relaxation. Structure A⁺ includes water molecules hydrogen-bonded to the distal N–H and the phenoxyl oxygen and structure B⁺ includes water molecules hydrogen-bonded at both distal and proximal N–H sites (see text). Carbon is shown in grey, hydrogen in white, nitrogen in blue, fluorine in cyan and oxygen in red.

a PCET process thought to be central to water oxidation in PSII. In this construct, just as in PSII^{15,43}, high-field EPR clearly detects the formation of phenoxyl radicals in two different states, a higher-energy state formed at 13 K and a relaxed state observed when the sample is warmed to 100 K. DFT calculations indicate that solvent molecules solvating the initial O–H⋯N site must reorganize to solvate the newly formed O⋯H–N site. This reorganization is blocked at 13 K, resulting in a higher-energy state with a g_x value of 2.0056. After warming to 100 K, the solvent molecules around the new O⋯H–N site reorganize to form a bifurcated hydrogen bond. Such solvent reorganization and structural rearrangements around the BiP result in the relaxed final structure with a g_x value of 2.0061. Thermodynamic considerations suggest that the PCET in the case of **triad-1** probably occurs by a concerted mechanism.

The thermal relaxation observed by high-field EPR in these systems is not ubiquitous. A construct similar to **triad-1**, but having a weaker intramolecular hydrogen bond and the benzimidazole group as part of the linkage between the porphyrin and phenol moieties, did not demonstrate such relaxation²⁰. Thus, it is

significant that **triad-1** mimics the thermal relaxation observed in the natural system. The simplicity of the structure allows us to identify the unusually strong intramolecular hydrogen bond between the phenol and the benzimidazole moiety, as the structural parameter that is responsible for the biomimetic behaviour.

It has been postulated that the PCET within the D1-Tyr_z-His190 group, which acts as a redox mediator/relay in PSII, plays a role in the high quantum efficiency of water oxidation by P680⁺ by providing a kinetic coupling between the fast initial electron transfer events and the slower process of water oxidation. In this connection, incorporation of a BiP redox mediator/relay in an artificial system significantly improved the quantum yield for transfer of electrons from a water-oxidizing catalyst to an oxidized dye in a nanoparticulate TiO₂-based photoanode in which the dye radical cation plays a role analogous to that of P680⁺ (ref. 44).

Methods

Synthesis. The porphyrin model (Supplementary Fig. 6 and Table 3)³⁵, BiP model²⁰, **dyad-2** and its carboxylic acid^{18,35} were prepared following previously reported procedures.

TiO₂ colloidal preparation. Transparent TiO₂ nanoparticle colloidal aqueous solutions were prepared by the dropwise addition of titanium(IV) chloride to cooled water. The temperature and component mixing rate of reactants were controlled by an apparatus developed for automatic colloid preparation⁴⁵. The pH of the solution was between 0 and 1, depending on the TiCl₄ concentration. Slow growth of the particles was achieved by using dialysis at 4 °C against water until the pH of the solution reached 3.5, indicating that particle growth was complete. The final concentration was 0.17 M TiO₂ with a particle size of 4.5 ± 1 nm. The solution was mixed with 0.6 mM of the carboxylic acid form of **dyad-2**, which was dissolved in THF and the resulting solution dried under a nitrogen atmosphere. The dried particles were redispersed in acetonitrile solution. Each solution contained, on average, 3.5 molecules of the carboxylic acid form of **dyad-2** per TiO₂ nanoparticle.

EPR. High-frequency EPR spectra were recorded at the D-band (130 GHz/4.6 T) with a continuous-wave/pulsed EPR spectrometer as described previously⁴⁶. A cylindrical single-mode cavity TE₀₁₁ was used, which had slits on the cylindrical side of the cavity to allow for optical excitation and field modulation. Samples were illuminated in the cavity of the EPR spectrometer. Light excitation was achieved with an optical parametric oscillator (Opotek) pumped by a Nd:YAG laser (Quantel). The output of the laser was coupled to a fibre-optic to deliver light to the cavity (1 mJ per pulse). The excitation wavelength was 532 nm. The sample temperature was regulated by an Oxford temperature controller (ITC 503) coupled to an Oxford continuous-flow cryostat (CF 1200). Theoretical simulations of the EPR spectra were performed with the SimFonia program (Version 1.25, Bruker BioSpin), using second-order perturbation theory. Annealing was tried at different temperatures. At $T < 70$ K the signal transformation was negligible at reasonable annealing times (~20 min). At $T > 120$ K a substantial decay of the EPR signal (which was recorded after freezing back to 13 K) was observed. Annealing at 100 K for 10 min led to spectra transformation without a large change in EPR intensity.

X-ray structures. The CCDC deposition number for **dyad-2** is 949079.

Received 11 July 2013; accepted 20 December 2013;
 published online 9 February 2014

References

- Babcock, G. T. *et al.* Water oxidation in photosystem II: from radical chemistry to multielectron chemistry. *Biochemistry* **28**, 9557–9565 (1989).
- Zouni, A. *et al.* Crystal structure of photosystem II from *Synechococcus elongatus* at 3.8 Å resolution. *Nature* **409**, 739–743 (2000).
- Umena, Y., Kawakami, K., Shen, J.-R. & Kamiya, N. Crystal structure of oxygen-evolving photosystem II at a resolution of 1.9 Å. *Nature* **473**, 55–60 (2011).
- Barry, B. A. & Babcock, G. T. Tyrosine radicals are involved in the photosynthetic oxygen-evolving system. *Proc. Natl Acad. Sci. USA* **84**, 7099–7103 (1987).
- Mamedov, F., Sayre, R. T. & Styring, S. Involvement of histidine 190 on the D1 protein in electron/proton transfer reactions on the donor side of photosystem II. *Biochemistry* **37**, 14245–14256 (1998).
- Hays, A.-M. A., Vassiliev, I. R., Golbeck, J. H. & Debus, R. J. Role of D1-His190 in proton-coupled electron transfer reactions in photosystem II: a chemical complementation study. *Biochemistry* **37**, 11352–11365 (1998).
- Meyer, T. J., Hang, M., Huynh, V. & Thorp, H. H. The role of proton coupled electron transfer (PCET) in water oxidation by photosystem II. Wiring for protons. *Angew. Chem. Int. Ed.* **46**, 5284–5304 (2007).
- Barry, B. A. Proton coupled electron transfer and redox active tyrosines in photosystem II. *J. Photochem. Photobiol. B* **104**, 60–71 (2011).

9. Hammarström, L. & Styring, S. Proton-coupled electron transfer of tyrosines in photosystem II and model systems for artificial photosynthesis: the role of a redox-active link between catalyst and photosensitizer. *Energy Environ. Sci.* **4**, 2379–2388 (2011).
10. Styring, S., Sjöholm, J. & Mamedov, F. Two tyrosines that changed the world: interfacing the oxidizing power of photochemistry to water splitting in photosystem II. *Biochim. Biophys. Acta* **1817**, 7–87 (2012).
11. Faller, P. *et al.* Rapid formation of the stable tyrosyl radical in photosystem II. *Proc. Natl Acad. Sci. USA* **98**, 14368–14373 (2001).
12. Rappaport, F. *et al.* Probing the coupling between proton and electron transfer in photosystem II core complexes containing a 3-fluorotyrosine. *J. Am. Chem. Soc.* **131**, 4425–4433 (2009).
13. Stubbe, J. A. & van der Donk, W. A. Protein radicals in enzyme catalysis. *Chem. Rev.* **98**, 705–762 (1998).
14. Faller, P., Rutherford, A. W. & Debus, R. J. Tyrosine D oxidation at cryogenic temperature in photosystem II. *Biochemistry* **41**, 12914–12920 (2002).
15. Faller, P., Goussias, C., Rutherford, A. W. & Un, S. Resolving intermediates in biological proton-coupled electron transfer: a tyrosyl radical prior to proton movement. *Proc. Natl Acad. Sci. USA* **100**, 8732–8735 (2003).
16. Gust, D., Moore, T. A. & Moore, A. L. Realizing artificial photosynthesis. *Faraday Discuss.* **155**, 9–26 (2012).
17. Gust, D., Moore, T. A. & Moore, A. L. Molecular mimicry of photosynthetic energy and electron transfer. *Acc. Chem. Res.* **26**, 198–205 (1993).
18. Megiatto, J. D. Jr *et al.* Mimicking the electron transfer chain in photosystem II with a molecular triad thermodynamically capable of water oxidation. *Proc. Natl Acad. Sci. USA* **109**, 15578–15583 (2012).
19. Rajh T., Nedeljkovic J. M., Chen L. X., Poluektov O. & Thurnauer M. C. Improving optical and charge separation properties of nanocrystalline TiO₂ by surface modification with vitamin C. *J. Phys. Chem. B* **103**, 3515–3519 (1999).
20. Moore, G. F. *et al.* A bioinspired construct that mimics the proton coupled electron transfer between P680⁺⁺ and the TyrZ–His190 pair of photosystem II. *J. Am. Chem. Soc.* **130**, 10466–10467 (2008).
21. Stone, A. J. *g* factors of aromatic free radicals. *Mol. Phys.* **6**, 509–515 (1963).
22. Smirnova, T. I., Smirnov, A. I., Paschenko, S. V. & Poluektov, O. G. Geometry of hydrogen bonds formed by lipid bilayer nitroxide probes: a high-frequency pulsed ENDOR/EPR study. *J. Am. Chem. Soc.* **129**, 3476–3477 (2007).
23. Orto, M. *et al.* Geometric and electronic structures of phenoxyl radicals hydrogen bonded to neutral and cationic partners. *Chem. Eur. J.* **18**, 5416–5429 (2012).
24. Thomas, F. *et al.* How single and bifurcated hydrogen bonds influence proton-migration rate constants, redox, and electronic properties of phenoxyl radicals. *Angew. Chem. Int. Ed.* **43**, 594–597 (2004).
25. Benisvy, L. *et al.* Phenoxyl radicals hydrogen-bonded to imidazolium: analogues of Tyrosyl D[•] of photosystem II: high-field EPR and DFT studies. *Angew. Chem. Int. Ed.* **44**, 5314–5317 (2005).
26. Un, S., Atta, M., Fontecave, M. & Rutherford, A. W. *g*-Values as a probe of the local protein environment: high-field EPR of tyrosyl radicals in ribonucleotide reductase and photosystem II. *J. Am. Chem. Soc.* **117**, 10713–10719 (1995).
27. Un, S., Gerez, C., Elleingand, E. & Fontecave, M. Sensitivity of tyrosyl radical *g*-values to changes in protein structure: a high-field EPR study of mutants of ribonucleotide reductase. *J. Am. Chem. Soc.* **123**, 3048–3054 (2001).
28. Saito, K., Shen, J.-R., Ishida, T. & Ishikita, H. Short hydrogen bond between redox-active tyrosine YZ and D1-His190 in the photosystem II crystal structure. *Biochemistry* **50**, 9836–9844 (2011).
29. Sibert, R. *et al.* Proton-coupled electron transfer in a biomimetic peptide as a model of enzyme regulatory mechanisms. *J. Am. Chem. Soc.* **129**, 4393–4400 (2007).
30. Markle, T. F., Rhile, I. J., Dipasquale, A. G. & Mayer, J. M. Probing concerted proton–electron transfer in phenol–imidazoles. *Proc. Natl Acad. Sci. USA* **105**, 8185–8190 (2008).
31. Costentin, C., Robert, M. & Saveant, J.-M. Electrochemical and homogeneous proton-coupled electron transfers: concerted pathways in the one-electron oxidation of a phenol coupled with an intramolecular amine-driven proton transfer. *J. Am. Chem. Soc.* **128**, 4552–4553 (2006).
32. Fecenko, C. J., Thorp, H. H. & Meyer, T. J. The role of free energy change in coupled electron–proton transfer. *J. Am. Chem. Soc.* **129**, 15098–15099 (2007).
33. Hammes-Schiffer, S. Theory of proton-coupled electron transfer in energy conversion processes. *Acc. Chem. Res.* **42**, 1881–1889 (2009).
34. Perrin, C. L. & Nielson, J. B. ‘Strong’ hydrogen bonds in chemistry and biology. *Annu. Rev. Phys. Chem.* **48**, 511–544 (1997).
35. Megiatto, J. D. Jr *et al.* Intramolecular hydrogen bonding as a synthetic tool to induce chemical selectivity in acid catalyzed porphyrin synthesis. *Chem. Commun.* **48**, 4558–4560 (2012).
36. Nurminen, E. J., Mattinen, J. K. & Lönnberg, H. Nucleophilic and acid catalysis in phosphoramidite alcoholysis. *J. Chem. Soc. Perkin Trans. 2*, 2159–2165 (2001).
37. Moore, G. F. *et al.* Effects of protonation state on a tyrosine–histidine bioinspired redox mediator. *J. Phys. Chem. B* **114**, 14450–14457 (2010).
38. Edwards, J. S., Soudackov, A. V. & Hammes-Schiffer, S. Analysis of kinetic isotope effects for proton-coupled electron transfer reactions. *J. Phys. Chem. A* **113**, 2117–2126 (2009).
39. Witwicki, M. & Jezierska, J. Protic and aprotic solvent effect on molecular properties and *g*-tensors of *o*-semiquinones with various aromaticity and heteroatoms: a DFT study. *Chem. Phys. Lett.* **493**, 364–370 (2010).
40. Witwicki, M., Jezierska, J. & Ozarowski, A. Solvent effect on EPR, molecular and electronic properties of semiquinone radical derived from 3,4-dihydroxybenzoic acid as model for humic acid transient radicals: high-field EPR and DFT studies. *Chem. Phys. Lett.* **473**, 160–166 (2009).
41. Barry, B. A. *et al.* Proton-coupled electron transfer and redox active tyrosines: structure and function of tyrosyl radicals in ribonucleotide reductase and photosystem II. *J. Phys. Chem. Lett.* **3**, 534–554 (2012).
42. Jenson D. L. & Barry, B. A. Proton-coupled electron transfer in photosystem II: proton inventory of a redox active tyrosine. *J. Am. Chem. Soc.* **131**, 10567–10573 (2009).
43. Chatterjee, R. *et al.* High-frequency electron nuclear double-resonance spectroscopy studies of the mechanism of proton-coupled electron transfer at the tyrosine-D residue of photosystem II. *Biochemistry* **52**, 4781–4790 (2013).
44. Zhao, Y. *et al.* Improving the efficiency of water splitting in dye-sensitized solar cells by using a biomimetic electron transfer mediator. *Proc. Natl Acad. Sci. USA* **109**, 15612–15616 (2012).
45. Rajh, T., Ostafin, A. E., Micic, O. I., Tiede, D. M. & Thurnauer, M. C. Surface modification of small particle TiO₂ colloids with cysteine for enhanced photochemical reduction: an EPR study. *J. Phys. Chem.* **100**, 4538–4545 (1996).
46. Lakshmi, K. V. *et al.* High-field EPR study of carotenoid and chlorophyll cation radicals in photosystem II. *J. Phys. Chem. B* **104**, 10445–10448 (2000).

Acknowledgements

This work was supported as part of the Center for Bio-Inspired Solar Fuel Production, an Energy Frontier Research Center funded by the US Department of Energy, Office of Science, Office of Basic Energy Sciences (award DE-SC0001016). D.D.M.H. was supported by the National Science Foundation Graduate Research Fellowship Program (NSF-GRFP; grant no. DGE-0802261), by the More Graduate Education at Mountain States Alliance (MGE@MSA) and by the Alliance for Graduate Education and the Professoriate (AGEP), National Science Foundation Cooperative agreement no. HRD-0450137. The high-frequency EPR work was supported by the US Department of Energy, Office of Basic Energy Sciences, Division of Chemical Sciences, Geosciences, and Biosciences (contract no. DE-AC02-06CH11357, O.G.P.). The work performed at the Center for Nanoscale Materials was supported by the US Department of Energy, Office of Science, Office of Basic Energy Sciences (contract no. DE-AC02-06CH11357).

Author contributions

J.D.M.J., D.G., T.A.M. and A.L.M. designed the research and experiments. J.D.M.J. and M.E.T.J. synthesized and characterized all chemical compounds. J.D.M.J. and T.L.G. are responsible for the crystal structure. D.D.M.H. and V.M. conducted theoretical calculations. O.G.P. and T.R. performed EPR experiments. A.L.T. carried out electrochemical measurements. M.J.L.P. and G.K. performed photophysical characterizations. J.D.M.J., D.D.M.H., M.J.L.P., G.K., O.G.P., T.R., V.M., D.G., T.A.M. and A.L.M. analysed and interpreted the data. J.D.M.J., D.D.M.H., D.G., T.A.M. and A.L.M. wrote the manuscript.

Additional information

Supplementary information and chemical compound information are available in the online version of the paper. Reprints and permissions information is available online at www.nature.com/reprints. Correspondence and requests for materials should be addressed to A.L.M.

Competing financial interests

The authors declare no competing financial interests.

Photoelectrochemical cells

Michael Grätzel

Institute of Photonics and Interfaces, Swiss Federal Institute of Technology, CH-1015, Lausanne, Switzerland (e-mail michael.gratzel@epfl.ch)

Until now, photovoltaics — the conversion of sunlight to electrical power — has been dominated by solid-state junction devices, often made of silicon. But this dominance is now being challenged by the emergence of a new generation of photovoltaic cells, based, for example, on nanocrystalline materials and conducting polymer films. These offer the prospect of cheap fabrication together with other attractive features, such as flexibility. The phenomenal recent progress in fabricating and characterizing nanocrystalline materials has opened up whole new vistas of opportunity. Contrary to expectation, some of the new devices have strikingly high conversion efficiencies, which compete with those of conventional devices. Here I look into the historical background, and present status and development prospects for this new generation of photoelectrochemical cells.

Ever since the French scientist Edmond Becquerel discovered the photoelectric effect, researchers and engineers have been infatuated with the idea of converting light into electric power or chemical fuels. Their common dream is to capture the energy that is freely available from sunlight and turn it into the valuable and strategically important asset that is electric power, or use it to generate fuels such as hydrogen. Photovoltaics takes advantage of the fact that photons falling on a semiconductor can create

electron–hole pairs, and at a junction between two different materials, this effect can set up an electric potential difference across the interface. So far, the science of solar cells has been dominated by devices in which the junction is between inorganic solid-state materials, usually doped forms of crystalline or amorphous silicon, and profiting from the experience and material availability resulting from the semiconductor industry. Recently, we have seen more use of devices made from compound semiconductors — the III/V compounds for high-efficiency aerospace components and the copper–indium–sulphide/selenide materials for thin-film, low-cost terrestrial cells. But the dominance of the field by inorganic solid-state junction devices faces new challenges in the coming years. Increasingly, there is an awareness of the possible advantages of nanocrystalline and conducting polymer devices, for example, which are relatively cheap to fabricate (the expensive and energy-intensive high-temperature and high-vacuum processes needed for the traditional devices can be avoided), can be used on flexible substrates, and can be shaped or tinted to suit domestic devices or architectural or decorative applications. It is now even possible to depart completely from the classical solid-state junction device, by replacing the phase in contact with the semiconductor by an electrolyte (liquid, gel or organic solid), thereby forming a photoelectrochemical device.

The development of these new types of solar cells is promoted by increasing public awareness that the Earth's oil reserves could run out during this century. As the energy needs of the planet are likely to double within the next 50 years, the stage is set for a major energy shortage, unless renewable energy can cover the substantial deficit left by fossil fuels. Public concern has been heightened by the disastrous environmental pollution arising from all-too-frequent oil spills and the frightening climatic consequences of the greenhouse effect caused by fossil fuel combustion. Fortunately the supply of energy from the Sun to the Earth is gigantic: 3×10^{24} joules a year, or about 10,000 times more than the global population currently consumes. In other words, covering 0.1% of the Earth's surface with solar cells with an efficiency of 10% would satisfy our present needs. But to tap into this huge energy reservoir remains an enormous challenge.

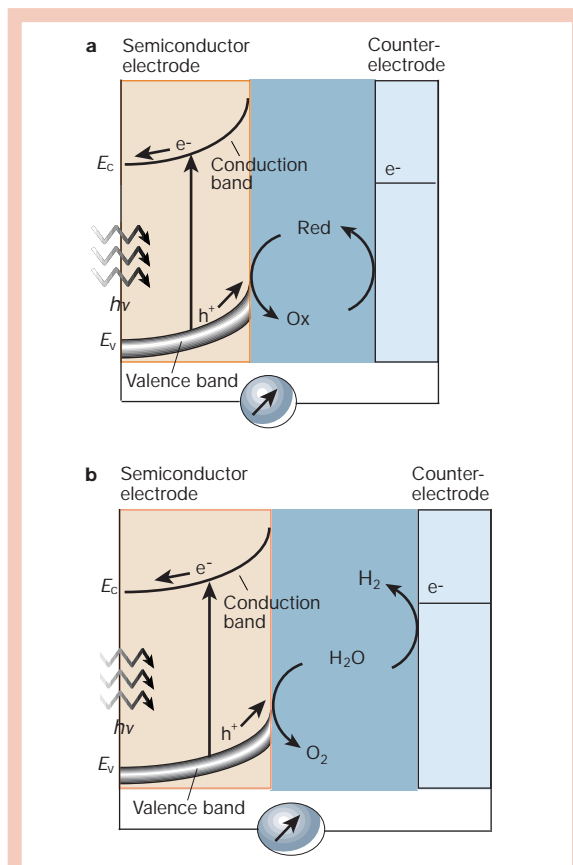
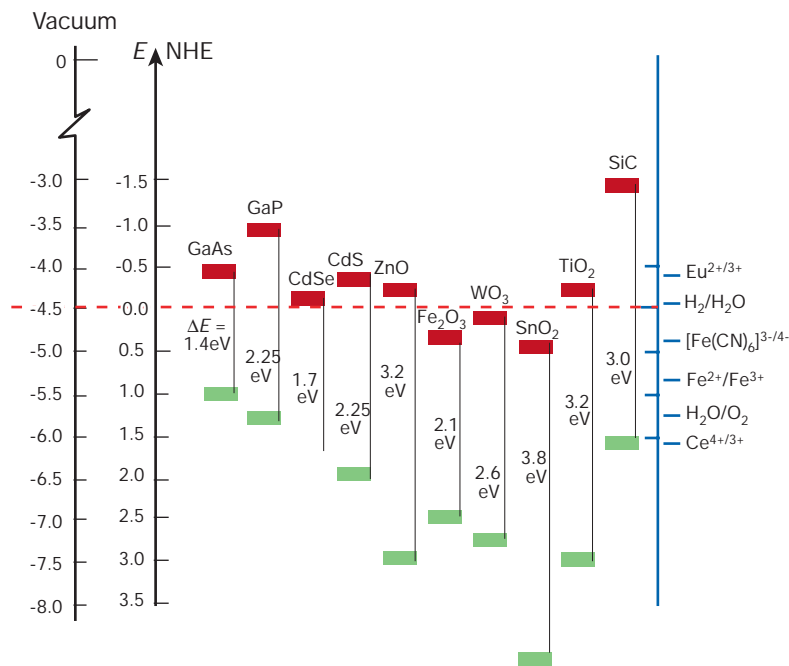


Figure 1 Principle of operation of photoelectrochemical cells based on *n*-type semiconductors. **a**, Regenerative-type cell producing electric current from sunlight; **b**, a cell that generates a chemical fuel, hydrogen, through the photo-cleavage of water.

Historical background

Becquerel's pioneering photoelectric experiments in 1839 were done with liquid not solid-state devices — a fact that is often ignored. His research, in which illumination of

Figure 2 Band positions of several semiconductors in contact with aqueous electrolyte at pH 1. The lower edge of the conduction band (red colour) and upper edge of the valence band (green colour) are presented along with the band gap in electron volts. The energy scale is indicated in electron volts using either the normal hydrogen electrode (NHE) or the vacuum level as a reference. Note that the ordinate presents internal and not free energy. The free energy of an electron–hole pair is smaller than the band gap energy due to the translational entropy of the electrons and holes in the conduction and valence band, respectively. On the right side the standard potentials of several redox couples are presented against the standard hydrogen electrode potential.



solutions containing a metal halide salt produced a current between two platinum electrodes immersed in the electrolyte, was motivated by photography. Daguerre had made the first photographic images in 1837, and Fox Talbot followed with the silver halide process in 1839. Although the art of formulating emulsions only became a science with the theoretical analysis of the process by Gurney and Mott² in 1938, there was constant empirical progress in the sensitivity of photographic films. Initially, films were particularly insensitive to mid-spectrum and red light. This is now recognized as being due to the semiconductor nature of the silver halide grains: they have a band gap (a gap in the allowed electronic energy levels) which ranges from 2.7 to 3.2 electron volts (eV) and negligible light absorption at wavelengths longer than 460 nm. Vogel's discovery³ in 1883 that silver halide emulsions could be sensitized by adding a dye extended the photosensitivity to longer wavelengths. Four years later, the concept of dye enhancement was carried over by Moser⁴ from photography to photoelectrochemical cells using the dye erythrosine on silver halide electrodes. This parallel between photography and photoelectrochemistry comes as a surprise to many chemists⁵. That the same dyes were particularly effective for both processes was recognized by Namba and Hishiki at the 1964 International Conference on Photosensitization of Solids in Chicago, which was a seminal event in the history of sensitization⁶. It was also recognized that the dye should be adsorbed on the semiconductor electrodes in a closely packed monolayer for maximum efficiency⁷. At this stage it was still debated whether sensitization occurred by transfer of electrons or of energy from the dye to the semiconductor⁸. Subsequent studies, notably by Hauffe⁹, Tributsch and Gerischer¹⁰, showed electron transfer to be the prevalent mechanism both for photographic and for photoelectrochemical sensitization processes.

Photosynthetic and regenerative cells

The foundation of modern photoelectrochemistry, marking its change from a mere support of photography to a thriving research direction on its own, was laid down by the work of Brattain and Garret¹¹ and subsequently Gerischer¹² who undertook the first detailed electrochemical and photoelectrochemical studies of the semiconductor–electrolyte interface. Research on photoelectrochemical cells went through a

frantic period after the oil crisis in 1973, which stimulated a worldwide quest for alternative energy sources. Within a few years well over a thousand publications appeared (see ref. 13 for a list).

Investigations focused on two types of cells whose principle of operation is shown in Fig. 1. The first type is the regenerative cell, which converts light to electric power leaving no net chemical change behind. Photons of energy exceeding that of the band gap generate electron–hole pairs, which are separated by the electric field present in the space-charge layer (see Box 1 for an explanation). The negative charge carriers move through the bulk of the semiconductor to the current collector and the external circuit. The positive holes are driven to the surface where they are scavenged by the reduced form of the redox relay molecule (R), oxidizing it: $h^+ + R \rightarrow O$. The oxidized form O is reduced back to R by the electrons that re-enter the cell from the external circuit. Much of the work on regenerative cells has focused on electron-doped (*n*-type) II/VI or III/V semiconductors using electrolytes based on sulphide/polysulphide, vanadium(II)/vanadium(III) or I₂/I⁻ redox couples. Conversion efficiencies of up to 19.6% have been reported for multijunction regenerative cells¹⁴.

The second type, photosynthetic cells, operate on a similar principle except that there are two redox systems: one reacting with the holes at the surface of the semiconductor electrode and the second reacting with the electrons entering the counter-electrode. In the example shown, water is oxidized to oxygen at the semiconductor photoanode and reduced to hydrogen at the cathode. The overall reaction is the cleavage of water by sunlight. Titanium dioxide has been the favoured semiconductor for these studies, following its use by Fujishima and Honda for water photolysis¹⁵. Unfortunately, because of its large band gap (3–3.2 eV, as shown in Fig. 2), TiO₂ absorbs only the ultraviolet part of the solar emission and so has low conversion efficiencies. Numerous attempts to shift the spectral response of TiO₂ into the visible, or to develop alternative oxides affording water cleavage by visible light, have so far failed.

In view of these prolonged efforts, disillusionment has grown about the prospects of photoelectrochemical cells being able to give rise to competitive photovoltaic devices, as those semiconductors with band gaps narrow enough for efficient absorption of visible light

Box 1

The semiconductor–electrolyte interface

When a semiconductor is placed in contact with an electrolyte, electric current initially flows across the junction until electronic equilibrium is reached, where the Fermi energy of the electrons in the solid (E_F) is equal to the redox potential of the electrolyte (E_{redox}), as shown in the figure. The transfer of electric charge produces a region on each side of the junction where the charge distribution differs from the bulk material, and this is known as the space-charge layer. On the electrolyte side, this corresponds to the familiar electrolytic double layer, that is, the compact (Helmholtz) layer followed by the diffuse (Gouy–Chapman) layer. On the semiconductor side of the junction the nature of the band bending depends on the position of the Fermi level in the solid. If the Fermi level of the electrode is equal to the flat band potential, there is no excess charge on either side of the junction and the bands are flat. If electrons accumulate at the semiconductor side one obtains an accumulation layer. If, however, they deplete from the solid into the solution, a depletion layer is formed, leaving behind a positive excess charge formed by immobile ionized donor states. Finally, electron depletion can go so far that their concentration at the interface falls below the intrinsic level. As a consequence, the semiconductor is *p*-type at the surface and *n*-type in the bulk, corresponding to an inversion layer. The illustration in the figure refers to *n*-type materials where electrons are the mobile charge carriers. For *p*-type semiconductors, analogous considerations apply. Positive holes are the mobile charge carriers and the immobile negatively charged states of the acceptor dopant form the excess space charge within the depletion layer.

The flat band potential is a very useful quantity in photoelectrochemistry as it facilitates location of the energetic position of the valence and conduction band edge of a given semiconductor material. It is obtained by measuring the capacity of the semiconductor–electrolyte junction. The semiconductor is subjected to reverse bias — that is, a voltage is applied to increase the potential step across the junction — and the differential capacity is determined as a function of the applied potential, V . The space-charge capacity of the semiconductor (C_{sc}) is in series with that of the Helmholtz layer (C_{H}) present at the electrolyte side of the interface. In the depletion regime the condition $C_{\text{H}} > C_{\text{sc}}$ applies, so the measured capacity is that of the space-charge layer. This depends on the applied bias voltage according to the Mott–Schottky equation: $1/(C_{\text{sc}})^2 = 2(\Delta\phi_{\text{sc}}RT/F)/(\epsilon_0\epsilon^1N)$, where $\Delta\phi_{\text{sc}} = V - V_{\text{fb}}$ is the voltage drop in the space-charge layer, R is the gas constant, F the Faraday number, ϵ the dielectric constant of the semiconductor, ϵ_0 the permittivity of vacuum and N the ionized donor dopant concentration. A plot of the square of the reciprocal capacity against the applied voltage gives a straight line and this is extrapolated to $1/(C_{\text{sc}})^2 = 0$ to derive the flat band potential V_{fb} .

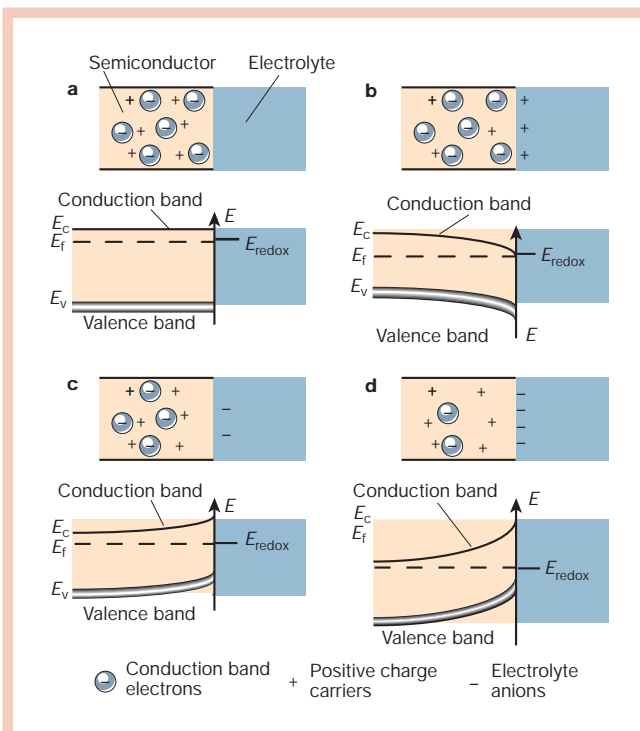
are unstable against photocorrosion. The width of the band gap is a measure of the chemical bond strength. Semiconductors stable under illumination, typically oxides of metals such as titanium or niobium, therefore have a wide band gap, an absorption edge towards the ultraviolet and consequently an insensitivity to the visible spectrum.

The resolution of this dilemma came in the separation of the optical absorption and charge-generating functions, using an electron transfer sensitizer absorbing in the visible to inject charge carriers across the semiconductor–electrolyte junction into a substrate with a wide band gap, and therefore stable. Figure 3 shows the operational principle of such a device.

Nanocrystalline junctions and interpenetrating networks

The need for dye-sensitized solar cells to absorb far more of the incident light was the driving force for the development of

Flat band potentials have been determined for a large number of materials⁴⁹ and some representative examples are shown in Fig. 2. Apart from the type of semiconductor they depend on the nature and composition of the electrolyte. In aqueous solution the flat band potentials of most oxide semiconductors shifts by 0.059 V when the pH is changed by one unit. This is a consequence of the fact that protons are potential-determining ions for these solids.



Box 1 Figure Schematic showing the electronic energy levels at the interface between an *n*-type semiconductor and an electrolyte containing a redox couple. The four cases indicated are: **a**, flat band potential, where no space-charge layer exists in the semiconductor; **b**, accumulation layer, where excess electrons have been injected into the solid producing a downward bending of the conduction and valence band towards the interface; **c**, depletion layer, where electrons have moved from the semiconductor to the electrolyte, producing an upward bending of the bands; and **d**, inversion layer where the electrons have been depleted below their intrinsic level, enhancing the upward band bending and rendering the semiconductor *p*-type at the surface.

mesoscopic semiconductor materials¹⁶ — minutely structured materials with an enormous internal surface area — which have attracted great attention during recent years. Mesoporous oxide films are made up of arrays of tiny crystals measuring a few nanometres across. Oxides such as TiO₂, ZnO, SnO₂ and Nb₂O₅, or chalcogenides such as CdSe, are the preferred compounds. These are interconnected to allow electronic conduction to take place. Between the particles are mesoscopic pores filled with a semiconducting or a conducting medium, such as a *p*-type semiconductor, a polymer, a hole transmitter or an electrolyte. The net result is a junction of extremely large contact area between two interpenetrating, individually continuous networks. Particularly intriguing is the ease with which charge carriers percolate across the mesoscopic particle network, making the huge internal surface area electronically addressable. Charge transport in such mesoporous

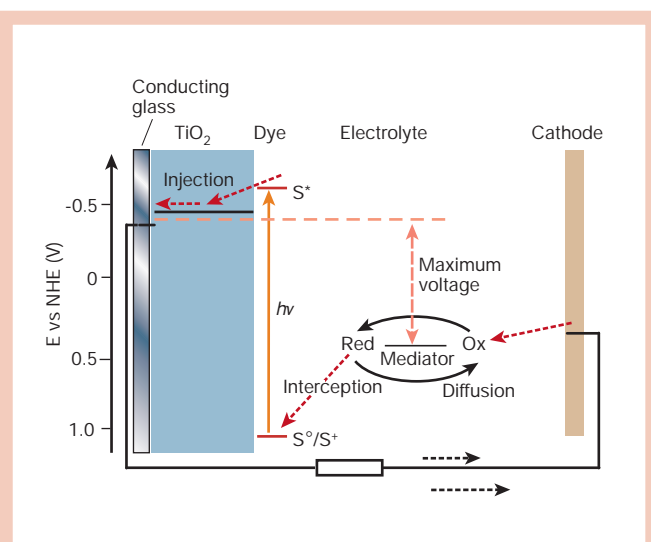


Figure 3 Schematic of operation of the dye-sensitized electrochemical photovoltaic cell. The photoanode, made of a mesoporous dye-sensitized semiconductor, receives electrons from the photo-excited dye which is thereby oxidized, and which in turn oxidizes the mediator, a redox species dissolved in the electrolyte. The mediator is regenerated by reduction at the cathode by the electrons circulated through the external circuit. Figure courtesy of P. Bonhôte/EPFL-LPI.

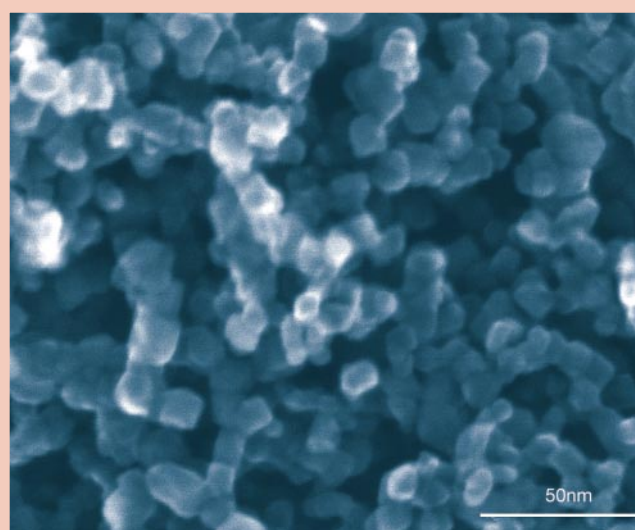


Figure 4 Scanning electron micrograph of the surface of a mesoporous anatase film prepared from a hydrothermally processed TiO_2 colloid. The exposed surface planes have mainly $\{101\}$ orientation.

systems is under intense investigation today^{17,18} and is best described by a random walk model¹⁹.

The semiconductor structure, typically 10 μm thick and with a porosity of 50%, has a surface area available for dye chemisorption over a thousand times that of a flat, unstructured electrode of the same size. If the dye is chemisorbed as a monomolecular layer, enough can be retained on a given area of electrode to provide absorption of essentially all the incident light. Figure 4 shows an electron micrograph of a nanocrystalline TiO_2 film with a grain size in the range of 10–80 nm. (For details of the hydrothermal deposition procedure, starting with hydrolysis of a titanium isopropoxide precursor and terminating with screen printing and firing of the semiconductor layer on a conductive transparent substrate, see ref. 20.)

The nanostructuring of the semiconductor introduces profound changes in its photoelectrochemical properties. Of great importance is the fact that a depletion layer (see Box 1) cannot be formed in the solid — the particles are simply too small. The voltage drop within the nanocrystals remains small under reverse bias, typically a few millivolts. As a consequence there is no significant local electric field present to assist in the separation of photogenerated electron–hole pairs. The photoresponse of the electrode is determined by the rate of reaction of the positive and negative charge carriers with the redox couple present in the electrolyte. If the transfer of electrons to the electrolyte is faster than that of holes, then a cathodic photocurrent will flow, like in a *p*-type semiconductor/liquid junction. In contrast, if hole transfer to the electrolyte is faster, then anodic photocurrent will flow, as in *n*-type semiconductor photoelectrochemical cells. Striking confirmation of the importance of these kinetic effects came with the demonstration²¹ that the same nanocrystalline film could show alternatively *n*- or *p*-type behaviour, depending on the nature of the hole or electron scavenger present in the electrolyte phase. This came as a great surprise to a field where the traditional thinking was to link the photoresponse to formation of a charge-depletion layer at the semiconductor–electrolyte interface.

What, then, is the true origin of the photovoltage in dye-sensitized solar cells? In the conventional picture, the photovoltage of photoelectrochemical cells does not exceed the potential drop in the space-charge layer (Box 1 Figure). But nanocrystalline cells can

develop photovoltages close to 1 V even though the junction potential is in the millivolt range. It has been suggested that a built-in potential difference at the back contact of the nanocrystalline film with the conducting glass is responsible for the observed photovoltage²². Other evidence²³ suggests that under illumination, electron injection from the sensitizer increases the electron concentration in the nanocrystalline electrode, raising the Fermi level of the oxide and thus shifting its potential²⁴. From recent electrical impedance studies²⁵, it seems that both changes — the potential drop across the back contact and the Fermi level shift of the TiO_2 nanoparticles — contribute to the photovoltage of dye-sensitized solar cells.

Accumulation layers (part b of Box 1 Figure) can be produced in the nanocrystals under forward bias when majority carriers are injected, rendering the film highly conductive. Under reverse bias the carriers are withdrawn, turning it into an insulator. Thus, by changing the applied potential, the film can be switched back and forth from a conducting to an insulating state. Space-charge limitation of the current (arising from limitation of the density of charge carriers because they are repelled by each other's electric field) is not observed as the injected majority carriers are efficiently screened by the electrolyte present in the pores surrounding the nanoparticles. The factors controlling the rate of charge carrier percolation across the nanocrystalline film are under intense scrutiny¹⁷. A technique known as intensity-modulated impedance spectroscopy has proved to be an elegant and powerful tool^{25,26} for addressing these and other important questions related to the characteristic time constants for charge carrier transport and reaction dynamics.

An interesting feature specific to nanocrystalline electrodes is the appearance of quantum confinement effects. These appear when the films are made up of small quantum dots, such as 8-nm-sized CdTe particles²⁷. Such layers have a larger band gap than the bulk material, the band edge position being shifted with respect to the positions indicated in Fig. 2 for macroscopic materials. The conduction band redox potential is lowered and that of the valence band is increased. As a consequence, electrons and holes can perform reduction and oxidation reactions that cannot proceed on bulk semiconductors.

The astounding photoelectrochemical performance of nanocrystalline semiconductor junctions is illustrated in Fig. 5 where we

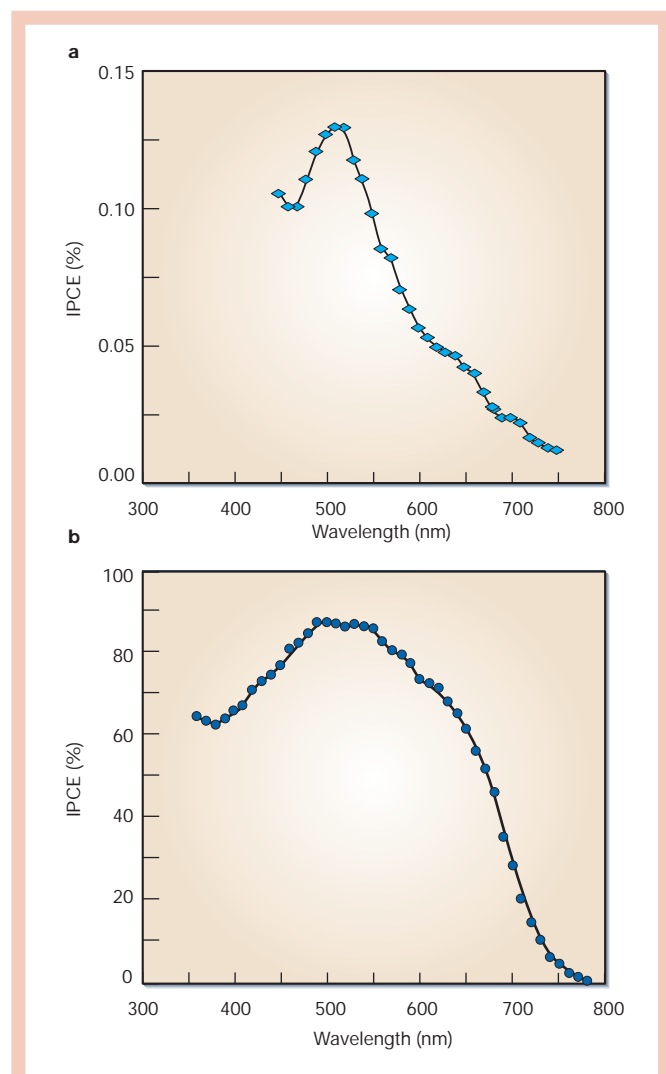


Figure 5 The nanocrystalline effect in dye-sensitized solar cells. In both cases, TiO₂ electrodes are sensitized by the surface-anchored ruthenium complex *cis*-RuL₂(SCN)₂. The incident-photon-to-current conversion efficiency is plotted as a function of the excitation wavelength. **a**, Single-crystal anatase cut in the (101) plane. **b**, Nanocrystalline anatase film. The electrolyte consisted of a solution of 0.3M I⁻ and 0.03M I₂ in acetonitrile.

compare the photoresponse of an electrode made of single-crystal anatase, one of the crystal forms of TiO₂, with that of a mesoporous TiO₂ film. Both electrodes are sensitized by the ruthenium complex *cis*-RuL₂(SCN)₂ (L is 2,2'-bipyridyl-4,4'-dicarboxylate), which is adsorbed as a monomolecular film at the titania surface. The incident-photon-to-current conversion efficiency (IPCE) is plotted as a function of wavelength. The IPCE value obtained with the single-crystal electrode is only 0.13% near 530 nm, where the sensitizer has an absorption maximum, whereas it reaches 88% with the nanocrystalline electrode²⁸ — more than 600 times as great. The photocurrent in standard sunlight augments 10³–10⁴ times when passing from a single crystal to a nanocrystalline electrode (standard, or full, sunlight is defined as having a global intensity (*I*) of 1,000 W m⁻², air mass 1.5; air mass is the path length of the solar light relative to a vertical position of the Sun above the terrestrial absorber). This striking improvement is due largely to the far better light harvesting of the dye-sensitized nanocrystalline film as compared with a flat single-crystal electrode, but is also due, at least in part, to the mesoscopic film texture favouring photogeneration and collection of charge carriers²⁹.

The overall conversion efficiency of the dye-sensitized cell is determined by the photocurrent density measured at short circuit (*i*_{ph}), the open-circuit photo-voltage (*V*_{oc}), the fill factor of the cell (*ff*) and the intensity of the incident light (*I*)

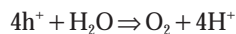
$$\eta_{\text{global}} = i_{\text{ph}} V_{\text{oc}} (\text{ff}/I)$$

Under full sunlight, short-circuit photocurrents ranging from 16 to 22 mA cm⁻² are reached with state-of-the-art ruthenium sensitizers, while *V*_{oc} is 0.7–0.8 V and the fill factor values are 0.65–0.75. A certified overall power conversion efficiency of 10.4% has been attained at the US National Renewable Energy Laboratory³⁰. Although this efficiency makes dye-sensitized cells fully competitive with the better amorphous silicon devices, an even more significant parameter is the dye lifetime achieved under working conditions. For credible system performance, a dye molecule must sustain at least 10⁸ redox cycles of photo-excitation, electron injection and regeneration, to give a device service life of 20 years. The use of solvents such as valeronitrile, or γ -butyrolactone, appropriately purified, in the electrolyte formulation provide a system able to pass the standard stability qualification tests for outdoor applications, including thermal stress for 1,000 h at 85 °C, and this has been verified independently³¹.

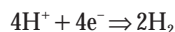
Tandem cells for water cleavage by visible light

The advent of nanocrystalline semiconductor systems has rekindled interest in tandem cells for water cleavage by visible light, which remains a highly prized goal of photoelectrochemical research. The 'brute force' approach to this goal is to use a set of four silicon photovoltaic cells connected in series to generate electricity that is subsequently passed into a commercial-type water electrolyser. Solar-to-chemical conversion efficiencies obtained are about 7%. Much higher efficiencies in the range of 12–20% have been reported for tandem cells based on III/V semiconductors^{14,32}, but these single-crystal materials cost too much for large-scale terrestrial applications.

A low-cost tandem device that achieves direct cleavage of water into hydrogen and oxygen by visible light was developed recently³³. This is based on two photosystems connected in series as shown in the electron flow diagram of Fig. 6. A thin film of nanocrystalline tungsten trioxide, WO₃ (ref. 34), or Fe₂O₃ (ref. 35) serves as the top electrode absorbing the blue part of the solar spectrum. The valence-band holes (h⁺) created by band-gap excitation of the film oxidize water to oxygen:



and the conduction-band electrons are fed into the second photosystem consisting of the dye-sensitized nanocrystalline TiO₂ cell discussed above. The latter is placed directly under the WO₃ film, capturing the green and red part of the solar spectrum that is transmitted through the top electrode. The photovoltage generated by the second photosystem enables hydrogen to be generated by the conduction-band electrons.



The overall reaction corresponds to the splitting of water by visible light. There is close analogy to the 'Z-scheme' (named for the shape of the flow diagram) that operates in photosynthesis. In green plants, there are also two photosystems connected in series, one that oxidizes water to oxygen and the other generating the compound NADPH used in fixation of carbon dioxide. As discussed above, the advantage of the tandem approach is that higher efficiencies can be reached than with single junction cells if the two photosystems absorb complementary parts of the solar spectrum. At present, the overall conversion efficiency from standard solar light to chemical

energy achieved with this device stands at 4.5%, and further improvements are being sought.

Dye-sensitized solid heterojunctions and ETA cells

Interest is growing in devices in which both the electron- and hole-carrying materials are solids, but are grown as interpenetrating networks forming a heterojunction of large contact area. From conventional wisdom one would have predicted that solar cells of this kind would work very poorly, if at all. The disordered character of the junction and the presence of the huge interface are features one tries to avoid in conventional photovoltaic cells, because the disruption of the crystal symmetry at the surface produces electronic states in the band gap of the semiconductor, enhancing the recombination of photogenerated carriers. The fact that molecular photovoltaic cells based on the sensitization of nanocrystalline TiO_2 were able to achieve overall conversion efficiencies from solar to electric power of over 10% encouraged work on solid-state analogues, that is, dye-sensitized heterojunctions. The first devices of this type used inorganic *p*-type semiconductors, for example CuI (ref. 36) or CuSCN (ref. 37), as hole conductors replacing the redox electrolyte. Respectable conversion efficiencies exceeding 1% have been reached with such cells. But the lack of photostability of the Cu(I) compounds and the difficulty of realizing a good contact between the two mesoscopic inorganic materials still present considerable practical challenges.

Organic charge-transport materials have advantages in this respect. An amorphous hole conductor can be introduced into the mesoporous TiO_2 film by a simple spin-coating process and readily adapts its form to the highly corrugated oxide surface. Cells based on a spirobisfluorene-connected arylamine hole transmitter³⁸, which fills the pores of a dye-sensitized nanocrystalline TiO_2 film, have reached a conversion efficiency of 2.56% at full sunlight³⁹. The high open-circuit voltage of these devices, exceeding 900 mV, is particularly noteworthy and promising for further substantial improvements in performance. In general, dye-sensitized heterojunction cells offer great flexibility because the light absorber and charge-transport material can be selected independently to obtain optimal solar energy harvesting and high photovoltaic output. The great advantage of such a configuration is that the charge carriers are generated by the dye precisely at the site of the junction where the electric field is greatest, enhancing charge separation.

Extremely thin absorber (ETA) solar cells are conceptually close to dye-sensitized heterojunctions. The molecular dye is replaced by an extremely thin (2–3 nm) layer of a small-band-gap semiconductor, such as CuInS_2 . A hole conductor such as CuSCN is placed on top of the absorber, producing a junction of the PIN type (*p*-type semiconductor/insulator/*n*-type semiconductor)⁴⁰. The structure has the advantage of enhanced light harvesting due to the surface enlargement and multiple scattering. Because photo-induced charge separation occurs on a length scale of a few nanometres, higher levels of defects and impurities can be tolerated than in flat thin-film devices, where the minority carriers are required to diffuse several microns. On the other hand, making PIN-junctions of such high contact area is difficult and this has hampered the performance of these cells. Their conversion efficiency so far has remained below 5%, which is less than one-third of the yield obtained with similar semiconductor materials in a flat junction configuration.

Soft junctions and organic solar cells

Organic materials have the advantage of being cheap and easy to process. They can be deposited on flexible substrates, bending where their inorganic competitors would crack. The choice of materials is practically unlimited, and specific parts of the solar spectrum can be selectively absorbed. Although organic cells are still considerably less efficient than single-crystal gallium arsenide or silicon, progress has been impressive over the past few years. In particular, solar cells based on interpenetrating polymer networks⁴¹, polymer/fullerene blends⁴²,

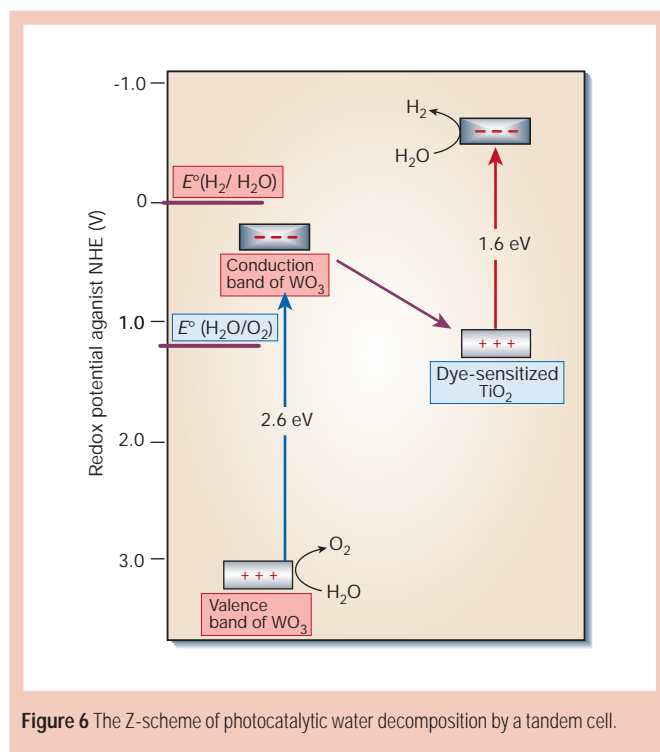


Figure 6 The Z-scheme of photocatalytic water decomposition by a tandem cell.

halogen-doped organic crystals⁴³ and the solid-state dye-sensitized devices mentioned above³⁸ have shown surprisingly high solar conversion efficiencies, currently reaching values of 2–3%.

Conducting polymers, for example poly-(phenylenevinylene) (PPV) derivatives or C_{60} particles, are attracting great interest as photovoltaic materials^{44,49}. Bulk donor–acceptor heterojunctions are formed simply by blending the two organic materials serving as electron donor (*p*-type conductor) and electron acceptor (*n*-type conductor). The advantage of these new structures over the flat-junction organic cells investigated earlier⁴⁵ is the interpenetration of the two materials that conduct positive and negative charge carriers, reducing the size of the individual phase domains to the nanometre range. This overcomes one of the problems of the first generation of organic photovoltaic cells: the unfavourable ratio of exciton diffusion length to optical absorption length. An exciton is a bound electron–hole pair produced by absorption of light; to be useful, this pair must reach the junction and there dissociate into two free charge carriers — but excitons typically diffuse only a few nanometres before recombining. Light is absorbed (and generates excitons) throughout the composite material. But in the composite, the distance the exciton has to travel before reaching the interface is at most a few nanometres, which is commensurate with its diffusion length. Hence photo-induced charge separation can occur very efficiently. A conversion efficiency from incident photons to current of over 50% has been achieved with a blend containing PPV and methanofullerene derivatives⁴⁶. The overall conversion efficiency from solar to electric power under full sunlight achieved with this cell was 2.5%. Although these results are impressive, the performance of the cell declined rapidly within hours of exposure to sunlight⁴⁷. In contrast, the output of dye-sensitized solar cells is remarkably stable even under light soaking for more than 10,000 h. Similar long-term stability will be required for large-scale application of polymer solar cells.

Summary

Photovoltaic devices based on interpenetrating mesoscopic networks have emerged as a credible alternative to conventional solar cells. Common to all these cells is an ultrafast initial charge separation step, occurring in femtoseconds, and a much slower back-reaction.

Table 1 Performance of photovoltaic and photoelectrochemical solar cells

Type of cell	Efficiency (%) [*]		Research and technology needs
	Cell	Module	
Crystalline silicon	24	10–15	Higher production yields, lowering of cost and energy content
Multicrystalline silicon	18	9–12	Lower manufacturing cost and complexity
Amorphous silicon	13	7	Lower production costs, increase production volume and stability
CuInSe ₂	19	12	Replace indium (too expensive and limited supply), replace CdS window layer, scale up production
Dye-sensitized nanostructured materials	10–11	7	Improve efficiency and high-temperature stability, scale up production
Bipolar AlGaAs/Si photoelectrochemical cells	19–20	—	Reduce materials cost, scale up
Organic solar cells	2–3	—	Improve stability and efficiency

^{*}Efficiency defined as conversion efficiency from solar to electrical power.

This allows the charge carriers to be collected as electric current before recombination takes place. Table 1 compares the performance of the new photoelectrochemical systems with conventional devices. Although still of lower efficiency, the nanostructured cells offer several advantages over their competitors. They can be produced more cheaply and at less of a cost in energy than silicon cells, for which 5 GJ have to be spent to make 1 m² of collector area. Unlike silicon, their efficiency increases with temperature, narrowing the efficiency gap under normal operating conditions. They usually have a bifacial configuration, allowing them to capture light from all angles. Transparent versions of different colour can readily be made that could serve as electric power-producing windows in buildings. These and other attractive features⁴⁸ justify the present excitement about these cells and should aid their entry into a tough market. □

- Bequerel, E. Recherches sur les effets de la radiation chimique de la lumière solaire, au moyen des courants électriques. *C.R. Acad. Sci.* **9**, 145–149 (1839).
- Gurney, R. W. & Mott, N. F. Theory of the photolysis of silver bromide and the photographic latent image. *Proc. R. Soc. Lond. A* **164**, 151–167 (1938).
- West, W. First hundred years of spectral sensitization. *Proc. Vogel Cent. Symp. Photogr. Sci. Eng.* **18**, 35–48 (1974).
- Moser, J. Notiz über die Verstärkung photoelectrischer Ströme durch optische Sensibilisierung. *Monatsh. Chem.* **8**, 373 (1887).
- Spitler, M. T. Dye photo-oxidation at semiconductor electrodes—a corollary to spectral sensitization in photography. *J. Chem. Educ.* **60**, 330–332 (1983).
- Namba, S. & Hishiki, Y. Color sensitization of zinc oxide with cyanide dyes. *J. Phys. Chem.* **69**, 774–779 (1965).
- Nelson, R. C. Minority carrier trapping and dye sensitization. *J. Phys. Chem.* **69**, 714–718 (1965).
- Boudon, J. Spectral sensitization of chemical effects in solids. *J. Phys. Chem.* **69**, 705–713 (1965).
- Gerischer, H. & Tributsch, H. Electrochemische Untersuchungen zur spectraleu sensibilisierung von ZnO-Einkristallen. *Ber. Bunsenges. Phys. Chem.* **72**, 437–445 (1968).
- Haufler, K., Danzmann, H. J., Pusch, H., Range, J. & Volz, H. New Experiments on the sensitization of zinc oxide by means of the electrochemical cell technique. *J. Electrochem. Soc.* **117**, 993–999 (1970).
- Brattain, W. H. & Garrett, C. G. B. Experiments on the interface between germanium and an electrolyte. *Bell Syst. Tech. J.* **34**, 129–176 (1955).
- Gerischer, H. Electrochemical behavior of semiconductors under illumination. *J. Electrochem. Soc.* **113**, 1174–1182 (1966).
- Kalyanasundaram, K. Photoelectrochemical cell studies with semiconductor electrodes: a classified bibliography (1975–1983). *Solar Cells* **15**, 93–156 (1985).
- Licht, S. Multiple band gap semiconductor/electrolyte solar energy conversion. *J. Phys. Chem.* **105**, 6281–6294 (2001).
- Fujishima, A. & Honda, K. Electrochemical photolysis of water at a semiconductor electrode. *Nature* **238**, 37–38 (1972).
- O'Regan, B. & Grätzel, M. A low-cost, high efficiency solar cell based on dye-sensitized colloidal TiO₂ films. *Nature* **353**, 737–740 (1991).

- Hagfeldt, A. & Grätzel, M. Molecular photovoltaics. *Acc. Chem. Res.* **33**, 269–277 (2000).
- Hilgendorff, M., Spanhel, L., Rothenhäusler, Ch. & Müller, G. From ZnO colloids to nanocrystalline highly conductive films. *J. Electrochem. Soc.* **145**, 3632–3637 (1998).
- Nelson, J. Continuous time random walk model of electron transport in nanocrystalline TiO₂ electrodes. *Phys. Rev. B* **59**, 15374–15380 (1999).
- Barbé, Ch. J. et al. Nanocrystalline titanium oxide electrodes for photovoltaic applications. *J. Am. Ceram. Soc.* **80**, 3157–3171 (1997).
- Hodes, G., Howell, I. D. J. & Peter, L. M. Nanocrystalline photoelectrochemical cells: a new concept in photovoltaic cells. *J. Electrochem. Soc.* **139**, 3136–3140 (1992).
- Schwarzburg, K. & Willig, F. Origin of photovoltage in dye sensitized electrochemical solar cells. *J. Phys. Chem. B* **103**, 5743–5746 (1999).
- Pichot, F. & Gregg, B. A. The photovoltage-determining mechanism in dye-sensitized solar cells. *J. Phys. Chem. B* **104**, 6–10 (1999).
- Cahen, D., Hodes, G., Grätzel, M., Guillemoles, J. F. & Riess, I. Nature of photovoltaic action in dye-sensitized solar cells. *J. Phys. Chem. B* **104**, 2053–2059 (2000).
- Van de Lagemaat, J., Park, N.-G. & Frank, A. J. Influence of electrical potential distribution, charge transport, and recombination on the photopotential and photocurrent conversion efficiency of dye-sensitized nanocrystalline TiO₂ solar cells: a study by electrical impedance and optical modulation techniques. *J. Phys. Chem. B* **104**, 2044–2052 (2000).
- Dloczik, L. et al. Dynamic response of dye-sensitized nanocrystalline solar cells: characterization by intensity-modulated photocurrent spectroscopy. *J. Phys. Chem. B* **101**, 10281–10289 (1997).
- Masatai, Y. & Hodes, G. Size quantization in electrodeposited CdTe nanocrystalline films. *J. Phys. Chem. B* **101**, 2685–2690 (1997).
- Nazeruddin, M. K. et al. Conversion of light to electricity by cis X2-Bis(2,2'-bipyridyl-4,4'-dicarboxylate) ruthenium(II) charge transfer sensitizers. *J. Am. Chem. Soc.* **115**, 6382–6390 (1993).
- Kavan, L., Grätzel, M., Gilbert, S. E., Klemenz, C. & Scheel, H. J. Electrochemical and photoelectrochemical investigations of single-crystal anatase. *J. Am. Chem. Soc.* **118**, 6716–6723 (1996).
- Nazeruddin, M. K. et al. Engineering of efficient panchromatic sensitizers for nanocrystalline TiO₂-based solar cells. *J. Am. Chem. Soc.* **123**, 1613–1624 (2001).
- Hinsch, A. et al. in *Proc. 16th Eur. PV Solar Energy Conf., Glasgow, May 2000* (eds Scheel, H. et al.) **32** (James & James, London, 2000).
- Khaselev, O. & Turner, J. A. A monolithic photovoltaic-photoelectrochemical device for hydrogen production via water splitting. *Science* **280**, 425–427 (1998).
- Grätzel, M. The artificial leaf, bio-mimetic photocatalysis. *Cattech* **3**, 3–17 (1999).
- Santato, C., Ulmann, M. & Augustynski, J. Photoelectrochemical properties of nanostructured tungsten trioxide films. *J. Phys. Chem. B* **105**, 936–940 (2001).
- Khan, S. U. M. & Akikusa, J. Photoelectrochemical splitting of water at nanocrystalline n-Fe₂O₃ thin-film electrodes. *J. Phys. Chem. B* **103**, 7184–7189 (1999).
- Tennakone, K., Kumara, G. R. R. A., Kumarasinghe, A. R., Wijayantha, K. G. U. & Sirimanne, P. M. A dye-sensitized nano-porous solid-state photovoltaic cell. *Semicond. Sci. Technol.* **10**, 1689–1693 (1995).
- O'Regan, B. & Schwarz, D. T. Large enhancement in photocurrent efficiency caused by UV illumination of dye sensitized heterojunctions. *Chem. Mater.* **10**, 1501–1509 (1998).
- Bach, U. et al. Solid-state dye-sensitized mesoporous TiO₂ solar cells with high photon-to-electron conversion efficiencies. *Nature* **395**, 583–585 (1998).
- Krüger, J., Bach, U. & Grätzel, M. High efficiency solid-state photovoltaic device due to inhibition of interface charge recombination. *Appl. Phys. Lett.* **79**, 2085–2087 (2001).
- Kaiser, I. et al. The eta-solar cell with CuInS₂: a photovoltaic cell concept using an extremely thin absorber. *Sol. Energy Mater. Sol. Cells* **67**, 89–96 (2001).
- Halls, J. J. M., Pickler, K., Friend, R. H., Morati, S. C. & Holmes, A. B. Efficient photodiodes from interpenetrating polymer networks. *Nature* **376**, 498–500 (1995).
- Yu, G., Gao, J., Hummelen, J. C., Wudl, F. & Heeger, A. J. Polymer photovoltaic cells: enhanced efficiencies via a network of internal donor acceptor heterojunctions. *Science* **270**, 1789–1791 (1995).
- Schön, J. H., Kloc, Ch., Bucher, E. & Batlogg, B. Efficient organic photovoltaic diodes based on doped pentacene. *Nature* **403**, 408–410 (2000).
- Brabec, C. J. & Sariciftci, N. S. Polymeric photovoltaic devices. *Mater. Today* **3–8** (2000).
- Wöhrle, D. & Meissner D. Organic solar cells. *Adv. Mat.* **3**, 129–138 (1991).
- Shaheen, S. E. et al. 2.5% efficient orga-nic plastic solar cells. *Appl. Phys. Lett.* **78**, 841–843 (2001).
- Tuladhar, D. et al. Abstract, Int. Workshop Nanostruct. Photovoltaics, Dresden, Germany <<http://www.mpipks-dresden.mpg.de>> (2001).
- Grätzel, M. Perspectives for dye-sensitized nanocrystalline solar cells. *Prog. Photovoltaic Res. Appl.* **8**, 171–185 (2000).
- Savenije, T. J., Warman, J. M. & Goossens, A. Visible light sensitization of titanium dioxide using a phenylene vinylene polymer. *Chem. Phys. Lett.* **278**, 148–153 (1998).

Acknowledgements

I thank the members of the Swiss Federal Institute of Technology (EPFL) electrochemical photovoltaics development team, some of whose work is referenced; the industrial organizations whose interest in this PV system has induced them to license the concept and thereby support the research; EPFL; and OFEN (Swiss Federal Office of Energy) for past encouragement and support.

Some Computational Challenges in Energy Research

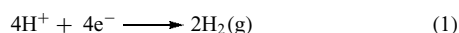
Victor S. Batista

Yale University, New Haven, CT, USA

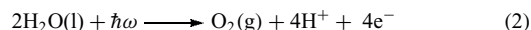
1	Introduction	1
2	Functionalization of Semiconductor Surfaces	2
3	Proton-Coupled Electron Transfer	4
4	Rectification of Interfacial Electron Transfer	5
5	Fuel Formation	6
6	Conclusions	7
7	Related Articles	7
8	Abbreviations and Acronyms	7
9	References	7

1 INTRODUCTION

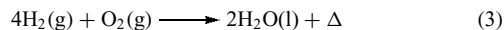
The development of cheap, robust, and efficient photocatalytic cells for water oxidation would allow the sustainable production of fuel from renewable resources.¹⁻⁴ An example of such a cell is shown in Figure 1, where hydrogen evolution at the cathode



is thermodynamically driven by photoanodic water oxidation:



The underlying photocatalytic process generates fuel (e.g., hydrogen) from water by using solar light to extract cheap electrons and protons from a renewable resource (e.g., water). The generated fuel is environmentally benign since, upon combustion, it generates only heat and water as follows:



The development of such type of photocatalytic solar cells based on inexpensive (e.g., earth-abundant) materials has been a long-standing challenge in photoelectrochemistry research,⁵ and significant effort has been invested since the discovery of ultraviolet (UV) water oxidation on *n*-TiO₂ electrodes.⁶ However, for many years, progress in the field has

been hindered by the lack of efficient catalytic materials as well as by the lack of fundamental understanding of the processes that limit the efficiency of the conversion mechanisms.

The main challenge has been to identify catalysts able to carry out the necessary multielectron transformations at energies and rates consistent with solar irradiance. This implies designing surface-bound complexes for catalyst turnover where solar irradiance is rate limiting, activating these catalysts by multiple single-electron injection events, designing cells with redox potentials sufficiently high as to drive the desired half-reactions, and designing and assembling robust molecular components. Such a design problem requires fundamental understanding of the factors affecting the elementary steps (numbered in Figure 1), including (1) photoexcitation; (2) interfacial electron transfer (IET) and surface charge separation; (3) charge transport; (4) storage of oxidizing equivalents for catalysis; and (5) irreversible carrier collection by sacrificial acceptors, or fuel-forming reactions at the cathode. The characterization of all these processes clearly surpasses the limits of traditional disciplines and therefore calls upon researchers to establish collaborative research programs combining synthesis, computational modeling, electrochemistry, and spectroscopy.

In recent years, we have witnessed a flurry of interest in the development of catalysts for water oxidation⁷⁻²² as well as on the development of fundamental studies of photocatalysis based on semiconductor surfaces.^{23,24} Current efforts are focused on the development of more efficient catalysts based on earth-abundant materials and on molecular

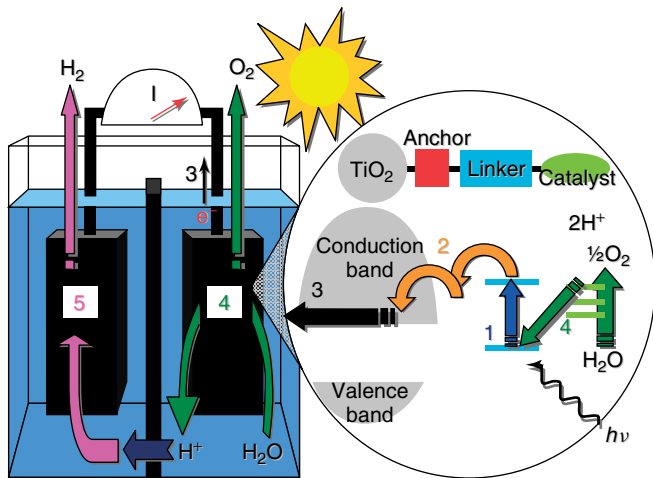


Figure 1 Photocatalytic cell for water oxidation and hydrogen evolution with schematic of elementary photoanodic processes

assemblies to efficiently couple multielectron photoanodic processes to fuel production cathodic processes. This article reviews recent advances in the field, with emphasis on computational work for the development and characterization of catalytic surfaces based on nanoporous TiO₂ thin films sensitized with manganese catalysts. The reviewed studies have been integrated with synthesis, electrochemistry, and spectroscopy in an interdisciplinary effort to advance our understanding of structure/function relationships in catalytic materials. The main aim has been to provide understanding of the fundamental processes that limit the efficiency of the reaction mechanisms and to develop guidelines for the design of novel photocatalytic materials for fuel production.

2 FUNCTIONALIZATION OF SEMICONDUCTOR SURFACES

Surface functionalization of nanoporous TiO₂ thin films is used in dye-sensitized solar cells (DSSCs) to maximize light harvesting.²⁵ Dye molecules on TiO₂ shift the absorption spectrum of the semiconductor to the visible region, leading to the efficient injection of electrons into the TiO₂ conduction band upon visible light absorption. The holes h^+ left behind usually have limited redox potentials since they are localized in the oxidized adsorbate molecule, rather than in the semiconductor valence band. Therefore, while efficient for light harvesting, such an approach has not led to photocatalysis.

Achieving photocatalysis with maximal light harvesting, requires sophisticated *surface catalysts* for IET. Recent studies have focused on the functionalization of TiO₂ surfaces by covalent attachment of biomimetic high-valent oxo-Mn complexes (Figure 2). These are known to be efficient catalysts

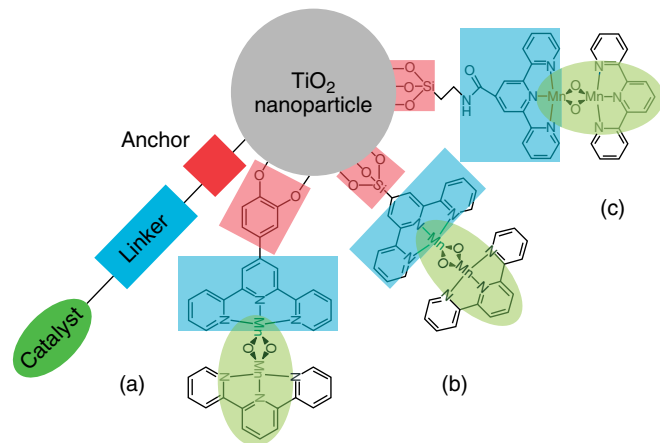
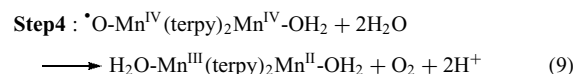
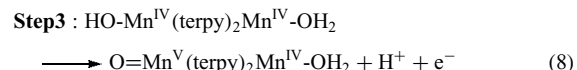
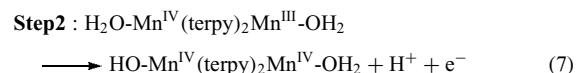
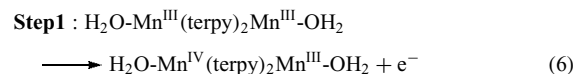
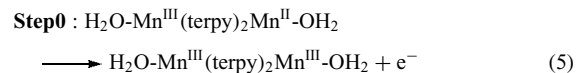


Figure 2 TiO₂ NP functionalized with Mn dimers by using various linkers including catechol (a) and siloxane-based (b and c) linkers

for selective C–H oxygenation,²⁶ and water splitting to O₂.¹⁰ Manganese catalysts are inspired by Nature, where only oxo-Mn complexes achieve redox potentials high enough to form O₂ at the oxygen-evolving complex (OEC) of photosystem II, as follows:^{27–30}



The following mechanism illustrates the underlying catalytic process of water oxidation by formation of high-valent Mn^{IV}Mn^{IV}-O* species, as illustrated for the complex [H₂O(terpy)Mn^{III}(O)₂Mn^{IV}(terpy)H₂O]³⁺ (terpy, 2,2':6,2''-terpyridine):



The Mn^{IV}Mn^{IV}-O* species is thought to be the activated form of the catalyst, normally formed by reaction of the Mn dimer with a primary oxidant (e.g., oxone), storing the four oxidizing equivalents that are necessary to oxidize water. In the photocatalytic case (Figure 1), however, such a species is formed through multiple one-electron injection processes and electron collection by the TiO₂ anode. The activation process thus avoids the use of a primary oxidant, yielding

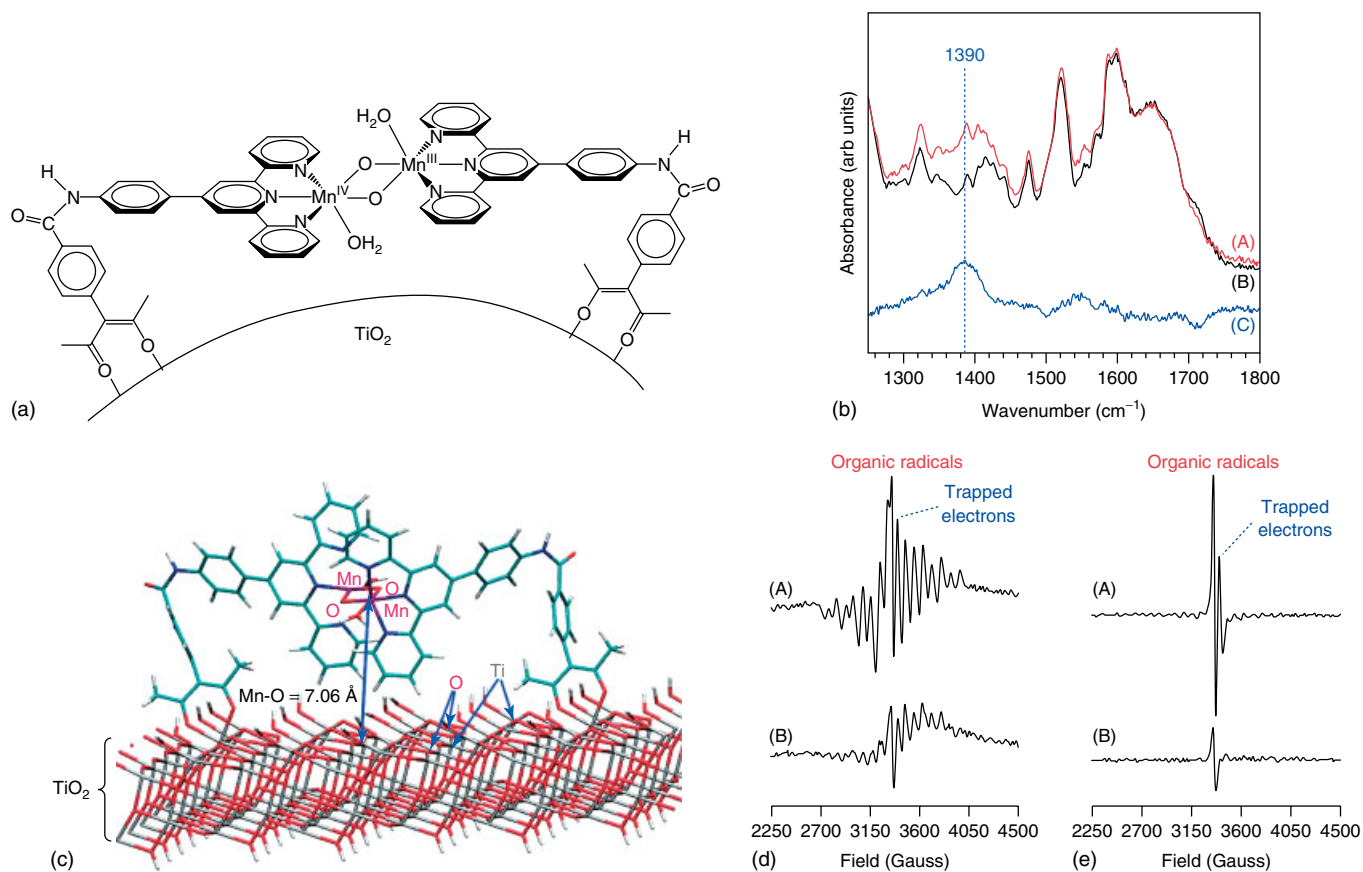


Figure 3 (a) DFT QM/MM configuration of **Mn-L-TiO₂**. (b) attenuated total reflection infrared (ATR-IR) spectra of (A) **Mn-L-P25**; (B) **Mn^{II}-L-P25**; and (C) shows the difference between spectra (A) and (B). (c) Resonances of organic radicals and TiO₂ lattice-trapped electrons (Ti³⁺) are labeled. (d,e) EPR difference spectra of (A) **Mn-L-P25** and (B) **Mn-L-D70**. (d) Light-*minus*-dark EPR spectra. (e) Postillumination dark *minus* preillumination dark EPR spectra. (Reproduced from Ref. 31. © American Chemical Society.)

a general approach for green oxidation chemistry driven by solar light.

Recent work has been focused on the direct deposition⁹ as well as on the covalent attachment³¹ of the Mn dimer [H₂O(terpy)Mn^{III}(μ-O)₂Mn^{IV}(terpy)H₂O](NO₃)₃, (terpy, 2,2′ : 6′, 2′′-terpyridine) onto nanoporous semiconductor surfaces by using a robust chromophoric linker **L**, a phenylterpy ligand attached to a 3-phenyl-acetylacetonate anchoring moiety via an amide bond (Figure 3). The resulting covalent binding to the semiconductor surface has been characterized by using quantum mechanics/molecular mechanics (QM/MM) hybrid methods in conjunction with UV–visible, IR (infrared), and EPR (electron paramagnetic resonance) spectroscopy. In addition, these studies have shown that **L** absorbs visible light, leading to photoinduced interfacial electron transfer into the semiconductor conduction band, reversibly advancing the Mn complex to the Mn(IV,IV) state. The reported work also showed that, in the absence of electron scavengers, the injected electron recombines back to form the Mn(III,IV) state in the dark.

2.1 Simulations of Interfacial Electron Transfer

Ab initio DFT (density functional theory) molecular dynamics simulations have been combined with quantum dynamics calculations of electronic relaxation to investigate IET in sensitized semiconductor nanostructures, providing fundamental understanding of IET at the detailed molecular level.^{9,31–39} The characteristic times for the excited-state IET from adsorbate complexes have been shown to be consistent with terahertz experiments and with ultrafast measurements in TiO₂ sensitized by small organic molecules, including biisonicotinic acid on rutile and alizarin on TiO₂.^{40,41}

2.2 Interfacial Electron Transfer

Quantum dynamics simulations have provided valuable insights on the nature of interfacial electron transfer processes leading to the activation of Mn catalysts anchored onto TiO₂ surfaces. For example, Figure 4 shows a series of snapshots for the distribution of electron density as it evolves

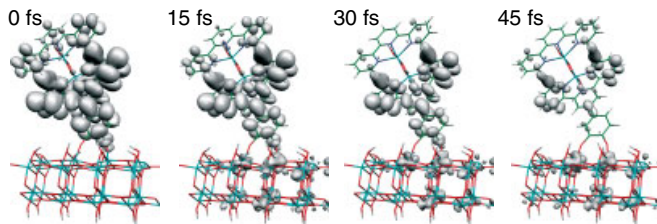


Figure 4 Snapshots, at 15-fs intervals, of the electronic charge distribution corresponding to IET after visible excitation (508 nm) of the catalyst surface complex depicted in Figure 2(a). Only the center semiconductor block is shown to allow a detailed view of the time-dependent charge distribution

during the early time dynamics of interfacial electron injection following photoexcitation of Mn dimer adsorbate. These simulations indicate that the interfacial electron injection is typically complete within an ultrafast, subpicosecond timescale when the initially populated electronic state localized in the adsorbate chromophore has suitable energy match with electronic states in the conduction band of the semiconductor surface.

Quantum dynamics simulations of interfacial electron transfer solve the time-dependent Schrödinger equation, yielding a detailed description of the time-dependent charge distribution after photoexcitation of the adsorbate. The resulting charge distribution provides information on the electronic orbitals responsible for hosting the injected electron in the semiconductor host substrate as well as the evolution of the spatial distribution of electronic population as it relaxes in the semiconductor conduction band. This type of atomistic simulations have also provided a description of the influence of thermal fluctuations on the underlying relaxation pathways.³³ Simulation studies beyond the low-temperature analysis have analyzed room-temperature conditions typical of photocatalytic cells, showing that thermal nuclear fluctuations can speed up the underlying interfacial electron transfer dynamics. The molecular/electronic origin of such effects has been traced to fluctuations that break the symmetry of otherwise orthogonal electronic states, creating additional relaxation pathways for carrier diffusion. Analogous computer simulations have also allowed the detailed analysis of the relaxation dynamics of holes, localized the monolayer of adsorbate molecules, created upon photoexcitation and interfacial electron transfer of sensitized TiO₂ nanoparticles (NPs) under cryogenic temperature conditions.^{34,42}

3 PROTON-COUPLED ELECTRON TRANSFER

Proton-coupled electron transfer (PCET) is often essential to achieve high catalytic turnovers of multielectron redox processes. Protonation/deprotonation processes can

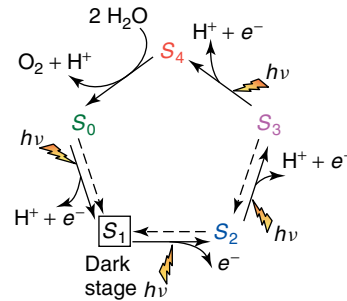


Figure 5 Catalytic cycle proposed by Joliot and Kok for water splitting into dioxygen, protons, and electrons at the OEC in PSII [1,2]. Dashed arrows indicate spontaneous interconversion processes in the dark. The steps for substrate water attachment and proton release are only tentatively proposed and might change with pH

facilitate reduction/oxidation state transitions, preventing charge buildup during the accumulation of multiple reducing (or oxidizing) equivalents. For example, PCET is thought to play an important role in keeping all of the redox steps in the Kok's catalytic cycle of water oxidation (Figure 5),^{43,44} over a narrow range of potential at ~ 1 V. The resulting “redox-leveling” effect prevents the accumulation of charge in the catalytic complex, allowing for the accumulation of four oxidizing equivalents in the OEC, embedded in the low dielectric environment of photosystem II (PSII).

The design of efficient catalysts for water oxidation often aims to develop molecular frameworks where the reactivity mimics the catalytic functionality of the OEC, leading to reaction pathways where the redox-leveling effect is induced by PCET. However, general design principles for efficient PCET mechanisms are still lacking. Computational modeling can play an important role in understanding catalytic processes of natural systems (e.g., photosystem II),^{11,12,45–51} as well as on the design and characterization of catalysts with similar functionality, by guiding the selection of suitable ligands for transition metal complexes that lead to redox-leveling mechanisms based on PCET. Recent studies of biomimetic oxomanganese complexes have been based on rigorous quantum chemistry calculations of redox potentials and pK_a values and direct comparisons with electrochemical measurements.⁵²

Figure 6 shows results of calculations of free energy changes associated with the oxidation state transition (III,III) \rightarrow (III,IV) in the mixed-valent Mn complex [(bpy)₂Mn^{III}(μ -O)₂Mn^{IV}(bpy)₂]³⁺ (bpy, 2,2'-bipyridyl), as obtained at the DFT B3LYP/cc-pVTZ(-f) level by using the standard thermodynamic cycle formalism applied in conjunction with continuum solvation models.⁵² It is shown that the pK_a values of the oxo-ligands depend strongly on the oxidation states of the complex, changing by approximately 10 pH units (i.e., from pH ~ 2 to pH ~ 12) upon III,IV \rightarrow III,III reduction of the Mn complex. These results are in good agreement with the experimental pK_a values determined by solution

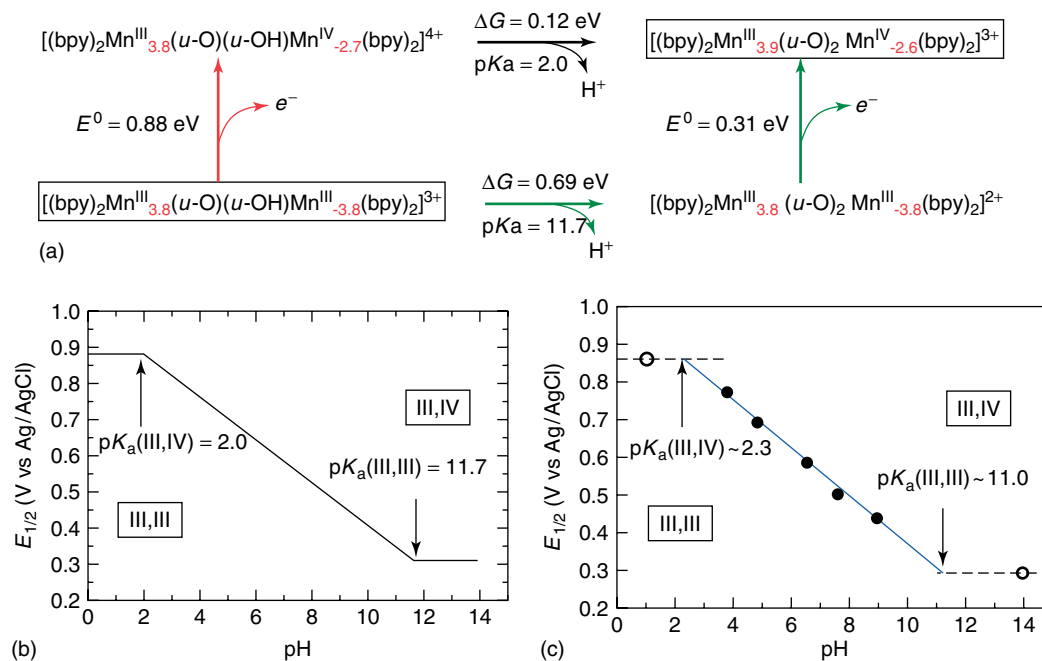


Figure 6 (a) Thermodynamic energy diagram of PCET for complex 1 in aqueous solutions at $pH = 0$, as described by DFT B3LYP/cc-pVTZ(-f) free energy calculations of redox potentials and pK_a values based on the Haber-Born cycle method applied in conjunction with a continuum solvation model. Formal oxidation numbers are indicated as superscripts in Roman numbers and the spin populations obtained according to the Mulliken population analysis are indicated as subscripts in red. (b) Pourbaix diagram for complex 1 in aqueous solutions, obtained (b) from free energy calculations of redox potentials at the DFT B3LYP/cc-pVTZ(-f) level of theory, and (c) experimental data (the circles). (Reproduced from Ref. 54. © American Chemical Society.)

magnetic susceptibility and near-IR spectroscopy,⁵³ as well as with the pH dependence of the redox potential previously reported by cyclic voltammogram (CV) measurements,⁵⁴ and provide fundamental understanding of the underlying changes in protonation and oxidation states leading to the pH dependence of redox potentials.

Figure 6(a) shows that the protonated reduced species $\mathbf{1}_{red}$ $[(bpy)_2Mn^{III}(\mu-O)(\mu-OH)Mn^{III}(bpy)_2]^{3+}$ can be oxidized via two possible pathways, including oxidation by a direct ionization process requiring a rather high free energy change of 0.88 eV (red arrow), or oxidation by the concerted removal of an electron from the complex and a proton from the μ -hydroxo bridge (green arrow). These results indicate that the underlying oxidation is strongly coupled to deprotonation of the μ -OH bridge for a wide range of values of pH (i.e., $pH = 2.0-11.7$). For $\mathbf{1}_{red}$, the oxidation free energy is constant (~ 0.88 V) at $pH < 2.0$ (oxidation takes the red path). Within the $2.0 < pH < 11.7$ range, the overall free energy requirement consists of two parts, including $0.69-0.059 \cdot pH$ eV for the deprotonation step and an extra 0.31 eV for the oxidation of the deprotonated species. Finally, at $pH > 11.7$, the oxidation free energy becomes constant since the green path dominates with spontaneous deprotonation.

Figure 6(b,c) shows the comparison of Pourbaix diagrams, illustrating the pH dependence of $E_{1/2}$, as computed at the DFT B3LYP/cc-pVTZ(-f) level of theory and directly

compared to CV measurements.⁵⁴ The agreement shows that theory can provide accurate descriptions of the regulatory effect of reduction state transitions on the pK_a values of the ligands and the effect of protonation of oxo-ligands on the redox potentials of metal centers. Therefore, it is natural to expect that analogous calculations and direct comparisons to experimental data will allow the study of PCET along the catalytic cycle of multielectron reactions catalyzed by other transition metal complexes.

4 RECTIFICATION OF INTERFACIAL ELECTRON TRANSFER

A common problem to any scheme where photoexcitation creates an electron-hole pair state is electron-hole pair recombination. In PSII, recombination is suppressed by an arrangement of redox cofactors that induce directionality of electron transfer after the initial charge separation. Molecular diodes can also induce directionality of electron transfer⁵⁵ and have been recently explored in the design of semiconductor materials where the covalent attachment of molecular linkers induces rectification of interfacial electron transfer (Figure 7). The electronic rectification properties of molecular linkers that covalently bind Mn catalysts to TiO_2 surfaces, including

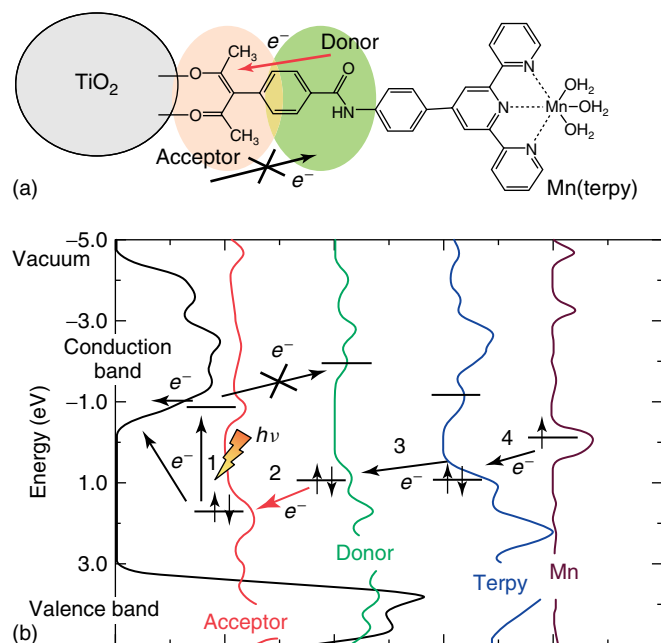


Figure 7 (a) Schematic diagram of a TiO₂ NP functionalized with [Mn^{II}(H₂O)₃]²⁺, where the Mn complex is covalently attached to the TiO₂ surface by the phenyl-acac anchor. (b) Density of electronic states and arrows indicating the electron transfer pathway, induced by photoexcitation and electron injection, leading to Mn oxidation. Favorable directionality of electron transfer is due to the positioning of electronic energy levels in the electron donor and acceptor parts of the ligand-linker chromophore. (Reproduced from Ref. 36. © American Chemical Society.)

Mn-complexes with phenylterpyridine ligands attached to 3-phenyl-acetylacetonate anchors via amide bonds, have been characterized by calculations of current–voltage characteristics at metallic junctions.⁵⁶ It was found that a suitable choice of the amide linkage can induce directionality of interfacial electron transfer. These findings were consistent with EPR measurements, confirming an asymmetry of electron transfer rates for linkers with significant rectification.⁵⁶ These studies are particularly relevant for the development of photovoltaic or photocatalytic devices based on functionalized TiO₂ thin films where the overall performance is often affected by recombination processes competing with interfacial electron injection.

Calculations of current–voltage (I – V) characteristics were performed with the software package SMEAGOL,^{57,58} integrating the nonequilibrium Green’s function (NEGF) method^{59,60} with DFT⁶¹ as implemented in the SIESTA package for electronic structure calculations.⁶² The systems were modeled in the usual three-subsystem segmentation with the molecular diode of interest in between metallic electrodes.⁵⁶ The surface Green’s functions, describing the current–voltage probes, were obtained as a direct summation of both open and closed scattering channels together with a regularization procedure of the Hamiltonian that provides a significant improvement over standard recursive methods.

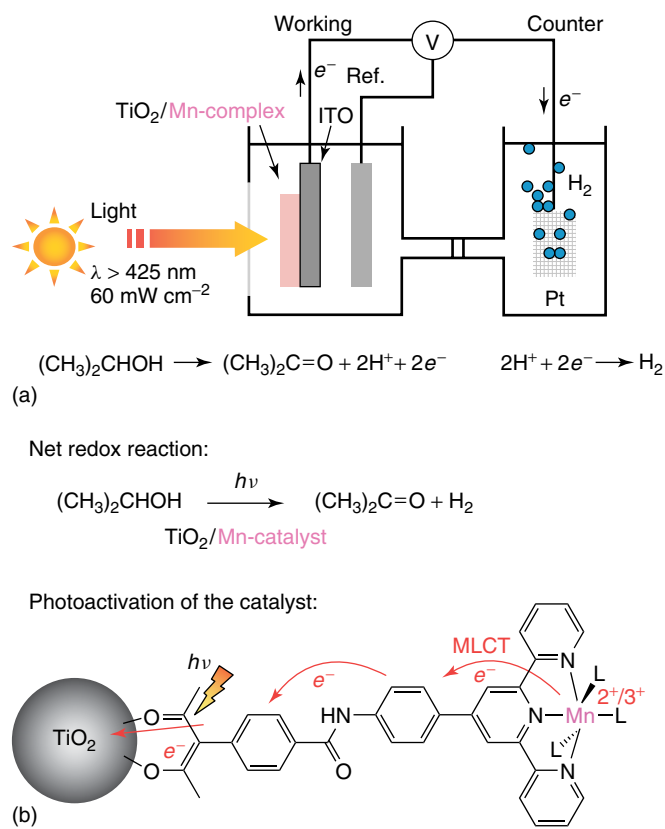


Figure 8 Photocatalytic cell for visible-light-driven oxidation chemistry and H₂ evolution (a), based on TiO₂ thin-film photoanodes functionalized with Mn catalysts covalently attached via chromophoric linkers (b)

5 FUEL FORMATION

Recent work on photocatalytic cells based on TiO₂ thin-film photoanodes functionalized with Mn-complexes has focused on coupling H₂ evolution driven to photoanodic oxidation reactions. Figure 8 shows a schematic diagram of a specific photocatalytic cell based on TiO₂ electrodes functionalized with Mn-terpy catalysts that can couple hydrogen evolution with oxidation of isopropanol to acetone. The reaction is catalyzed by the Mn-terpy complex adsorbate, activated by interfacial electron injection into the TiO₂ host substrate, upon absorption of visible light ($\lambda > 425$ nm).⁶³ The activation process induces the oxidation-state transition Mn(II) \rightarrow Mn(III) in the metal center, generating Mn(III) with sufficient oxidizing power to transform isopropanol in acetone. The injected electrons are combined with protons in the counter-electrode to produce hydrogen. It has been shown that such a mechanism, involving photoexcitation, interfacial electron injection, charge carrier collection, and irreversible hydrogen evolution, can be accomplished when the Mn-terpy catalysts are covalently attached to the TiO₂ surface by using robust chromophoric linkers that are stable in aqueous solutions under oxidative conditions.

Similar results have been reported for other “proof-of-concept” visible-light-driven photocatalytic cells, including cells based on other (although more expensive) transition metal catalysts,^{13,24} indicating that the functionalization of semiconductor surfaces by covalent attachment of transition metal complexes yields a general approach for the development of photocatalytic solar cells.

6 CONCLUSIONS

The emergence of photocatalytic solar cells based on semiconductor materials functionalized with earth-abundant transition metal complexes represent a promising development for the sustainable production of fuel from renewable resources (e.g., water). Recent advances in the study of fundamental aspects that affect the overall efficiency of the underlying catalytic mechanisms suggest that control over photoabsorption, PCET, and IET can be achieved by implementing the ligand design methodology that has been so successful for many years in the development of homogeneous catalysts. When fundamentally informed by structural and mechanistic characterization based on computational modeling, high-resolution spectroscopy, and electrochemistry, in conjunction with the comparative analysis of analogous catalytic processes in nature, the resulting methodology constitutes a powerful “bottom-up” synthetic tool for the development of new catalytic materials. These emerging methods are thus expected to continue making significant contributions in the development of novel semiconductor materials for photocatalytic solar cells.

7 RELATED ARTICLES

Dye-Sensitized Solar Cells: an Overview; Energy Conversion in Photosynthesis; Hydrogen Economy; Molecular Catalysis for Fuel Cells; Molecular Catalysts for Oxygen Production from Water; Photocatalytic Hydrogen Production from Water; Toward Solar Fuels Using a Biomimetic Approach: Progress in the Swedish Consortium for Artificial Photosynthesis; Recent Advances in Photo-Initiated Electron-Transfer at the Interface between Anatase TiO₂ Nanocrystals and Transition-Metal Polypyridyl Compounds.

8 ABBREVIATIONS AND ACRONYMS

CV = cyclic voltammogram; DFT = density functional theory; DSSC = dye-sensitized solar cells; EPR = electron paramagnetic resonance; IET = interfacial electron transfer; IR = infrared; NEGF = nonequilibrium green’s

function; NP = nanoparticle; OEC = oxygen-evolving complex; PCET = proton coupled to electron transfer; QM/MM = quantum mechanics/molecular mechanics; UV = ultraviolet.

9 REFERENCES

1. A. J. Bard and M. A. Fox, *Acc. Chem. Res.*, 1995, **28**, 141.
2. E. E. Benson, C. P. Kubiak, A. J. Sathrum, and J. M. Smieja, *Chem. Soc. Rev.*, 2009, **38**, 89.
3. A. J. Morris, G. J. Meyer, and E. Fujita, *Acc. Chem. Res.*, 2009, **42**, 1983.
4. M. Rakowski-Dubois and D. L. Dubois, *Acc. Chem. Res.*, 2009, **42**(12), 1974.
5. A. J. Bard and M. A. Fox, *Acc. Chem. Res.*, 1995, **28**, 141.
6. A. Fujishima and K. Honda, *Nature*, 1972, **238**, 37.
7. N. D. McDaniel, F. J. Coughlin, L. L. Tinker, and S. Bernhard, *J. Am. Chem. Soc.*, 2008, **130**, 210.
8. J. F. Hull, D. Balcells, J. D. Blakemore, C. D. Incarvito, O. Eisenstein, G. W. Brudvig, and R. H. Crabtree, *J. Am. Chem. Soc.*, 2009, **131**, 8730.
9. G. H. Li, E. M. Sproviero, R. C. Snoeberger, N. Iguchi, J. D. Blakemore, R. H. Crabtree, G. W. Brudvig, and V. S. Batista, *Energy Environ. Sci.*, 2009, **2**, 230.
10. J. Limburg, J. S. Vrettos, L. M. Liable-Sands, A. L. Rheingold, R. H. Crabtree, and G. W. Brudvig, *Science*, 1999, **283**, 1524.
11. E. M. Sproviero, J. A. Gascon, J. P. McEvoy, G. W. Brudvig, and V. S. Batista, *Curr. Opin. Struct. Biol.*, 2007, **17**, 173.
12. E. M. Sproviero, J. A. Gascon, J. P. McEvoy, G. W. Brudvig, and V. S. Batista, *Coord. Chem. Rev.*, 2008, **252**, 395.
13. W. J. Youngblood, S. H. A. Lee, K. Maeda, and T. E. Mallouk, *Acc. Chem. Res.*, 2009, **42**, 1966.
14. M. W. Kanan and D. G. Nocera, *Science*, 2008, **321**, 1072.
15. M. W. Kanan, Y. Surendranath, and D. G. Nocera, *Chem. Soc. Rev.*, 2009, **38**, 109.
16. Z. F. Chen, J. J. Concepcion, J. W. Jurss, and T. J. Meyer, *J. Am. Chem. Soc.*, 2009, **131**, 15580.
17. J. J. Concepcion, J. W. Jurss, M. K. Brennaman, P. G. Hoertz, A. O. T. Patrocinio, N. Y. M. Iha, J. L. Templeton, and T. J. Meyer, *Acc. Chem. Res.*, 2009, **42**, 1954.
18. J. J. Concepcion, J. W. Jurss, M. R. Norris, Z. F. Chen, J. L. Templeton, and T. J. Meyer, *Inorg. Chem.*, 2010, **49**, 1277.
19. S. W. Gersten, G. J. Samuels, and T. J. Meyer, *J. Am. Chem. Soc.*, 1982, **104**, 4029.
20. R. Brimblecombe, A. M. Bond, G. C. Dismukes, G. F. Swiegers, and L. Spiccia, *PCCP*, 2009, **11**, 6441.
21. R. Brimblecombe, G. F. Swiegers, G. C. Dismukes, and L. Spiccia, *Angew. Chem.-Int. Ed.*, 2008, **47**, 7335.

22. G. C. Dismukes, R. Brimblecombe, G. A. N. Felton, R. S. Pryadun, J. E. Sheats, L. Spiccia, and G. F. Swiegers, *Acc. Chem. Res.*, 2009, **42**, 1935.
23. A. Mills and S. Le Hunte, *J. Photochem. Photobiol.*, 1997, **108**, 1.
24. J. A. Treadway, J. A. Moss, and T. J. Meyer, *Inorg. Chem.*, 1999, **38**, 4386.
25. B. O'Regan and M. Gratzel, *Nature*, 1991, **353**, 737.
26. S. Das, C. D. Incarvito, R. H. Crabtree, and G. W. Brudvig, *Science*, 2006, **312**, 1941.
27. R. Manchanda, G. W. Brudvig, and R. H. Crabtree, *Coord. Chem. Rev.*, 1995, **144**, 1.
28. E. M. Sproviero, J. A. Gascon, J. P. McEvoy, G. W. Brudvig, and V. S. Batista, *J. Chem. Theory Comput.*, 2006, **2**, 1119.
29. J. Limburg, J. S. Vrettos, H. Y. Chen, J. C. de Paula, R. H. Crabtree, and G. W. Brudvig, *J. Am. Chem. Soc.*, 2001, **123**, 423.
30. E. M. Sproviero, J. A. Gascon, J. P. McEvoy, G. W. Brudvig, and V. S. Batista, *J. Inorg. Biochem.*, 2006, **100**, 786.
31. G. Li, E. M. Sproviero, W. R. McNamara, R. C. Snoeberger, R. H. Crabtree, G. W. Brudvig, and V. S. Batista, *J. Phys. Chem. B*, 2010, DOI: 10.1021/jp908925z (Submitted).
32. L. G. C. Rego and V. S. Batista, *J. Am. Chem. Soc.*, 2003, **125**, 7989.
33. S. G. Abuabara, L. G. C. Rego, and V. S. Batista, *J. Am. Chem. Soc.*, 2005, **127**, 18234.
34. L. G. C. Rego, S. G. Abuabara, and V. S. Batista, *J. Chem. Phys.*, 2005, **122**(15), 122.
35. S. Jin, R. C. Snoeberger, A. Issac, V. S. Batista, and T. Lian, *J. Phys. Chem. B*, 2010, DOI: 10.1021/jp911662g (Submitted).
36. W. R. McNamara, R. C. Snoeberger, G. Li, J. M. Schleicher, C. W. Cady, M. Poyatos, C. A. Schmittenmaer, R. H. Crabtree, G. W. Brudvig, and V. S. Batista, *J. Am. Chem. Soc.*, 2008, **130**, 14329.
37. W. R. McNamara, R. C. Snoeberger, G. H. Li, C. Richter, L. J. Allen, R. L. Milot, C. A. Schmittenmaer, R. H. Crabtree, G. W. Brudvig, and V. S. Batista, *Energy Environ. Sci.*, 2009, **2**, 1173.
38. L. G. C. Rego, R. da Silva, J. A. Freire, R. C. Snoeberger, and V. S. Batista, *J. Phys. Chem. C*, 2010, **114**, 1317.
39. R. C. Snoeberger, T. Lian, and V. S. Batista, *Proc. SPIE*, 2010, **7396**, 739604.
40. R. Huber, J. E. Moser, M. Gratzel, and J. Wachtveitl, *J. Phys. Chem. B*, 2002, **106**, 6494.
41. J. Schnadt, P. A. Bruhwiler, L. Patthey, J. N. O'Shea, S. Sodergren, M. Odellius, R. Ahuja, O. Karis, M. Bassler, P. Persson, H. Siegbahn, S. Lunell, and N. Martensson, *Nature*, 2002, **418**, 620.
42. L. G. C. Rego, S. G. Abuabara, and V. S. Batista, *Quantum Inf. Comput.*, 2005, **5**, 318.
43. P. Joliot, G. Barbieri, and R. Chabaud, *Photochem. Photobiol.*, 1969, **10**, 309.
44. B. Kok, B. Forbush, and M. McGloin, *Photochem. Photobiol.*, 1970, **11**, 457.
45. E. M. Sproviero, J. A. Gascon, J. P. McEvoy, G. W. Brudvig, and V. S. Batista, *J. Chem. Theory Comput.*, 2006, **2**, 1119.
46. E. M. Sproviero, J. A. Gascon, J. P. McEvoy, G. W. Brudvig, and V. S. Batista, *J. Inorg. Biochem.*, 2006, **100**, 786.
47. E. M. Sproviero, J. A. Gascon, J. P. McEvoy, G. W. Brudvig, and V. S. Batista, *J. Am. Chem. Soc.*, 2008, **130**, 6728.
48. E. M. Sproviero, J. A. Gascon, J. P. McEvoy, G. W. Brudvig, and V. S. Batista, *J. Am. Chem. Soc.*, 2008, **130**, 3428.
49. E. M. Sproviero, J. P. McEvoy, J. A. Gascon, G. W. Brudvig, and V. S. Batista, *Photosynth. Res.*, 2008, **97**, 91.
50. E. M. Sproviero, M. B. Newcomer, J. A. Gascon, E. R. Batista, G. W. Brudvig, and V. S. Batista, *Photosynth. Res.*, 2009, **102**, 455.
51. E. M. Sproviero, K. Shinopoulos, J. A. Gascon, J. P. McEvoy, G. W. Brudvig, and V. S. Batista, *Philos. Trans. R. Soc. B-Biol. Sci.*, 2008, **363**, 1149.
52. T. Wang, G. Brudvig, and V. S. Batista, *J. Chem. Theory Comput.*, 2010, **6**, 755.
53. S. R. Cooper and M. Calvin, *J. Am. Chem. Soc.*, 1977, **99**, 6623.
54. H. H. Thorp, J. E. Sarneski, G. W. Brudvig, and R. H. Crabtree, *J. Am. Chem. Soc.*, 1989, **111**, 9249.
55. M. Elbing, R. Ochs, M. Koentopp, M. Fischer, C. von Hanisch, F. Weigend, F. Evers, H. B. Weber, and M. Mayor, *Proc. Natl. Acad. Sci. U.S.A.*, 2005, **102**, 8815.
56. J. A. Palma, W. R. McNamara, R. C. Snoeberger, C. Richter, R. L. Milot, C. A. Schmittenmaer, R. H. Crabtree, G. W. Brudvig, and V. S. Batista, *J. Am. Chem. Soc.*, 2010, submitted.
57. A. R. Rocha, V. Garcia-Suarez, S. W. Bailey, C. J. Lambert, and J. S. S. Ferrer, *J. Chem. Phys.*, 2005, **4**, 335.
58. A. R. Rocha, V. Garcia-Suarez, S. W. Bailey, C. J. Lambert, J. Ferrer, and S. Sanvito, *Phys. Rev. B*, 2006, **73**, 085414.
59. L. V. Keldysh, *Sov. Phys. JETP*, 1965, **20**, 1018.
60. S. Datta, 'Electronic Transport in Mesoscopic Systems', Cambridge University Press, Cambridge, 1997.
61. W. Kohn and L. J. Sham, *Phys. Rev. A*, 1965, **140**(4A), 1133.
62. J. M. Soler, E. Artacho, J. D. Gale, A. Garcia, J. Junquera, P. Ordejon, and D. Sanchez-Portal, *J. Phys. Cond. Matt.*, 2002, **14**, 2745.
63. G. Li, W. R. McNamara, R. C. Snoeberger, R. H. Crabtree, G. W. Brudvig, and V. S. Batista, *J. Am. Chem. Soc.*, 2010, submitted.